3. Characterisation and purification trials with the M_2 Muscarinic Receptor and the H_1 Histamine Receptor

3.1. Acknowledgements

Dr Wayne Leifert and Mrs Sharon Burnard taught me G-protein purification and the [^{35}S]-GTPγS binding assay. Dr Olgatina Bucco optimised the [^{35}S]-GTPγS assay to a 96-well plate format. Wayne and Olgatina helped with interpretation of some of the early receptor/G-protein reconstitution assay results.

Dr Olgatina Bucco purified the $G\alpha_q$ and $G\alpha_o$ subunits used in reconstitution assays with the histamine receptor.

Dr Ian Menz gave very useful advice about the technique of IMAC and helped with analysis of results.

Dr Ross Fernley patiently taught me how to use the HPLC and then allowed me the rare opportunity of unlimited, unsupervised use. Ross also provided helpful advice in regards to purification techniques, receptor/ligand affinities and analysis of HPLC profiles.

Dr Connie Darmanin recognised the potential of the initial $His6_CM_2R$ solubilisation experiments and was crucial in taking the purification to near completion. Connie also provided helpful advice for the $His10_CH_1R$ purification and gave advice on experimental design.

3.2. Introduction

Purification of functional, homogeneous, mammalian seven transmembrane receptors has proven to be extremely difficult to date. The failure rate is very high, as emphasised by the fact that there are only two mammalian 7TMR structures solved to atomic resolution (Cherezov, et al., 2007; Palczewski, et al., 2000; Rasmussen, et al., 2007). If the proteins could by easily produced and purified in functional form, diffracting protein crystals would be much more readily forthcoming. Whilst expression of the receptor in large yields is the first challenge, the second challenge of stripping the protein from its native membrane environment in order to purify it is an equal, if not greater challenge. There are several purification protocols for retrieving the M_2R from native tissue (Florio and Sternweis, 1985; Haga and Haga, 1983; Rinken, 1996) and from cell cultures including *Sf*9 (Parker, et al., 1991) and CHO cells (Peterson, et al., 1995). Purification using hexa-Histidine tagging on the N or C terminus of a mutant M_2R, lacking 147 residues from the third intracellular loop and an N terminal glycosylation sequence, has been reported (Hayashi and Haga, 1996). Whilst the H_1R has mainly been solubilised and/or purified from tissue sources (Osband and McCaffrey, 1979; Ruat, et al., 1992; Toll and Snyder, 1982) and only a single report exists for the purification of recombinant H_1R from *Sf*9 cells (Ratnala, et al., 2004).

In this study the aim was to purify at least one seven transmembrane receptor from, a choice of two receptor families (muscarinic and histamine) and four receptor constructs. Prior to purification the signalling activity of the receptor constructs was assessed by reconstitution with purified G-proteins. The expression levels reported in chapter 2 were high enough that with large scale cell culture, sufficient quantities of receptor could be produced for initial purification trials.

3.3. Methods

3.3.1. Reagents

Unless otherwise stated, all reagents were of analytical grade and were purchase from Sigma Aldrich. All buffers were prepared with milliQ purified water (mQH_2O)

3.3.2. G-protein baculoviruses

Baculoviruses for a terminal hexa-Histidine tagged $G\alpha_{i1}$ ($His6_NG\alpha_{i1}$), $G\alpha_q$, β_1, γ_2 and hexa-Histidine tagged γ_2 were generously supplied by Professor Richard Neubig (University of Michigan). $G\alpha_o$ virus was kindly supplied by Dr Andrejs Kumans of Professor Alfred Gilman's laboratory (University of Texas, Southwestern Medical School).

3.3.3. Purification of the G-Protein subunits

*Sf*9 cells (up to 2 L) were infected with the recombinant baculoviruses $His6_NG\alpha_{i1}$, β_1, and γ_2 for 72 h and were subsequently harvested by centrifugation at 1000xg for 10 min. All further operations were performed on ice or at 4^{o}C, using a modification of published methods (Hepler, et al., 1993). The cell pellet was gently resuspended in ice-cold phosphate-buffered saline (PBS; 137 mM NaCl, 2.7 mM KCl, 10 mM Na_2HPO_4, 1.8 mM KH_2PO_4, pH 7.4) and centrifuged at 1000xg for 10 min. The supernatant was discarded and the pellet was resuspended in ice-cold lysis buffer (50mM HEPES pH 8.0, 0.1mM EDTA, 3mM $MgCl_2$, 10 mM β-Mercaptoethanol and 10 μM GDP). Cells were lysed using a Nitrogen cavitation chamber (500psi, 15 min). The lysate was centrifuged at 750xg (10 min, 4 °C) to remove intact cells and nuclei. The supernatant (containing the crude membrane fraction) was centrifuged at 100,000xg for 30 min. The membrane pellet was then resuspended in wash buffer (50 mM Hepes, 3 mM $MgCl_2$, 50 mM NaCl, 10 mM β-mercaptoethanol, 10 μM GDP and protease inhibitors as for the lysis buffer, pH 8.0) using a large Dounce homogeniser. The membranes were centrifuged at 100,000xg for 30 min before resuspension in a small volume of wash buffer to maintain total protein concentration of ≥ 5 mg/mL. Protein concentration was then determined by the Bradford protein assay (Bradford, 1976) and adjusted to 5mg/mL. Sodium cholate was added to a final concentration of 1% w/v from a 20% w/v stock. Membranes were extracted with detergent by stirring on ice for one hour. The detergent/membrane suspension was then centrifuged (100,000xg, 40 min) and the supernatant containing soluble proteins collected.

The soluble fraction was diluted five fold with buffer A (20 mM Hepes, 10 mM NaCl, 1 mM $MgCl_2$, 10 mM β-mercaptoethanol, 0.5% (w/v) polyoxyethylene-10-lauryl ether, and 10 μM GDP, pH 8.0) and then loaded onto an equilibrated column consisting of nickel–nitrilotriacetic acid (Ni–NTA) agarose beads (2mL, 50% suspension, Qiagen) to allow selective binding of histidine-tagged proteins. The column was washed with 50 mL of buffer A containing 5 mM imidazole and 300 mM NaCl to remove proteins not specifically bound to the column via Ni^{2+}–histidine interaction. One column volume (1mL) of buffer E (20mM NaHEPES pH8.0, 50mM NaCl, 50mM $MgCl_2$, 5mM imidazole, 10mM β-mercaptoethanol, 10μM GDP, 1% w/v sodium cholate) with additional Aluminium fluoride (10mM sodium fluoride, 30μM Aluminium chloride) was passed through the column and the column placed at room temperature for 15 minutes to allow interaction of Aluminium fluoride with the $His6_N G\alpha_{i1}/\beta_1\gamma_2$ trimer. Aluminium fluoride is a GTP analogue and causes dissociation of the βγ dimer from Gα. Fractions (5 to 7 void volumes) were eluted using buffer E plus Aluminium fluoride. Since Aluminium fluoride dissociates the G-proteins at this time the non-Histidine tagged protein ($\beta_1\gamma_2$) is collected. The Histidine tagged subunit, $His6_N G\alpha_{i1}$, was then eluted using buffer E (no Aluminium fluoride) with added 150mM imidazole and 5 to 7 void volume fractions were collected. Fractions were analysed by SDS-PAGE with Coomassie staining. Fractions containing $His6_N G\alpha_{i1}$ were combined, as were fractions containing $\beta_1\gamma_2$, to produce one fraction for $His6_N G\alpha_{i1}$ and one for $\beta_1\gamma_2$. Pooled $His6_N G\alpha_{i1}$ or $\beta_1\gamma_2$ was injected into a dialysis cassette (Slide-A-Lyzer, Pierce) with a molecular weight cut-off of 3.5kDa. G-proteins were dialysed against 200mL of buffer F (20mM NaHEPES pH8.0, 3mM $MgCl_2$, 10mM NaCl, 0.1% w/v sodium cholate, 10mM β-mercaptoethanol and 1μM GDP) to remove imidazole and Aluminium fluoride. Buffer was changed every 1 – 2 hours to a total of ~600mL before overnight dialysis against 300mL of buffer F and another 2 changes the following morning. G-proteins were analysed again by Coomassie stained SDS-PAGE and protein concentration determined using either gel densitometry or the Bradford protein assay. G-protein aliquots were snap frozen in liquid nitrogen and stored at -80°C.

$G\alpha_q$ and $G\alpha_o$, which were used in experiments with the $His10_C H_1 R$, were purified by Dr Olgatina Bucco (AusBiotech, formerly CSIRO). The $G\alpha_{q/o}$ proteins were purified by interaction with a Histidine tagged βγ complex (associated with a Nickel IMAC resin).

3.3.4. The [^{35}S]-GTPγS binding assay

7TM receptor/G-protein interaction was measured using a modification of the [^{35}S]GTPγS binding technique (Windh and Manning, 2002). All concentrations given are the final assay concentrations. A reconstitution mix consisting of 7TMR containing membranes (0.1 mg/mL), GDP (5 μM), AMP-PNP (10 μM), $His6_NG\alpha_{i1}$, or other Gα subunit as stated, (20nM) and βγ (20 nM), and [^{35}S]-GTPγS (0.2 nM) was prepared in TMND buffer (50 mM Tris, pH 8.0, 100 mM NaCl, 1 mM $MgCl_2$, and 1 mM DTT) on ice. The assays were prepared in a 96 v-well plate (Axygen) to a final volume of 75μL. Reactions were initiated by addition of either buffer (basal), acetylcholine (10 μM) for M_2R containing membranes or histamine (10μM) for $His10_CH_1R$ containing membranes. Non receptor induced [^{35}S]-GTPγS binding was determined in the presence of atropine (100 μM) for the muscarinic receptors or triprolidine (100μM) for the histamine receptor. Assay plates were incubated at 27 °C with shaking (500rpm) on a Xtron heated plate shaker (Xtron) for 90 minutes. 25μL of the assay was transferred to a MultiScreen^{TM} 96 well glass fibre filter plate (Millipore) for rapid filtration using a Multiscreen^{TM} Separation System (Millipore). Each well was washed with 5 x 200μL of TMN buffer. The filtration plate was fitted to the white plastic base and 50μL of Microscint scintillant (Perkin Elmer) was added to each well. The plate was covered with a translucent plastic sheet and [^{35}S] presence determined by liquid scintillation counting in a Top Count Microplate Scintillation Counter (Perkin Elmer Life Sciences) with 1 minute counts per well.

3.3.5. Data Analysis

Graphs were produced using Prism4 (GraphPad Software).

3.3.6. Large scale expression of the $His6_CM_2R$ and $His10_CH_1R$

Whilst for preliminary M_2R work, cells were cultured on the small scale (as described in chapter 2), for final purification experiments using either M_2R or H_1R, large scale cultures were produced. Large scale (~5L) *Sf*9 cultures of the Histidine tagged muscarinic and histamine receptors were grown and infected at the fermentation facilities of CSIRO, Molecular and Health Technologies, Parkville, by Dr Louis Lu and Ms Tram Phan. Cells were grown using serum free media (Sf900 II, Invitrogen) in a Celligen Plus Bioreactor. Cells were collected by centrifugation, immediately frozen in liquid nitrogen and stored at -80^{o}C for future use. In one experiment freezing was shown to have little effect on the receptor, as determined by radioligand binding.

3.3.7. SDS-PAGE

Experiments in this chapter were performed in two laboratories, there were slight variations between the two laboratories in the protocols used for SDS-PAGE.

Criterion pre-cast gels for SDS-PAGE

Samples were diluted 1:1 with 2x reducing sample buffer (BioRad) and heated at 100^{o}C for 3 minutes. Diluted sample (20µL, per well) was loaded onto a 15% Tris-HCl gel (Criterion, BioRad) and run at 150V for approximately 20 minutes and then 200V until the dye front neared the end of the separating gel. Either Kaleidoscope pre-stained or Kaleidoscope Precision Plus pre-stained (BioRad) standards were used.

NuSep gels for SDS-PAGE

The quality of results obtained with NuSep gels was substantially lower than that observed with BioRad gels (e.g. compare Figures 1, 13 and 26 to Figures 14, 15 and 17). Samples run on NuSep gels, including the marker, often appeared smeared on staining, there was also a tendency of samples to warp during electrophoresis and background staining of the silver appeared higher. A slight improvement was obtained by using NuSep prepared sample buffer.

For NuSep gels, samples were prepared in 1x reducing buffer (5x stock, 0.2M Tris pH6.8, 25% w/v glycerol, 12.5% v/v β-mercaptoethanol, 12.5%w/v bromophenol blue, 5%v/v SDS). Later in the study, samples were prepared by combination of sample, NuSep sample buffer (which is non-reducing) and 5x reducing buffer (as just described) at a ratio of 1:0.9:0.1. Samples were heat-treated at 96^{o}C for 5 minutes and loaded (20µL per well) into 4-20% Tris-HCl precast gels (NuSep). Benchmark^{TM} protein ladders (Invitrogen) were used. Gels were run at 175V/150mA for 45 minutes. SDS-PAGEs were stained using silver staining.

Coomassie Staining

Gels were stained in Bio-Safe Coomassie stain (BioRad) for 1 hour at room temperature with rocking and then washed with several changes of mQH_2O.

Silver Staining

All steps were carried out at room temperature with gentle rocking. Gels were incubated in fixer (50% v/v methanol and 10% v/v acetic acid) for 30 minutes. Fixer was gradually removed by soaking the gel in methanol (5% v/v) and acetic acid (7% v/v) for 30 minutes and then washing with several changes of mQH_2O, followed by overnight washing in mQH_2O. The gel was sensitised by soaking in dithiothreitol (DTT, 5µg/mL) for 30 minutes. DTT was removed and the gel immediately placed in silver stain ($AgNO_3$, 0.1% w/v) for 30 minutes. The gel was washed rapidly in mQH_2O and then twice with developer (3% w/v Na_2CO_3, 0.05% v/v formaldehyde) before soaking in developer until the desired level of staining was obtained. Development was stopped by placing the gel in acetic acid (5% v/v) for 10-20 minutes before washing with mQH_2O. Gels were scanned to produce a digital image and then discarded.

3.3.8. Western Blot

For Western blot analysis proteins were transferred (110V, 1 hour) from SDS-PAGE gel onto a nitrocellulose membrane (Biorad). All proceeding steps were performed at room temperature and with gently rocking.

Colorometric detection of the $His6_C M_2R$

The nitrocellulose membrane was blocked in 3% BSA (20mL, in PBS) for 1 hour. Rabbit anti-M_2R antibody (2µL) was added directly to the blocking solution and incubated with the membrane overnight. The following morning the membrane was washed in TBST (20mM Tris, 500mM NaCl, pH7.5, 0.1% Tween-20 v/v) for 3 x 5 minutes, and then placed in alkaline phosphatase (AP) conjugated anti-Rabbit (1:20,000, in PBS containing 1% w/v BSA) for 1 hour. The membrane was washed in TBST (3 x 5 minutes) and then TMN pH9.5 (2 x 5 minutes), before being placed again in TMN pH9.5 (20mL). Nitro blue tetrazolium (66µL, 10mg/mL stock) and 5-bromo-4-chloro-3indolyl phosphate (660µL, 50mg/mL stock) were added. After sufficient colour development the membrane was washed under running water for 2 minutes to stop development.

Chemiluminescent detection of $His6_C M_2R$ and $His10_C H_1R$.

All antibody dilutions were prepared in TBST.

The membrane was blocked in 3% BSA in TBS (20mM Tris, 500mM NaCl, pH7.5) overnight. This was followed by washing for 2 x 10 minutes in TBST and then incubation in either mouse anti-polyHistidine (1:5,000), rabbit anti-M_2R (1:6,000, Abcam) or rabbit

anti-H_1R for 2 hours. The membrane was washed for 3 x 10 minutes in TBST before being incubated with either HRP anti-mouse (1:15,000, ImmunStar, BioRad) or HRP anti-Rabbit (1:15,000, ImmunStar, BioRad) depending on the primary antibody, for 1 hour. The membrane was washed again for 3 x 10 minutes in TBST. The membrane was developed using the ECL plus Western Blot detection kit (Amersham) according to manufacturers instructions. Chemiluminescence was detected by BioMax photographic film (Kodak). The film was soaked in GBX developer (Kodak) for 1 minute, washed under running water (30 seconds), soaked in GBX fixer (Kodak) and then washed under running water for 2 minutes before overnight drying at room temperature.

3.3.9. Solubilisation of $His6_CM_2R$ containing *Sf*9 membranes

All steps were performed on ice or at 4°C.

Infected *Sf*9 cells (1.25L) containing the $His6_CM_2R$ (as determined by [^{3}H]-scopolamine binding, chapter 2) were resuspended in 125mL of lysis buffer (50mM NaHEPES pH8.0, 0.1mM EDTA pH8.0, 3mM $MgCl_2$, 10mM β-mercaptoethanol and the protease inhibitors: 200µg/mL PMSF, 300µg/mL benzamidine, 250µg/mL bacitracin, 300µg/mL soya bean trypsin inhibitor). Resuspended cells were subjected to Nitrogen cavitation (500psi, 15 minutes). Cavitated cells were centrifuged (750xg, 10 minutes) to pellet unbroken cells and nuclei and the supernatant was re-centrifuged (100,000xg, 30 minutes) to collect the crude *Sf*9 membranes. The membrane pellets were resuspended in ~ 100mL of 'muscarinic solubilisation buffer' (20mM Trizma® base, 150mM NaCl, 5% w/v glycerol, protease inhibitors as above and 20µM of the muscarinic receptor inverse agonist atropine, pH7.4) to a final protein concentration of 3mg/mL as determined by the Bradford protein assay. The membrane suspension was split into 3 x 30mL aliquots and 10mM (final concentration) of DDM, CHAPS or (sodium) cholate added to each aliquot. Detergents were added from 90mM stocks making the final protein concentration at the solubilisation step ~2.7mg/mL. Membrane/detergent suspensions were rotated at 4°C for 2 hours and then centrifuged (100,000xg, 60 minutes, 4°C). A 1mL sample of the soluble supernatant was kept for analysis, the remainder of each soluble fraction (~ 25mL) was mixed with 1mL of solubilisation buffer equilibrated HisLink resin (50% suspension, Promega). After overnight rotation at 4°C, a column was prepared of the soluble-protein/resin suspension and the flow through was loaded twice more on the column. The column was washed with solubilisation buffer (40mL) containing 5mM imidazole and the appropriate detergent and then eluted with five column volumes (500µL) of solubilisation buffer containing 500mM

imidazole. For columns that become blocked during washing a 10mL syringe, which fitted tightly to the top of the column, was used to apply the pressure required for flow through. Samples and fractions were snap frozen in liquid nitrogen and stored at -80^{o}C.

For solubilisation of large scale cultures with DDM volumes were scaled accordingly.

3.3.10. Solubilisation of His10$_C$H$_1$R

7M urea treated membranes (from 5L of cells, see chapter 2) were homogenised with 125mL of 'histamine solubilisation buffer' (20mM Bis-Tris propane, 1M NaCl, 1mM Histidine, 10% (w/v) glycerol, pH7.6, 5mM β-mercaptoethanol and protease inhibitors as above). The H_1R ligand triprolidine was added to a final concentration of 20μM and the suspension rocked gently at room temperature for 15 minutes. This concentration of ligand was maintained for the remainder of the purification protocol. Finely dispersed n-Octyl-β-D-glucopyranoside (0.730g, nOG, Calbiochem) was gradually added to the suspension to a final concentration of 20mM. The suspension was rotated at 4^{o}C for 2 hours and then centrifuged at 80,000xg for 15 minutes. The pellet was discarded and the slightly yellow and turbid supernatant was added to 10mL of Profinity^{TM} IMAC resin (50% suspension, BioRad) which had been equilibrated with solubilisation buffer. The resin/protein suspension was rotated at 4^{o}C overnight.

3.3.11. Immobilised Metal Affinity Chromatography (IMAC)

In early work described in this study, the His6$_C$M$_2$R IMAC was performed in the absence of a HPLC workstation. In later work (all large scale purifications) columns were connected to a BioLogic workstation (BioRad) allowing for control of column flow using the pump. Flow rate was set to maintain a constant but slow elution rate, generally a rate of 1mL/min was used. For large scale His6$_C$M$_2$R purification, the IMAC column was washed with 'muscarinic solubilisation buffer' containing 5mM imidazole and then eluted with 10, 20, 100, 200 and 500mM imidazole. This was later standardised to a two step process of 5mM imidazole washing followed by 20mM imidazole elution of the receptor. For large scale His10$_C$H$_1$R purification, the IMAC column was washed with 'histamine solubilisation buffer' 10mM imidazole and eluted with a gradient of 20, 50, 100, 200, 500 and 750mM imidazole. This was later standardised to a two step process of washing with 50mM imidazole and eluting with 200mM imidazole.

Fractions containing either $His6_CM_2R$ or $His10_CH_1R$, as shown by SDS-PAGE with protein staining and/or Western blot, were pooled and concentrated using a centrifugal filter device with a 10kDa cut off (Amicon® Ultra, Millipore). These devices were always re-used (with the same receptor) to minimise loss of protein in the filter. Between uses they were stored in 30% (v/v) ethanol.

3.3.12. HPLC Sepharose-75 Gel Filtration.

Concentrated receptor containing IMAC fractions were further purified using high performance liquid chromatography (HPLC) on a Superdex-75 10/300 (Pharmacia Biotech/ GE Healthcare) gel filtration column (GF-HPLC). HPLC was carried out using a BioLogic HR Workstation and a Model 2128 Fraction Collector (both from BioRad). In addition to being a purification step, GF-HPLC allowed for buffer exchange of the protein into a more suitable buffer for crystallisation trials. This was particularly important for the $His10_CH_1R$ due to the high salt concentration used in the solubilisation buffer. For the $His10_CH_1R$, GF-HPLC was carried out in 'histamine gel filtration buffer' (20mM Bis-Tris propane, 150mM NaCl, 10% w/v glycerol, 5mM β-mercaptoethanol, 20µM triprolidine, 20mM nOG, pH7.6). For the $His6_CM_2R$ 'muscarinic gel filtration buffer' (20mM Trizma® base, 150mM NaCl, 5% w/v glycerol, 20µM atropine, 5mM β-mercaptoethanol, 10mM DDM, pH7.4) was used. The column and lines were first washed with $sMQH_2O$ (0.2mL/min, 40 minutes) to remove storage ethanol and then equilibrated with the appropriate gel filtration buffer (0.2mL/min, 60 minutes). 500µL of IMAC purified receptor was injected in each GF-HPLC column. The flow rate during purification was 0.2mL/min and 500µL fractions were collected after 5mL of flowthrough was discarded (void volume of the column is 6mL). An A_{280} and conductivity profile was prepared for each GF-HPLC run.

3.3.13. Soluble protein binding assay

The assay protocol for soluble protein was developed based on published protocols which have been used with a number of solubilised membrane proteins (Brandt, et al., 2001; Schonwetter, et al., 1989; Sigel, et al., 1983). Assays were prepared as described in section 2.3.5 (chapter 2). At the termination of the assay an equal volume of PEG 8-10K (30% w/v in TMN) was added to the assay. Assays were placed on ice for 20 minutes before being filtered over glass fibre filters (GF/B, Whatman) and washed with 3 x 3mL of ice cold PEG 8-10K (10% w/v in TMN). This process is referred to as PEG filtration.

For H_1R samples containing triprolidine (any samples after addition of nOG), dialysis was performed prior to [^{3}H]-pyrilamine binding. Up to 100µL of the sample was added to a Slide-A-Lyzer mini dialysis unit with a molecular weight cut-off of 10kDa (Pierce). The dialysis tube was floated in 100mL of sample buffer, minus triprolidine. Buffer was changed once an hour for 4 hours with the sample being mixed after each buffer change. The buffer was changed 3 times (such that a total of 400mL was used for each sample). Samples were then assayed as described above.

3.4. Results and Discussion

3.4.1. Purification of the G-proteins

Detailed methods have been published for the purification of the membrane associated G-protein subunits (Hayashi and Haga, 1996; Kozasa, 2004; Lim and Neubig, 2001). Since the proteins are peripheral membrane proteins and not integral membrane proteins, they were substantially easier to purify than the 7TMRs and published purification protocols were simpler to successfully reproduce. In this study, *Sf*9 cells were co-infected with hexa-Histidine tagged $G\alpha_{i1}$ ($His6_NG\alpha_{i1}$), β_1 and γ_2 baculoviruses. G-proteins were extracted in the presence of GDP allowing the protein trimer to be immobilised on Nickel resin through the interaction of $His6_NG\alpha_{i1}$ with the resin. Addition of Aluminium fluoride (AlF_4^-) removed a protein of ~ 37kDa as shown by Coomassie stained SDS-PAGE (Figure 1, lanes 3 and 4). This is the expected molecular weight of β_1, $\gamma 2$ was not generally visualised on SDS-PAGE due to its low molecular weight (8kDa).

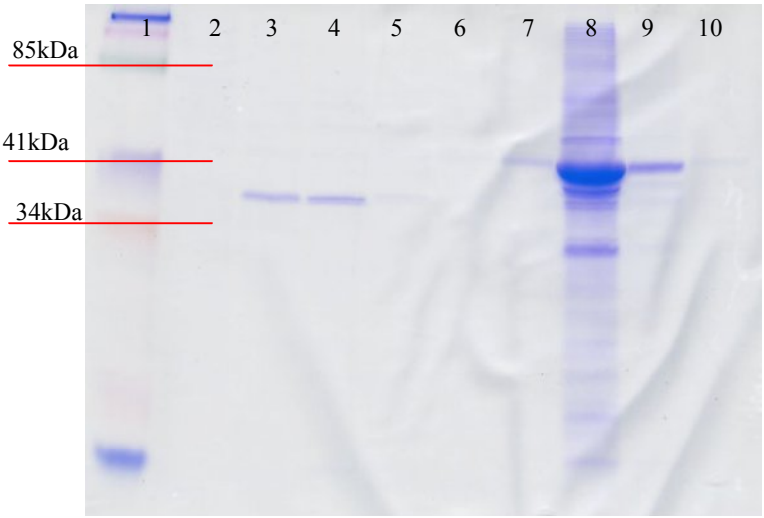

Figure 1. Coomassie stained SDS-PAGE (Criterion, BioRad) of IMAC purified G-proteins. Lane Descriptions: 1 – Kaleidoscope Molecular Weight Marker (5µL, BioRad); 2 – 6 AlF_4^- eluted fractions 1 – 5; 7 – 10 imidazole eluted fractions 1 – 4. 20µL of sample was loaded per well.

Imidazole elution of the column eluted a protein of ~41kDa, which is the expected molecular weight for $His6_NG\alpha_{i1}$ (Figure 1, lanes 7 – 9). The imidazole eluted His-tagged protein was not homogeneous (purity was estimated 70 – 90%) but the purity was of sufficient standard for the reconstitution assays used in this study. Western blot analysis of the G-protein purification was not used in this study, but was later used by a fellow

laboratory member, Ms Tamara Cooper (CSIRO MHT), to confirm the presence of the G-proteins.

3.4.2. Characterisation and Purification of the $His10_CH_1R$

Characterisation (G-protein coupling) and purification experiments performed on the $His10_CH_1R$ are summarised in Figure 2. Each of these steps is discussed in the proceeding sections. Although purification of the $His10_CH_1R$ has been reported (Ratnala, et al., 2004), the purification method reported here is different to that published.

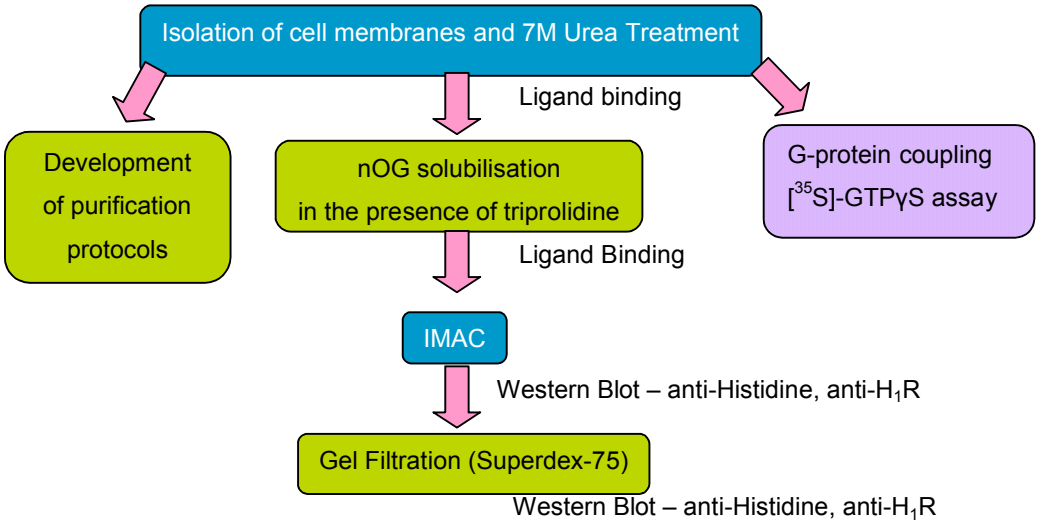

Figure 2. Flow diagram of the steps used for purification of the $His10_CH_1R$

3.4.3. Reconstitution of the H_1R with purified G-protein subunits

Prior to reconstitution with G-proteins, urea-treated membranes containing the $His10_CH_1R$ were prepared since urea-treatment removes endogenous G-proteins. Since this step also acts as a receptor purification step, it will be discussed later in this chapter (refer to section 3.4.6). The $G\alpha_q$ and $G\alpha_o$ protein used in this study were purified by Dr Olgatina Bucco (AusBiotech, formerly CSIRO).

In the cell the H_1 histamine receptor signals through $G\alpha_q$ (Bakker, et al., 2002). *Sf*9 membranes containing the $His10_CH_1R$ histamine receptor (see chapter 2) could be functionally reconstituted with purified $G\alpha_q$ and $\beta_1\gamma_2$ as demonstrated by a 1.8 fold increase in $[^{35}S]$-GTPγS binding in the presence of the receptor agonist histamine (Figure 3B). Addition of both histamine and pyrilamine (a receptor antagonist/inverse agonist)

returned [^{35}S]-GTPγS binding to near basal levels and demonstrated that the increase in [^{35}S]-GTPγS binding was receptor specific (Figure 3C).

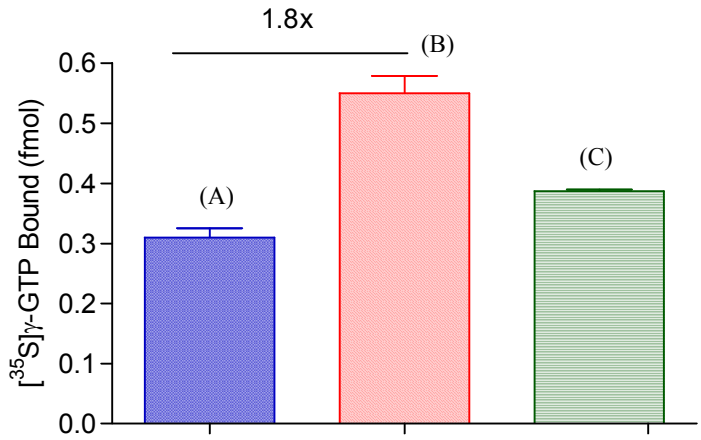

Figure 3. Reconstitution of *Sf*9 membranes containing His10$_C$H$_1$R with purified Gα$_q$ and β$_1$γ$_2$. Bars represents [^{35}S]-GTPγS binding to reconstituted proteins in (A) the absence of receptor ligand; (B) the presence of the receptor agonist histamine; (C) in the presence of histamine and the receptor inverse agonist pyrilamine. Data represents the mean ± S.E.M., n = 3.

His10$_C$H$_1$R could also be functionally reconstituted with Gα$_o$ and Gα$_{i1}$ (Figures 4A/B and 5A/B). In the presence of histamine, [^{35}S]-GTPγS binding to the reconstituted proteins increased by 1.5 (Gα$_o$, Figure 4) or 7.5 fold (Gα$_{i1}$, Figure 5) compared to the binding of the radionucleotide in the absence of receptor ligand. [^{35}S]-GTPγS binding returned to near basal levels when both histamine and pyrilamine were included with the reconstituted proteins (Figure 4C and 5C).

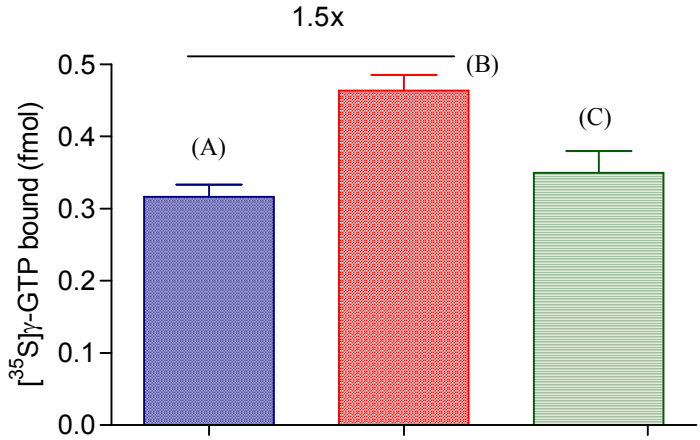

Figure 4. Reconstitution of *Sf*9 membranes containing His10$_C$H$_1$R with purified Gα$_o$ and β$_1$γ$_2$. Bars represents [^{35}S]-GTPγS binding to reconstituted proteins in (A) the absence of receptor ligand; (B) the presence of the receptor agonist histamine; (C) in the presence of histamine and the receptor inverse agonist pyrilamine. Data represents the mean ± S.E.M., n = 3.

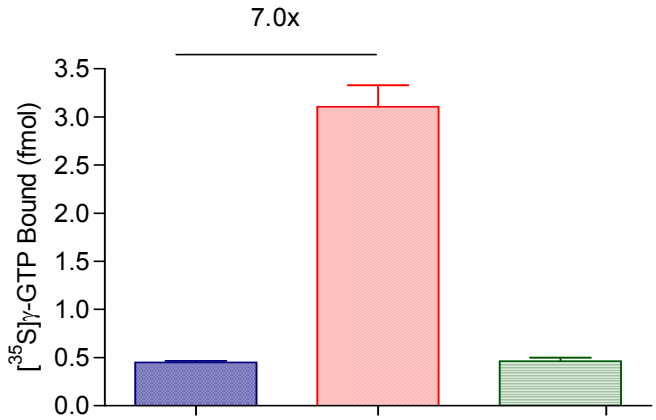

Figure 5. Reconstitution of *Sf*9 membranes containing $His10_CH_1R$ with purified $His6_NG\alpha_{i1}$and $\beta_1\gamma_2$. Bars represents [^{35}S]-GTPγS binding to reconstituted proteins in (A) the absence of receptor ligand; (B) the presence of the receptor agonist histamine; (C) in the presence of histamine and the receptor inverse agonist pyrilamine. Data represents the mean ± S.E.M., n = 3.

Interaction of the $His10_CH_1R$ with G-proteins produced variable quantities of [^{35}S]-GTPγS binding (in particular, compare Figures 3 and 4 to Figure 5). Measurement of [^{35}S]-GTPγS binding to purified Gα proteins in the absence of receptor gave a partial explanation for the observation of variable [^{35}S]-GTPγS binding in the receptor/G-protein reconstituted system (Figure 6). In this experiment the G-protein concentration was increased to 50nM (from 20nM which was used in the reconstitution assays) to enable detectable quantities of [^{35}S]-GTPγS to become bound to the G-protein subunit, particularly for the case of $G\alpha_q$ and $G\alpha_o$. Hence, the total [^{35}S]-GTPγS binding appears higher than results presented in Figures 3, 4 and 5. In the absence of receptor, [^{35}S]-GTPγS binding to $His6_NG\alpha_{i1}$ was 5.0 fold higher than that to $G\alpha_q$ and 3.6 fold higher than [^{35}S]-GTPγS binding to $G\alpha_o$. This suggests that it is, at least in part, the Gα proteins themselves that lead to the observed differences in the fold increase of [^{35}S]-GTPγS binding in the $His10_CH_1R$/G-protein reconstitution assays. For example $G\alpha_i$ can more readily exchange GDP for GTP than can $G\alpha_q$. Alternatively, the purified $His6_NG\alpha_{i1}$ preparation may simply have a higher percentage of functional protein than the $G\alpha_o$ or $G\alpha_q$ preparations.

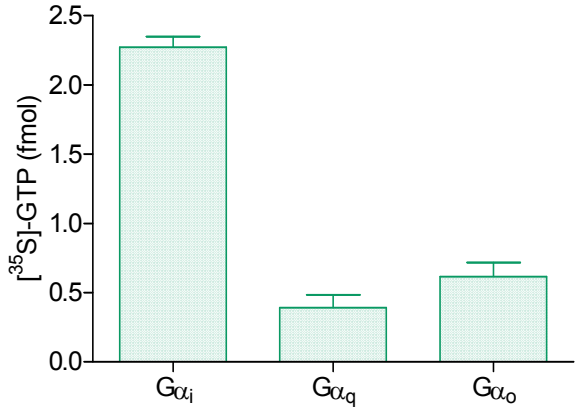

Figure 6. [^{35}S]-GTPγS binding to Gα proteins in the absence of receptor. 50nM of G-protein subunit was combined with 0.2nM [^{35}S]-GTPγS and incubated at 27°C for 90 minutes with shaking. Data represents the mean ± S.E.M., n = 3.

However, as well as being higher than [^{35}S]-GTPγS binding to $G\alpha_o$ or $G\alpha_q$, the total amount of [^{35}S]-GTPγS bound to histamine activated $His6_N G\alpha_{i1}$ is higher than that bound to $His6_N G\alpha_{i1}$ which was activated by M_2R (results presented in section 3.4.12). This suggests that receptor interaction with the G-protein also plays some part in the amount of [^{35}S]-GTPγS bound to the different Gα subunits.

In one report H_1R expressed in HL-60 monocytes was shown to be involved in pertussis-toxin sensitive increases in calcium influx, suggesting the involvement of $G\alpha_i$ proteins (Seifert, et al., 1994). Wang and Kotlikoff, (2000) used antibodies directed to $G\alpha_i$ to show involvement of the G-protein in H_1R activation of non-selective cation channels. Interestingly, activation of these channels also required interaction of the H_1R with $G\alpha_q$ proteins and subsequent intracellular calcium release (Wang and Kotlikoff, 2000). However, the majority of reports show a role for H_1R only in pertussis-toxin insensitive signalling (Fitzsimons, et al., 2004; Leopoldt, et al., 1997; Maruko, et al., 2005). For example, studies with the H_1R expressed in CHO cells have reported involvement of the receptor in increases in cellular cAMP, calcium and inositol phosphate concentrations, all of which were pertussis-toxin insensitive (Moguilevsky, et al., 1994). Furthermore, an interaction of H_1Rs with $G\alpha_o$ proteins has not previously been reported. The relevance of the *in vitro* results presented here to the *in vivo* interactions of the H_1R remains to be determined but they may play a role in the explanation of histamine receptor physiological functions as future studies reveal new roles for the receptor.

Interaction of the $His10_CH_1R$ with the G-proteins in combination with work presented in chapter 2 confirmed the presence and functionality of the H_1R in the *Sf*9 membranes. Furthermore, the high expression levels of the receptor (chapter 2) made it a useful receptor on which to develop protocols for purification of 7TMRs. Development of protocols for detection of the receptor throughout the purification was particularly difficult since the purification protocol itself was being developed i.e. there was no positive control to enable definitive analysis of the effectiveness of a detection/purification protocol (such as Western blot or assays for detergent solubilised proteins).

3.4.4. Optimisation of chemiluminescent Western blot of 7TMRs

Preliminary work with the $His10_CH_1R$ used Western blot for detection of the receptor since this method was initially more straight-forward than developing a radioligand binding assay amenable to the various stages of receptor purification. For this purpose protocols for Westerns using chemiluminescent detection were developed, as opposed to using colormetric detection as was standard in the laboratory at the time. Colormetric detection is around 10x less sensitive than chemiluminescent detection (information from BioRad "Guide to Blot Detection"). Furthermore, chemiluminescent films are more amenable to digital scanning since faint colour signals may be difficult to visualise when the blot is scanned and printed. Use of horse radish peroxidise (HRP) conjugated antibodies and chemiluminescence detection increases sensitivity to around 100x over that which can be achieved with colourimetric alkaline phosphatase conjugated secondary antibodies, and allows for detection of protein quantities as low as 1pg. The ability to detect such small quantity of protein was a prerequisite in this study since receptor quantities would be minimal and therefore sensitive detection methods require less protein to be used. Considerable effort was put into finding the optimal conditions for Western blot of the receptor samples – which ranged from membranous impure samples to pure detergent solubilised receptor. Transfer conditions (from gel to nitrocellulose) were fairly standard at 110V for one hour. Initially 0.1% (w/v) SDS was incorporated in the transfer buffer but this was later deemed as unnecessary. The cost of bovine serum albumin (BSA) made skim milk powder a desirable alternative for blocking of the nitrocellulose membrane, but for the antibodies used in this study at least, BSA proved a more effective blocking agent (Figure 7). Western blot conditions for the anti-polyHistidine antibody were determined by experimenting with purified $His6_N G\alpha_{i1}$. Serial dilutions of $His6_N G\alpha_{i1}$ (1µL) and membranes prepared from M_2R baculovirus infected *Sf*9 cells (1µL) were spotted directly

onto a nitrocellulose membrane. Membranes were blocked in either 5% skim milk powder (Figure 7A) or 3% BSA (Figure 7B and 7C). Following washing, the membranes were incubated with either a 1:1000 dilution (Figure 7A and 7B) or a 1:5000 dilution (Figure 7C) of anti-polyHistidine antibody. This was followed by washing of the membrane and then incubation in either a 1:5000 dilution (Figure 7A and 7B) or 1:20000 dilution (Figure 7C) of HRP-anti-Mouse. Under these conditions, skim milk powder was not as effective as BSA in blocking the membrane from non-specific binding (compare Figure 7A and 7B).

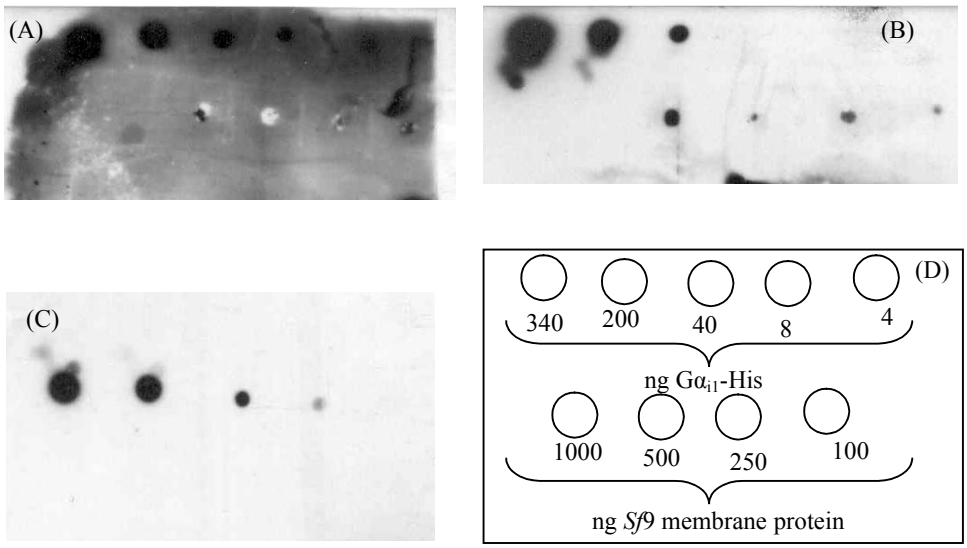

Figure 7. Anti-Histidine dot blot using purified $G\alpha_{i1}$-His and *Sf*) membranes. (A) Membrane blocked with 5% skim milk powder, 1:1000 anti-Histidine, 1:5000 HRP-anti-Mouse. (B) Membrane blocked with 3% BSA, 1:1000 anti-Histidine, 1:5000 HRP-anti-Mouse. (C) Membrane blocked with 3% BSA, 1:5000 anti-Histidine, 1:20000 anti-Mouse. (D) schematic of dot blot membranes showing nano-gram quantities of protein applied to the membrane.

The results of this experiment meant that BSA was used as the blocking agent for all subsequent blots with overnight blocking always giving the best results. Reduction in non-specific anti-polyHistidine antibody binding was optimised by finding Western conditions which allowed detection of the purified $His6_NG\alpha_{i1}$ but did not show binding of the antibodies to *Sf*9 membranes which contained M_2R, *Sf*9 cell and baculoviral proteins. Antibody concentrations of 1:5000 for the primary antibody and 1:20000 for the secondary antibody fulfilled this requirement (Figure 7B and 7C). Titration of the $His6_NG\alpha_{i1}$ gave a sensitivity level for the antibodies (under the conditions described) of between 4 and 8ng of His-tagged Gα (Figure 7C and 7D).

Since there was no purified positive control for the anti-H_1R antibody, the optimal antibody concentration was determined by testing a wide variety of antibody concentrations and H_1R samples and observing Western blots with minimal background. Ultimately the conditions developed for the anti-polyHistidine worked with the anti-H_1R (Figure 8B) and the anti-M_2R when these primary antibodies were used at a 1:6000 dilution.

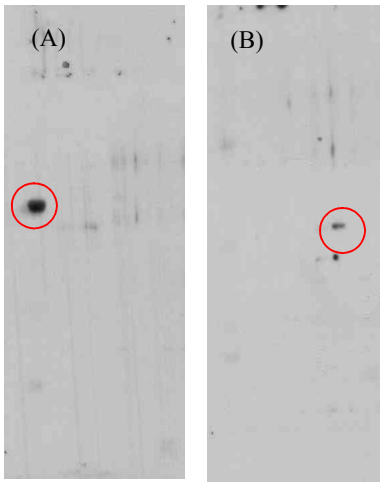

Figure 8. Development of the Western blot for the $His10_CH_1R$. Anti-H_1R was used at a concentration of 1:6,000 in combination with conditions developed for the anti-polyHistidine antibody (Figure 16). A protein of between 50 and 75kDa in an IMAC purified sampled was detected using both anti-polyHistidine (A) and anti-H_1R antibodies (B) and is circled.

3.4.5. Development of an assay for soluble $His10_CH_1R$

To this point, the $His10_CH_1R$ was described as functional by a combination of the [^{3}H]-ligand binding assay (chapter 2) and the ability of the receptor to functionally interact with the G-proteins (refer to section 3.4.3). For purification of the $His10_CH_1R$, functionality of the receptor is defined only by the ability of the receptor to bind [^{3}H]-pyrilamine. Though this is a common definition during purification of 7TMRs (Grisshammer, et al., 1999; Kobilka, 1995; Ratnala, et al., 2004), ideally future work should examine the interaction of purified $His10_CH_1R$ with the G-proteins.

In chapter 2, detection of functional 7TMRs was achieved by [^{3}H]-ligand binding filtration assays, which is a simple method for detection of the receptors. An initial difficulty encountered when purifying 7TMRs is determining a simple method for detecting soluble functional receptor, since soluble receptor will pass through the filter using the conventional assay. This can be achieved either by adaptation of the normal filtration

assay, or by alternate methods such as scintiplate assays, scintillation proximity assay (SPA) beads, or more complex methods such as surface plasmon resonance (Harding, et al., 2007). Scintiplate or SPA assays use capture of the radioligand bound soluble receptor to a scintillant containing source (plate or bead). [^{3}H] detection then relies on proximity of the receptor bound radiolabel to the scintillant. A scintiplate assay has been reported for use with soluble α_{2B} adrenergic receptor (Sen, et al., 2002). However this technique is lengthy and requires the use of expensive antibodies and therefore was not used. SPA beads require the receptor to be either glycosylated (for use with wheat germ agglutinin SPA beads) or biotinylated (streptavidin beads) or an antibody to be available for functionalisation of the SPA beads. Availability of Nickel presenting SPA beads may have been useful, but these were not found during this study. Filtration of radioligand binding assays over glass fibre filters is a simple method of capturing membrane associated receptor whilst separating bound [^{3}H]-ligand from free and it relies on the large lipid/protein clumps being trapped by the small pore size of the filter. Adaptation of the [^{3}H]-ligand filtration assays must meet the requirement of capturing soluble receptor whilst, at the same time, separating bound radioligand from free. Two methods are commonly reported for modification of the filtration binding assay for specific capture of radioligand bound soluble receptor – polyethylenimine (PEI) treatment of the glass fibre filters prior to their use in assay filtration (Ratnala, et al., 2004; Treherne and Young, 1988), or PEG precipitation of the radioligand binding assay (and theoretically the solubilised protein) followed by washing of the filters with PEG (Brandt, et al., 2001; Harding, et al., 2007; Schonwetter, et al., 1989). In this study, PEG precipitation was used for radioligand binding assays on soluble proteins.

An important lesson learnt from the work of Ratnala, et al., (2004) was the incorporation of a H_1R ligand during, and in all steps following, detergent addition to the membranes. Intuitively the ligand stabilises the structure of the receptor, an important property during removal of the receptor from the natural membrane environment. Ideally a labelled ligand would be incorporated during receptor solubilisation and purification, allowing for simultaneous tracking and stabilisation of the receptor throughout. However this was not deemed as viable in this study due to a desire to contain the use of [^{3}H] and, additionally, due to the high cost involved in incorporating radioligand through out large scale purification. Failing the use of a labelled ligand, incorporation of the ligand throughout the purification is somewhat hinderous since it must be removed prior to detecting receptor

levels using binding of a labelled ligand. In this case, it would be desirable to incorporate a ligand with relatively low affinity for the receptor throughout the purification protocol but of course this decreases the effectiveness of the ligand for its original purpose of receptor stabilisation. In this study the high affinity H_1R antagonist triprolidine was incorporated throughout the purification protocol.

Thus, two problems needed to be overcome to enable detection of the 7TMR throughout the purification – removal of the ligand used for receptor stabilisation during purification and capture of the solubilised [^{3}H]-ligand bound receptor whilst allowing removal of unbound radioligand. The later of these problems was investigated by solubilisation of the $His10_CH_1R$ in the absence of triprolidine, this allowed for some verification of receptor presence and determination of the appropriateness of PEG filtration for capturing soluble receptor (Figure 9).

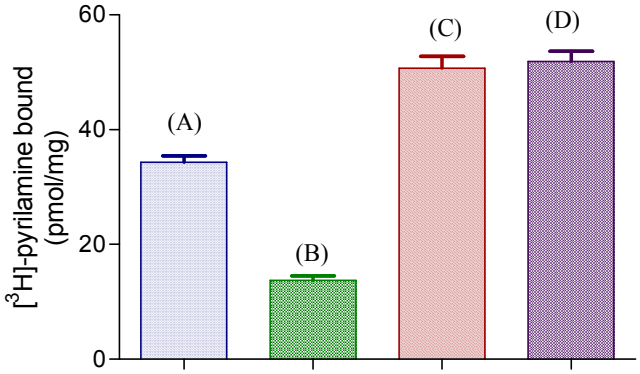

Figure 9. PEG filtration for capture of soluble $His10_CH_1R$. $His10_CH_1R$ *Sf*9 membranes were solubilised in the absence of triprolidine. [^{3}H]-pyrilamine bound was determined at 60nM [^{3}H]-pyrilamine (free). Error bars are for assay duplicates. (A) Soluble fraction, assay filtered with PEG; (B) Soluble fraction, TMN filtration; (C) $His10_CH_1R$ membranes, assay filtered with PEG; (D) $His10_CH_1R$ membranes, assay filtered with TMN. Non-specific binding was ≤ 15%.

PEG precipitation and filtration of membrane associated $His10_CH_1R$ did not change the amount of [^{3}H]-pyrilamine bound compared to normal filtration (compare Figure 9C and 9D). Nor was free radioligand retained during PEG filtration (results not shown). Encouragingly a ~3 fold increase in specific [^{3}H]-pyrilamine binding was observed when PEG filtration was used on detergent soluble proteins extracted from $His10_CH_1R$ containing membranes, as compared to the same assay filtered in the absence of PEG (compare Figure 9A and 9B). This suggests both the presence of the histamine receptor in the soluble fraction and the ability of the PEG filtration method to capture soluble receptor.

Furthermore, at 37pmol/mg of total protein it suggests that approximately 53% of the $His10_CH_1R$ has been solubilised with the caveat that it is difficult to quantify whether all the soluble protein is being captured by PEG precipitation and filtration. An alternative is the use of gel filtration to remove free-radioligand and so avoid the possibility of lost soluble receptor in the assay using the filtration technique. GF-HPLC or other methods on this scale are completely in-practical when working with such small quantities of protein, but it has since been discovered that there are available mini-gel filtration columns which may be useful for performing radioligand binding assays with soluble receptor.[1] These columns will be trialled with purified $His10_CH_1R$ in future work.

The problem of detection of receptor purified with ligand was demonstrated by the experiment presented in Figure 10.

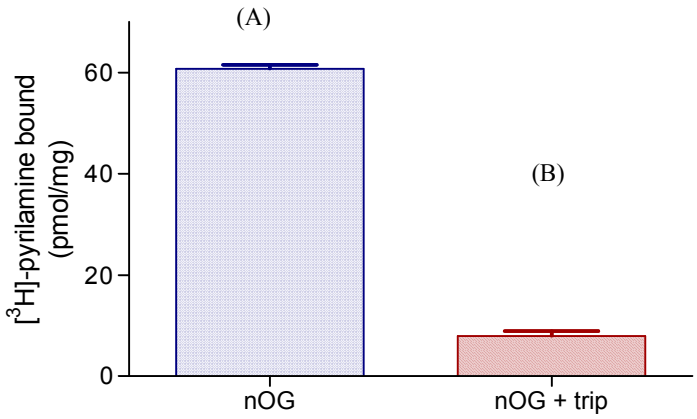

Figure 10. Specific [^{3}H]-pyrilamine binding to $His10_CH_1R$ membranes in the presence of (A) nOG; (B) nOG plus 20µM triprolidine. Error bars represent assay duplicates. 50nM of (free) [^{3}H]-pyrilamine was used.

Detergent (nOG, see section 3.4.7) was added to $His10_CH_1R$ containing membranes (membrane/detergent suspension was not centrifuged). A sample was taken and immediately proceeding this, triprolidine was added to a final concentration of 20µM and another sample taken. Both samples were dialysed against solubilisation buffer which did not contain triprolidine (as described in methods section 3.3.13), and then used in a [^{3}H]-pyrilamine binding assay with PEG filtration. Thus the samples are identical with the exception of the added triprolidine in one sample, yet [^{3}H]-pyrilamine binding decreased by ~8 fold in the sample containing unlabelled ligand. That binding in the triprolidine containing sample was evident suggests either, that some receptors have lost bound

[1] Micro Bio-Spin chromatography columns, available from BioRad, Cat# 732-6204 as at February 2008.

triprolidine in exchange for [^{3}H]-pyrilamine (though the concentration of triprolidine used was saturating), or it may simply represent non-specific binding of the radioligand. Ideally a large molar excess of [^{3}H]-pyrilamine would be used in the assay though this approach is difficult since the purchased stock concentration was approximately 25µM. Despite this limitation, in one experiment 8.2µM (final concentration) of the radioligand was used in a 9 hour incubation with purified His10$_C$H$_1$R, in an attempt to at least partially out compete the bound triprolidine (Figure 11). The PEG filtration method was used to capture the soluble receptor.

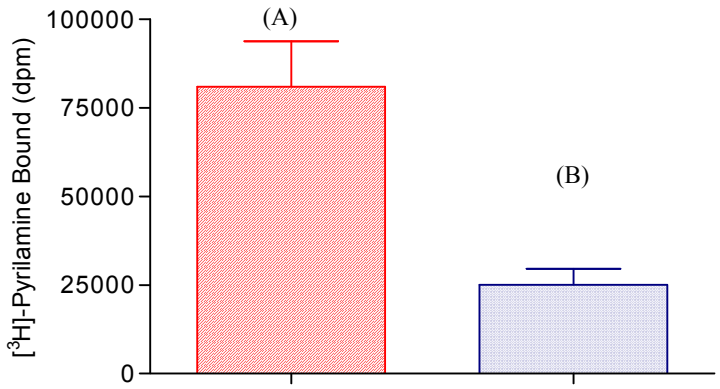

Figure 11. [^{3}H]-pyrilamine binding to purified His10$_C$H$_1$R. (A) Radioligand detected in the presence of His10$_C$H$_1$R (0.5µg) ; (B) radioligand detected in the absence of His10$_C$H$_1$R. [^{3}H]-pyrilamine concentration was 8.2µM (15µL filtered), which corresponded to 8,573,374 dpm in each assay. Bars represent duplicate assays

In this case non-specific radioligand binding is defined as that which is detected in the absence of purified receptor (Figure 11B). At such high radioligand concentration, non-specific association of [^{3}H] with the filter was high, but it appears that at least some receptor has captured [^{3}H]-pyrilamine (Figure 11A).

Whilst the ability to capture soluble receptor was demonstrated, the problem of removing or out competing receptor bound ligand used during purification was not resolved. Preliminary purification experiments for both the muscarinic and histamine receptors carried out in the absence of ligand did not result in receptor detection using Western blot analysis after the IMAC step. This is interesting since Western blot should detect both functional and non-functional receptor (as long as the antibody epitope is present). It confirms the pivotal role the presence of ligand plays during receptor purification.

Whilst the soluble assay was being developed, purification trials with the $His10_CH_1R$ were ongoing with Western blot being used to assess for the presence of the $His10_CH_1R$. As time limitations became an issue, it was decided that incorporation of a high affinity ligand during purification was more important then the ability to detect all functional receptors. It was a conundrum - incorporate high affinity ligand for receptor stabilisation and it is difficult to remove the ligand, or purify without the ligand and produce inactive receptor. So whilst [^{3}H]-pyrilamine binding assays were carried out on the solubilised and final $His10_CH_1R$, it is unlikely a true representation of functional receptor amounts. For these reasons, the focus of H_1R work was the end point – obtaining purified receptor in a manner that would maximize the possibility of retaining functional receptor. The strategy was the incorporation of the inverse agonist triprolidine, low temperature and a rapid protocol. In hindsight it would have been beneficial to screen for receptor ligands which both stabilised the receptor but could also be readily removed. In this regard, tripelennamine may have been useful as described in the work of Ratnala, et al., (2004). A preliminary purification experiment using this ligand did not result in the isolation of $His10_CH_1R$, whilst a duplicate experiment with triprolidine did. Once the purification experiment was successful, there was a reluctance to change the protocol. A useful approach, avoiding the use of expensive and potentially hazardous labelled ligands throughout the purification would be the use of allosteric ligands or other binding partners for the receptor, i.e. compounds which have high affinity to the receptor but do not bind to the (orthosteric) ligand binding site. Allosteric ligands have been well documented for the M_2R (May, et al., 2005) and are likely also available for the H_1R. Alternatively, small receptor targeting peptides may be useful in this regard. CADEN Biosciences (Wisconson, United States) develops high affinity G-protein based peptides to the intracellular loops of 7TMRs. Having ligands to two distinct sites on the receptor would enable one ligand to be incorporated throughout the purification and the other to be labelled and used for detection.

3.4.6. 7M urea treatment of $His10_CH_1R$ membranes

In addition to removing endogenous *Sf*9 cell G-proteins, the 7M urea treatment method used in this study enriches for membrane associated receptor and, as such, was the first step used for purification of the receptor. This is demonstrated by an increase in specific [^{3}H]-pyrilamine binding per mg of total protein (Figure 12).

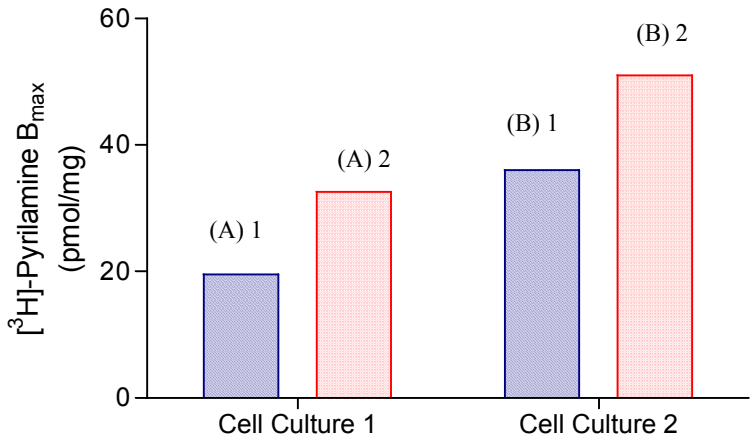

Figure 12. [^{3}H]-pyrilamine binding to *Sf*9 cell lysates and 7M urea treated membranes from 2 His10$_C$H$_1$R cell cultures. (A) 1: [^{3}H]-pyrilamine binding to *Sf*9 cell lysates; 2: [^{3}H]-pyrilamine binding to 7M urea treated membranes. (B) As for (A), assays were performed on a different cell culture of the receptor.

Although 7M urea treatment method is a purification step, there can be substantial losses (up to 40%) of total receptor, as determined by [^{3}H]-pyrilamine binding. Since the cells are at least partially lysed (due to the freezing process), [^{3}H]-pyrilamine binding measurements at this stage would detect all H_1 receptors including intracellular, partially folded or fragmented receptors (which may still be capable of binding ligand (Ratnala, et al., 2004)). Hence the loss of total receptor may represent the loss of receptors that are fragmented and may be more susceptible to removal by 7M urea. The higher starting expression of the His10$_C$H$_1$R allowed for some receptor loss, but with future developments to the purification protocol, it may prove advantageous to remove/modify this step, giving a higher final yield. (This was trialled once in this study but without exceptional success and, due to time limitations, was not examined further).

3.4.7. Solubilisation of the His10$_C$H$_1$R

As opposed to the approach used with the His6$_C$M$_2$R (refer to section 3.4.13), for the His10$_C$H$_1$R very little time was spent on optimisation of the solubilisation step due firstly to the detailed report of (Ratnala, et al., 2004), secondly to early success with n-octyl-β-D-glucopyranoside (nOG), and thirdly, the time limitations of the study. Ratnala, et al., (2004) tested six detergents for their ability to solubilise His10$_C$H$_1$R from *Sf*9 cells and reported 40-50% solubilisation of H_1R using N-dodecyl-β-D-maltoside (DDM), whilst n-nonyl-β-D-glucopyranoside (nG) achieved only 30-35% solubilisation efficiency. Whilst in

this study some preliminary His10$_C$H$_1$R solubilisation experiments were performed with DDM, nOG was initially trialled in a complete purification due to the availability of the detergent from a previous study, and because of its significantly lower cost compared to DDM. Furthermore, nOG has a high CMC (20 – 25mM) allowing for efficient detergent removal by dialysis. Since nOG solubilisation followed by IMAC produced His10$_C$H$_1$R in a preliminary study, this detergent was routinely used for solubilisation. The solubilisation buffer components used in this study were kept similar to those reported in Ratnala, et al., (2004), with the exception that the glycerol concentration was decreased to 10% (w/v) since the reported glycerol concentration (20% w/v) was found to be difficult to work with, particularly in regards to the chromatography steps. Solubilisation time was increased to 2 hours.

3.4.8. Histidine Nickel Affinity Chromatography

The nOG soluble fraction was incubated overnight (at 4^{o}C) with IMAC resin to allow sufficient time for binding of the C terminal deca-Histidine tag to the nickel resin. Washing of the IMAC column with 100mM imidazole eluted 2 proteins of between 50 and 75kDa (Figure 13A). The smaller of the two proteins was detected on anti-polyHistidine (Figure 13B) and anti-H$_1$R (Figure 13C) Western blot.

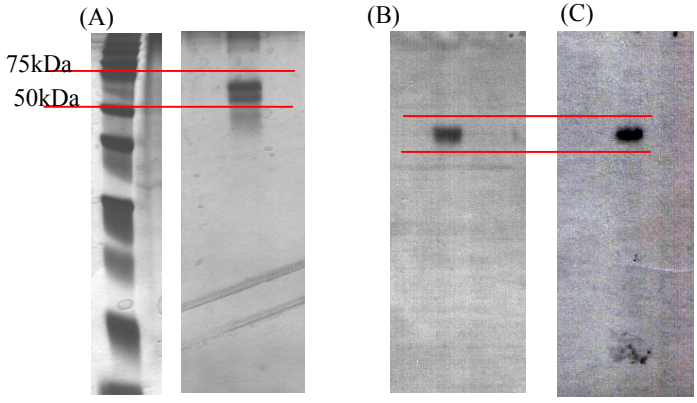

Figure 13. IMAC purification of the His10$_C$H$_1$R. (A) Silver stained SDS-PAGE (Criterion, BioRad); (B) anti-polyHistidine Western blot; (C) anti-H$_1$R Western blot. Red lines represent the position of a 75 and 50kDa protein. The SDS-PAGE used for the Western blots had a longer resolving time and so proteins have migrated further.

Thus the higher molecular weight protein does not appear to be glycosylated His10$_C$H$_1$R since it is not detected by either the anti-Histidine or anti-H$_1$R anitbodies. Through the several large scale purifications done during this study, this band was seen on more than one occasion (but not consistently) in SDS-PAGE gels of IMAC fractions, however, it was

never detected by Western blot. The identity of this larger protein remains unclear but it may in some way be related to the receptor.

Initial IMAC experiments with solubilised $His10_CH_1R$ used an imidazole concentration gradient of between 10 and 750mM imidazole for elutions. However, after determination of the imidazole concentration at which $His10_CH_1R$ began to elute (Figure 13A), a two step elution protocol was adopted to decrease the time spent on this purification step. The column was washed with 30 void volumes of 50mM imidazole and then eluted with 250mM imidazole and fractions (2 – 3x void volume) collected (Figure 14). Elutions of the column with 500mM imidazole did not show the presence of $His10_CH_1R$, suggesting the receptor was completely eluted using 250mM imidazole. This is consistent with the work of Ratnala, et al., (2004) who report elution of the $His10_CH_1R$ from IMAC using 100mM imidazole.

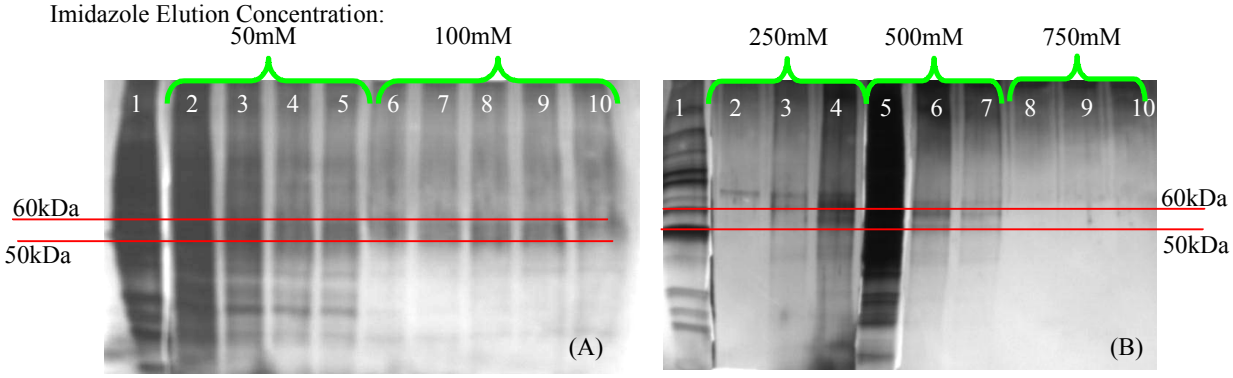

Figure 14. Silver stained SDS-PAGE (NuSep) of imidazole eluted IMAC fractions. (A) Lane Descriptions: 1 – BenchMark Marker (3µL, Invitrogen); 2-5 – 50mM imidazole wash; 6-10 – 100mM imidazole elutions. (B) Lane Descriptions: 1 – BenchMark Marker (1.5µL, Invitrogen); 2-4 – 250mM imidazole elutions; 5-7 – 500mM imidazole wash; 8-10 – 750mM imidazole wash. 15µL of sample was loaded per well.

Increasing incubation time of the soluble proteins with the resin from 24 to 48 hours resulted in $His10_CH_1R$ elution at concentrations greater than 250mM (Figure 15) and an estimated increase in total yield, but this was not used routinely due to a desire to keep the purification protocol rapid in order to preserve functional receptor.

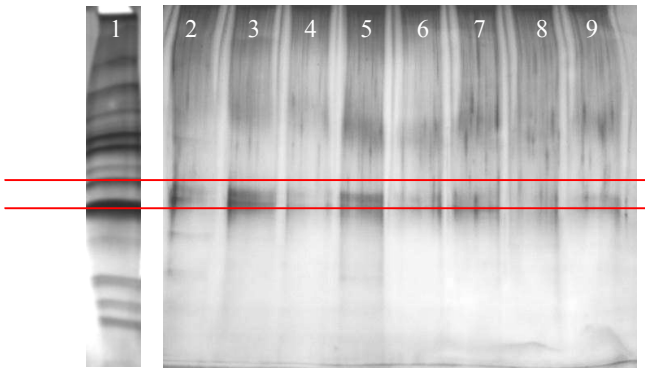

Figure 15. Silver stained SDS-PAGE (NuSep) of imidazole eluted IMAC fractions following 48 hours incubation of soluble protein with Nickel resin. Lane Descriptions: 1 – BenchMark Marker (1.5µL, Invitrogen); 2-4 – 250mM imidazole elutions; 5-9 – 500mM imidazole elutions. 15µL of sample was loaded per well.

Fractions containing the $His10_CH_1R$, as determined by SDS-PAGE, were pooled and concentrated in preparation for gel filtration. In initial purifications, Western blot analysis was used to confirm the presence of receptor at this stage. In later experiments only SDS-PAGE was used and Western blot was performed following the next purification step (GF-HPLC).

3.4.9. Gel Filtration HPLC

As well as providing a final purification step, GF-HPLC allowed for buffer exchange of the protein to a simple, low salt buffer which would be more compatible with crystallisation trials. A protein which elutes as a single peak from a gel filtration column is highly desirable (if not essential) for crystallisation of the protein. The purity of $His10_CH_1R$ from GF-HPLC, as shown by the GF-HPLC absorbance profile, did vary but SDS-PAGE was used to confirm a protein purity of greater than 90%, prior to use of the protein in crystallisation trials. The exact volume at which $His10_CH_1R$ eluted from the Superdex-75 column also varied but this was believed to be due to difficulties in running the GF-HPLC at high detergent concentrations; (bubbles in the column lines/absorbance reader can affect the perceived elution volume of the protein). Typically the $His10_CH_1R$ eluted between fractions 11 to 17 of the GF-HPLC (Figure 16, boxed).

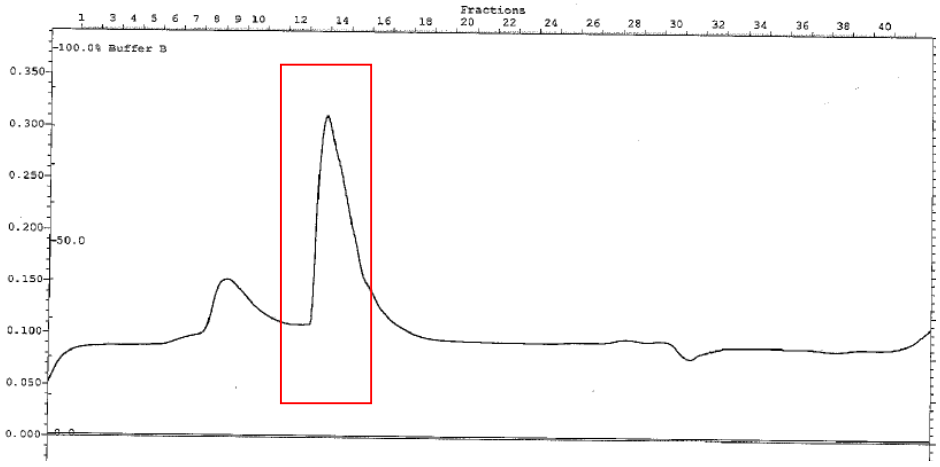

Figure 16. GF-HPLC A_{280} profile for chromatography of concentrated IMAC fractions containing $His10_CH_1R$. Flow rate was 0.2mL/min, 500µL fractions were collected.

At a flow rate of 0.2mL/min and an estimated elution time of 47 – 62 minutes, the predicted molecular mass of these fractions is between 32 and 12kDa which is substantially lower than the SDS-PAGE observed size of the protein (Figure 17, lane 8).

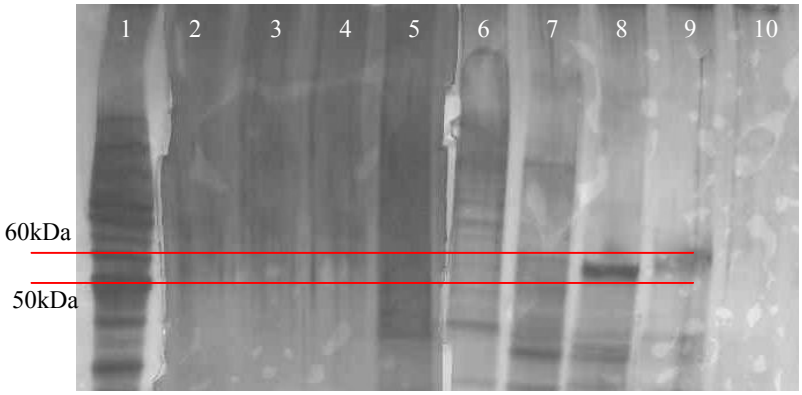

Figure 17. Silver stained SDS-PAGE of fractions from GF-HPLC. Lane Descriptions: 1 – BenchMark Marker (2µL, Invitrogen); 2 –fraction 1; 3 – fraction 3; 4 – fraction 5; 5 – fraction 7; 6 – fraction 9; 7 – fraction 11; 8 – fraction 13; 9 – fraction 15; 10 – fraction 19. 10µL of sample was loaded per well.

On one occasion during this study, the receptor eluted substantially later from the Sepharose-75 column (Figure 18) but still appeared at between 50 and 60kDa on an SDS-PAGE gel (results not shown). Results in Figures 16, 17 and 18 may suggest that the receptor is interacting with the Sepharose-75 resin, which can particularly occur if the protein is glycoslated. The observed weight of the $His10_CH_1R$ on SDS-PAGE (and in results presented in Figure 13) do not suggest the receptor is glycosylated under the expression conditions used in this study, though work by Sansuk, et al., (2008) has

demonstrated that baculovirus/insect cell produced H_1R shows in homogenous glycosylation at Asn[5]. However, given the variety of profiles that were observed during this study and the comments previously discussed regarding the use of detergent in the GF-HPLC, the profiles may simply be due to technical problems with this chromatographic step.

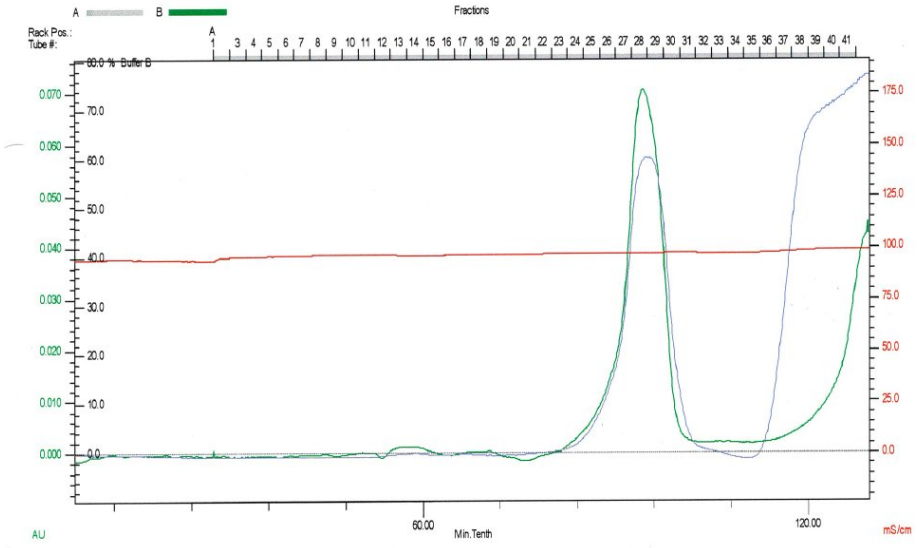

Figure 18. GF-HPLC A_{280} (green) and conductance profile (red) for chromatography of concentrated IMAC fractions containing $His10_CH_1R$. Flow rate was 0.2mL/min, 500µL fractions were collected.

If a first run of GF-HPLC did not produce $His10_CH_1R$ of sufficient purity for crystallisation (for example, Figure 17, lane 8), fractions containing the receptor were pooled and run again on the Superdex-75 column to produce a single band on SDS-PAGE and anti-H_1R Western blot (Figure 19B and 19C).

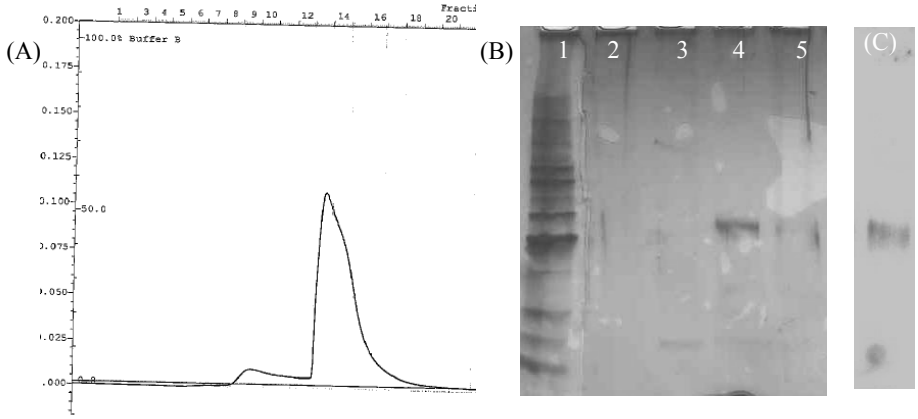

Figure 19. (A) GF-HPLC A_{280} profile for chromatography of concentrated IMAC fractions containing $His10_CH_1R$. (B) Silver stained SDS-PAGE of fractions from GF-HPLC. Lane Descriptions: 1 – BenchMark Marker (2µL, Invitrogen); 2 – fraction 2; 3 – fraction 10; 4 – fraction 13; 5 – fraction 17. 10µL of sample was loaded per well. (C) anti-H_1R western blot of GF-HPLC purified $His10_cH_1R$.

Of course with each additional purification step, the yield of the receptor is decreased, and this must be considered when modifying the purification. For the purpose of this study pure protein was of the utmost importance, increase in yield could be achieved by repeating the purification process. On one occasion ion exchange chromatography (MonoQ) was used to produce pure $His10_CH_1R$ but, although successful, was not further utilised in this study since the same results could be obtained using GF-HPLC.

Fractions containing pure H_1R, as determined by SDS-PAGE and Western blot, were pooled and concentrated to ~5mg/mL. Receptor to be used within 3 days was frozen at -20°C. For longer term storage, $His10_CH_1R$ was rapidly frozen in liquid nitrogen and stored at -80°C.

3.4.10. Yield and Functionality of the $His10_CH_1R$

The difficulties in detecting soluble functional receptor have been discussed in detail in section 3.4.5. A summary of estimated quantities of functional receptor from a typical purification from 5L of *Sf*9 cells, in combination with results presented in section 3.4.5 are given in Table 1.

Table 1. Estimated functional quantities of $His10_CH_1R$ as determined by [^{3}H]-pyrilamine binding. Samples from (B) onwards were prepared in the presence of triprolidine, unless otherwise stated (C). UT = urea treated

Sample	pmol/mg	mg functional H_1R
(A) UT membranes	55	3.85
(B) nOG soluble	4.5	0.25
(C) nOG soluble, no triprolidine	37	2.03
(D) nOG insoluble	2	0.04
(E) Purified $His10_CH_1R$	558	0.03

Sample C represents binding to receptor solubilised in the absence of triprolidine which, under these conditions indicates that approximately 53% of functional $His10_CH_1R$ is being solubilised from the urea treated membranes. From purification of 5L of *Sf*9 cells, 1mg of $His10_CH_1R$ was obtained as determined by absorbance measurement. When incubated with 8μM of [^{3}H]-pyrilamine, a specific activity of 558pmol/mg of total protein was calculated for the purified $His10_CH_1R$ (Table 1, sample E), corresponding to 0.03mg of functional

receptor and a value of 3% functional receptor in the final purified sample. However with the limitations of the assay measurement, the relevance of this value is difficult to determine. Undoubtedly functional receptor is lost during the purification protocol, but the exact extent to which this occurs was not definitively determined in this study.

Unfortunately reports of pmol/mg ligand binding activities during 7TMR purification are discouragingly scarce. Two notable exceptions are purification reports of the β_2 adrenergic receptor (Chelikani, et al., 2006; Kobilka, 1995) and of the neurotensin receptor (Grisshammer, et al., 1999) for which extensive reports have been written. Some reports give "dpm" (disintegrations per minute, of the radioligand) values as a representation of receptor functionality but with the absence of quantity (μg) of protein in the assay and specific activity of the radioligand used, these values mean little in regards to the yield of functional receptor. Others report pmol/mg values but are not so ready to quantify the % of functional receptor (Hayashi and Haga, 1996) or report only EC_{50} values for the ligand interaction with the receptor binding site (Furukawa and Haga, 2000). For a receptor of 55kDa, assuming one site ligand binding, the value for activity of 100% functional and pure protein is calculated to be 18181pmol/mg (18nmol/mg). However, no reports exist for purified M_2R or H_1R exhibiting such activity following the purification steps required. Hayashi and Haga, (1996) reported purification of a mutant M_2R to specific activity of 1.6nmol/mg (~5% functional for the ~32kDa mutant). Peterson, et al., (1995) purified porcine M_2R from CHO cells to a specific activity of 12nmol/mg (67% functional), they were particularly fortunate to have a starting expression of 51pmol/mg (which is particularly high for the M_2R). Ruat, et al., (1992) solubilised H_1R from guinea pig cerebellum to a specific activity of 220fmol/mg (<< 1% functional) but did not report activity following further purification. Ratnala, et al., (2004) report recovery of 85% functional $His10_CH_1R$ which, if determined by radioligand binding assay, would correspond to [^{3}H]-pyrilamine binding of ~15452pmol/mg. This value for ligand binding was not reported, though competition binding assays certainly verified the presence of functional purified receptor (but not the amount of functional receptor).

Although there were limitations in the assay method used in this study (in conjunction with the strategy to maintain high-affinity ligand during the purification), it is certainly not disregarded that the final purified receptor may consist of a very low percentage population of functional receptor. Despite this unknown, the $His10_CH_1R$ was trialled in both two

dimensional and three dimensional crystallisation attempts as is reported in chapter 4 of this study.

3.4.11. Purification of the $His6_CM_2R$, a summary

Prior to receiving the $His10_CH_1R$ baculovirus, purification of the $His6_CM_2R$ was attempted. Work with the muscarinic receptor was paused whilst techniques for receptor purification were being learnt with the $His10_CH_1R$. Towards the end of this study follow up work on the $His6_CM_2R$ was carried out. A flowchart for work with the $His6_CM_2R$ is shown in Figure 20.

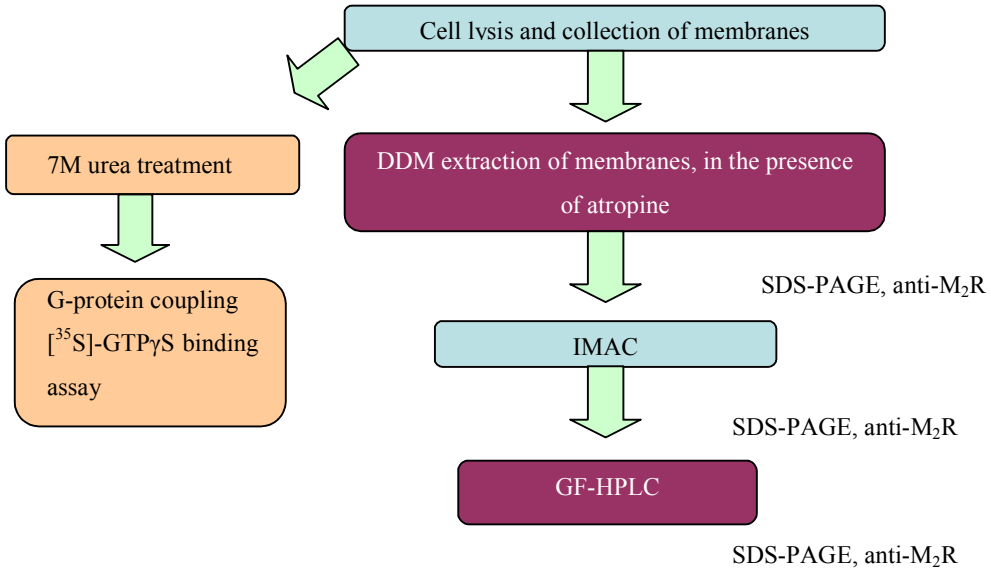

Figure 20. Purification flow chart for the $His6_CM_2R$

Prior to purification attempts, functionality of the $His6_CM_2R$ was confirmed by reconstitution with purified G-protein subunits.

3.4.12. Reconstitution of the M_2R with purified G-protein subunits

Expression of un-tagged and poly-Histidine tagged M_2Rs were reported in chapter 2. Receptor identity and functionality was further confirmed by reconstitution of the M_2R containing *Sf*9 membranes with the purified G-protein subunits, $His6_N G\alpha_{i1}$ and $\beta_1\gamma_2$ (Figure 21A). All *Sf*9 membranes used in this work were 7M urea treated as this method inactivates endogenous G-proteins in the *Sf*9 cell (Lim and Neubig, 2001). G-protein coupling ability of the muscarinic receptor was maintained despite the presence of a Histidine tag on either the C (Figure 21B and 21C) or N (Figure 23) terminus of the M_2R. Addition of the M_2R agonist acetylcholine to a mixture of $His6_CM_2R/His6_N G\alpha_{i1}\beta_1\gamma_2$

produced a 2.4 fold increase in bound [^{35}S]-GTPγS compared to [^{35}S]GTPγS binding to the reconstituted proteins in the absence of M_2R agonist. This demonstrates the activation of $His6_N G\alpha_{i1}$ by agonist bound $His6_C M_2R$. $His12_C M_2R$ was also able to interact with $His6_N G\alpha_{i1}$ as demonstrated by a 2.4 fold increase in [^{35}S]-GTPγS binding, in the presence of acetylcholine (Figure 21C). *Sf*9 membranes containing un-tagged M_2R produced a 3.4 fold increase in [^{35}S]-GTPγS binding in the presence of acetylcholine (Figure 21A).

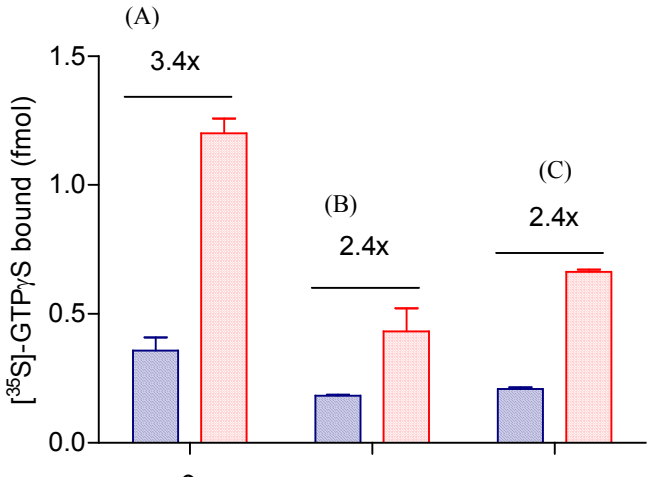

Figure 21. Reconstitution of *Sf*9 membranes containing M_2R or C terminal His tagged M_2R with purified $G\alpha_{i1}$ and $\beta_1\gamma_2$. (A) *Sf*9 membranes containing M_2R. (B) *Sf*9 membranes containing $His6_C M_2R$. (C) *Sf*9 membranes containing $His12_C M_2R$. Striped blue bars show [^{35}S]-GTPγS binding to the reconstituted proteins in the absence of M_2R ligand. Spotted red bars show [^{35}S]-GTPγS binding in the presence of the muscarinic receptor agonist acetylcholine. 2.5µg of total membrane protein was used in each 25µL assay. Data represents the mean ± S.E.M., n = 3. Fold increase is shown above each basal/acetycholine set.

The higher fold increase in [^{35}S]-GTPγS binding in the presence of untagged M_2R was not a reflection of the higher receptor density in these membranes as compared to the $His6/12_C M_2R$ containing membranes (compare chapter 2 Figures 8 and 10), since assays prepared using double the concentration of total membrane protein (and thus the concentration of either $His6_C M_2R$ or $His12_C M_2R$) did not increase agonist induced [^{35}S]-GTPγS binding (Figure 22).

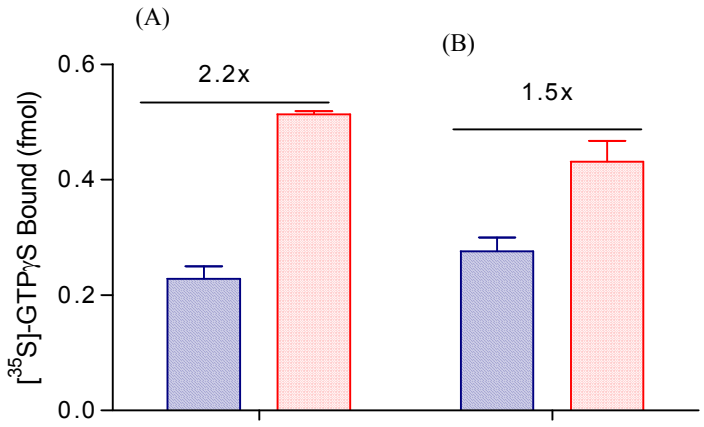

Figure 22. Increasing total membrane protein concentration in a His-tagged M_2R/G-protein reconstitution assay. (A) G-protein reconstitution with $His6_CM_2R$. (B) G-protein reconstitution with $His12_CM_2R$. Blue striped bars show [^{35}S]-GTPγS binding to the reconstituted proteins in the absence of M_2R ligand. Red spotted bars show [^{35}S]-GTPγS binding in the presence of the M_2R agonist acetylcholine. 5µg of total membrane protein was used in each 25µL assay. Data represents the mean ± S.E.M., n = 3. Fold increase is shown above each basal/acetycholine set.

Reconstitution of *Sf*9 membranes containing the N terminal tagged M_2R, $His6_NM_2R$, resulted in only a 1.4 fold increase in bound [^{35}S]-GTPγS (Figure 23A). $His6_NM_2R$ density was approximately equivalent to that exhibited by $His6_CM_2R$ membranes (Chapter 2, Figure 10). Thus it is unlikely that receptor density was not the cause of the lower fold increase in agonist induced [^{35}S]-GTPγS binding. Furthermore, the higher level of basal [^{35}S]-GTPγS binding (which may have masked the effect of agonist addition) could not readily explain the smaller increase in radionucleotide binding by $His6_NM_2R$ activated $His6_NG\alpha_{i1}$ compared to $His6_CM_2R$ activated G-protein. Increasing the concentration of GDP in the reconstitution, decreased both the basal and acetylcholine induced [^{35}S]-GTPγS binding (Figure 23B and 23C).

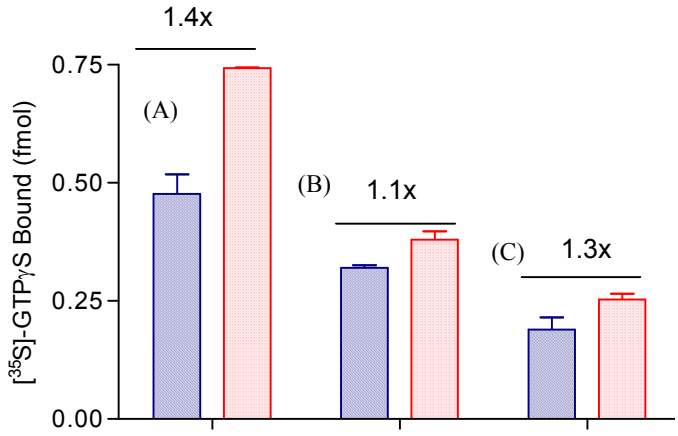

Figure 23. Reconstitution of *Sf*9 membranes containing N terminal His tagged M_2R, $His6_NM_2R$, with purified $G\alpha_{i1}$ and $\beta_1\gamma_2$. (A) In the presence of 1μM GDP (B) In the presence of 5μM GDP. (C) In the presence of 10μM GDP. Blue striped bars show [^{35}S]-GTPγS binding to the reconstituted proteins in the absence of M_2R ligand. Red spotted bars show [^{35}S]-GTPγS binding in the presence of the muscarinic receptor agonist acetylcholine. Data represents the mean ± S.E.M, n = 3.

Thus, interestingly, it was observed that addition of a hexa-Histidine tag to the C terminus of the M_2R appeared to have less effect on receptor mediated $G\alpha_{i1}$ GTP exchange. This was not a result of difference in expression level of the tagged receptors, as these were previously shown to be almost identical (Chapter 2). Homology modelling and mutagenesis data of rhodopsin and the β_2R suggest the involvement of the intracellular second loop (including side chains) as well as side chain extensions of transmembrane helices 3 and 6 in receptor/G-protein coupling (Gether, 2000; Gether, et al., 1997). The variability in amino acid sequences in the third intracellular loop of 7TMRs, as well as the ability of artificial peptides to interact with G-proteins, suggest that it is both the conformation and charge presented by the receptor domains that is important in G-protein coupling. Thus it could be hypothesised that addition of the Histidine tag modifies the domains of the receptor presented to the G-proteins upon agonist binding to the receptor. Alternatively, the addition of the Histidine tag and TEV protease cleveage sequence to the N terminus of the receptor may be interfering with agonist/receptor binding and this is effecting the observed receptor/G-protein interaction.

Taken with results presented in Chapter 2, it can be concluded that baculovirus infected *Sf*9 cells contained M_2R, $His6_CM_2R$, $His12_CM_2R$ or $His6_NM_2R$ as appropriate and furthermore, that all receptors were able to interact with G-proteins to some extent. Since the C terminal Histidine tagged M_2Rs showed G-protein interaction most comparable to the untagged

M_2R, it was decided to use these receptors in future purification attempts. Initially the $His6_CM_2R$ was used in purification trials with the stratagem that protocols developed for this receptor could be transferred to the $His12_CM_2R$ at a later date if necessary.

3.4.13. Solubilisation of *Sf*9 cells containing M_2R

The presence of M_2R in *Sf*9 membranes was always confirmed by [^{3}H]-scopolamine binding prior to solubilisation/purification trials. However following the difficulties encountered with the $His10_CH_1R$ radioligand, such binding assays were not performed throughout the purification. Preliminary work with the M_2R was to focus on assessing the ability to extract the receptor from the membrane and detecting such activity. Thus solubilisation and purification attempts with the $His6_CM_2R$ were assessed by Western blot using a receptor specific antibody.

The loss in total receptor yield was the reason 7M urea treatment was not used prior to solubilisation of the $His6_CM_2R$, which was already expressing at much lower levels than the histamine receptor. Given that starting quantities of M_2R were low, a two step purification step was desired. CHAPS, DDM and (sodium) cholate were trialled for solubilisation of the $His6_CM_2R$ from small scale (<2L) *Sf*9 cell cultures containing the receptor. Together these detergents covered the three detergent classes – zwitterionic (CHAPS), non-ionic (DDM) and ionic (cholate). Previous studies had demonstrated cholate and DDM as effective detergents for M_2R solubilisation (Rinken, 1996). At 10mM all three detergents were used above their reported CMC value. Solubilisation was performed on whole cell lysates using a simplified IMAC protocol (refer to methods section 3.3.9) to concentrate the solubilised receptor and so ensure its detection by Western blot. Briefly, the soluble fraction was incubated with Nickel resin and a column prepared. The column was washed with buffer containing 5mM imidazole and then eluted with 500mM imidazole and 5 void volume fractions collected. At this stage IMAC was not being optimised as a purification step but rather as a method to concentrate the receptor.

IMAC fractions prepared from sodium cholate (10mM) solubilised *Sf*9 membranes material showed a protein signal between the 45 – 85kDa marker protein range on an anti-M_2R Western blot (Figure 24, circled). This is in the expected size range for the $His6_CM_2R$ which has a predicted molecular mass of 52.5kDa but has 4 potential sites of glycosylation (Chapter 1, Figure 5) meaning observed receptor size may be higher. The observed size of

$His6_CM_2R$ is in agreement with reports of receptor solubilisation and/or purification from *Sf*9 cells. Park, et al., (2001) reported the observation of recombinant M_2R between 50 and 60kDa when probed with an anti-FLAG antibody. Park and Wells, (2003) reported the presence of a 50 – 60kDa protein in silver stained SDS-PAGE of solubilised *Sf*9 membranes containing M_2R.

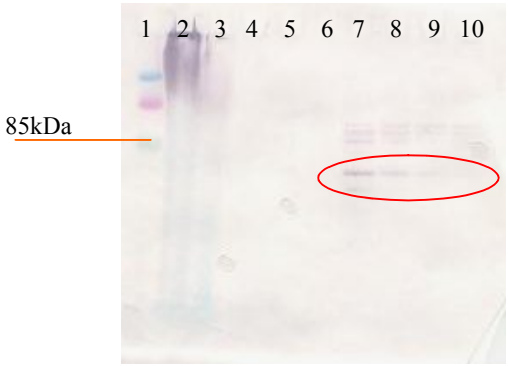

Figure 24. Solubilisation of $His6_CM_2R$ membranes with 10mM cholate. Western blot with anti-M_2R. Lane Descriptions: 1 – Kaleidoscope Marker (5µL, BioRad); 2 – urea treated $His6_CM_2R$ membranes; 3 – cholate insoluble; 4 – cholate soluble; 5 – IMAC column flow through; 6-10 – 500mM imidazole eluted fractions 20µL of sample was loaded per well.

Encouragingly, membranes solubilised with either DDM (10mM, Figure 25) or CHAPS (10mM, Figure 26) gave a similar result to membranes extracted with cholate (Figures 24), with a band being evident between the 41 and 85kDa marker proteins. Furthermore, antibody binding was specific (Figures 25B and 26B), selectively binding the receptor from the variety of proteins observed in the SDS-PAGE. The receptor was not detected in the insoluble or soluble samples, since at this stage the receptor concentration is probably below the limit of detection. Interestingly, all anti-M_2R blots showed a triplicate of bands between the 85 and 128kDa marker proteins. Whether these are non-specific antibody binding, non SDS-PAGE denatured receptor/protein complexes, or glycosylated receptor forms, was not definitively determined in this study.

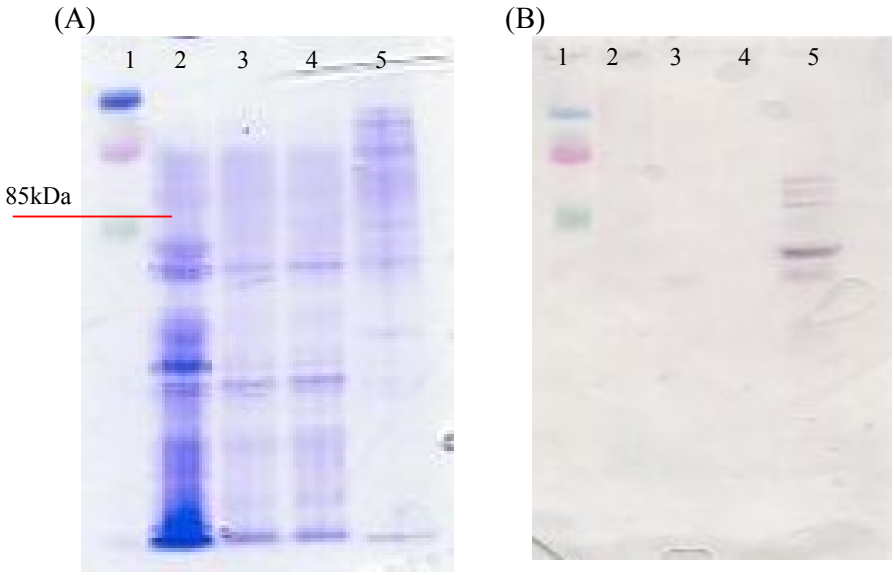

Figure 25. Solubilisation of $His6_CM_2R$ membranes with 10mM DDM. (A) – Coomassie stained SDS-PAGE (Invitrogen gel). Lane Descriptions: 1 – Kaleidoscope Marker (5µL, BioRad) .; 2 – DDM insoluble; 3 – DDM soluble; 4 – IMAC column flow through; 5 – 500mM imidazole elution, fraction #2. (B) – Western Blot with anti-M_2R. Lane descriptions: as for (A). Samples were prepared as described in the methods section (for Invitrogen pre-cast gels); 20µL of sample was loaded per well

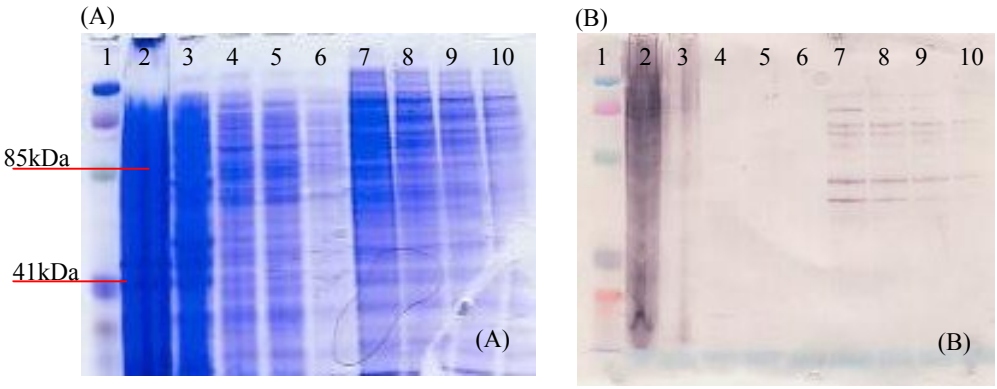

Figure 26. Solubilisation of $His6_CM_2R$ with 10mM CHAPS. (A) – Coomassie stained SDS-PAGE. Lane Descriptions: 1- Kaleidoscope Marker (5µL, BioRad); 2 – urea treated M_2R membranes (100µg); 3 – CHAPS insoluble; 4 – CHAPS soluble; 5 – IMAC column flow through; 6 – 10 - 500mM imidazole eluted fractions. (B) – Western blot with anti-M_2R. Lane description: As for (A). Samples were prepared as described in method section; 20µL of sample was loaded per well.

There appeared to be little difference in the ability of cholate, CHAPS and DDM to solubilise the $His6_CM_2R$ from the *Sf*9 membranes, as observed by Western blot (compare Figures 24, 25B and 26B in which the same total protein amount was loaded). It was a theoretical decision to utilise the detergent DDM for future purifications based on the assumption that being a non-ionic detergent, it was expected to aid in the maintenance of a

functional receptor form. Ligand binding on the solubilised/purified receptor was, at this stage, a goal of future work.

3.4.14. IMAC of the $His6_CM_2R$

At this stage of the project expression of the $His6_CM_2R$ was increased to 5L cultures using fermentation facilities at CSIRO MHT Parkville (Victoria). Attempts at purification of the $His6_CM_2R$ were an extension from the solubilisation step, which already included a simple form of IMAC. Solubilisation studies demonstrated that the $His6_CM_2R$ was retained on the nickel column at 5mM imidazole. Following 5mM imidazole washing, an imidazole gradient of 10, 20, 100, 200 and 500mM imidazole was used to elute protein bound to the Nickel resin. A protein of between 50 and 60kDa in size was eluted at between 10 and 20mM imidazole (Figure 27, lanes 2 – 5). 20mM imidazole appeared sufficient to completely elute this protein since it was not visible in subsequent fractions (Figure 27, lanes 6 – 15). These 10 and 20mM imidazole eluted IMAC fractions (20mL in total) were pooled, concentrated (to ~ 2mL), and analysed by anti-M_2R Western blot (Figure 28B, lane 2). Despite the concentrated, non-homogeneous IMAC sample, a single band of ~62kDa was detected on the Western blot.

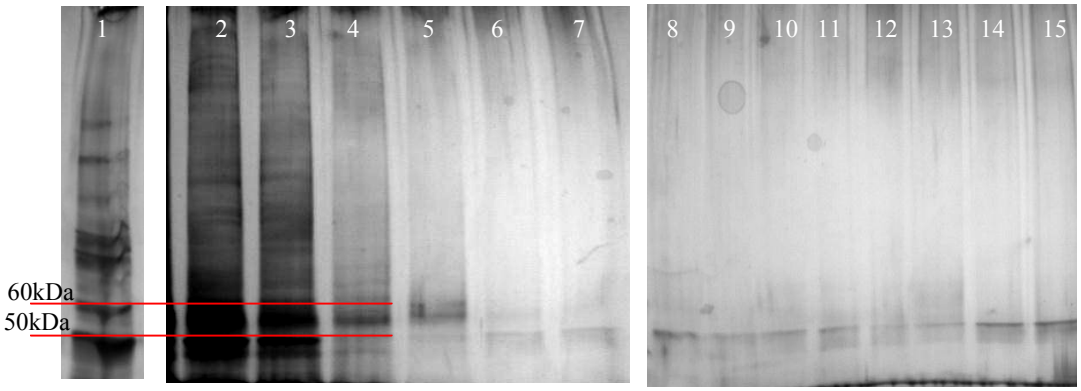

Figure 27. Silver stained SDS-PAGE of Nickel chromatography fractions of DDM solubilised *Sf*9 membranes containing $His6_CM_2R$. Lane descriptions: 1 – BenchMark Marker (2µL, Invitrogen); 2 – 3 10mM imidazole eluted fractions; 4 – 5 20mM imidazole eluted fractions; 6 – 9 100mM imidazole eluted fractions; 10 – 12 200mM imidazole eluted fractions; 13 – 15 500mM imidazole eluted fractions. 20µL of sample was loaded per well.

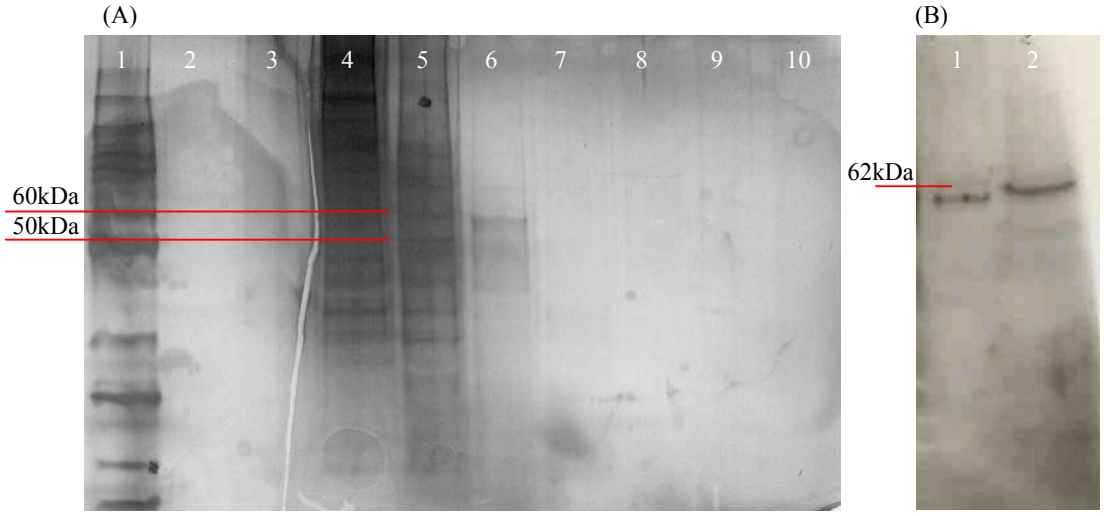

Figure 28. (A) Silver stained SDS-PAGE gel of gel filtration HPLC fractions. Lane Descriptions: 1 – BenchMark unstained marker (2µL, Invitrogen); 2 – Fraction 3; 3 – Fraction 7; 4 – Fraction 9; 5 – Fraction 14; 6 – Fraction 28; 7 – Fraction 32; 8 – Fraction 34; 9 – Fraction 38; 10 – Fraction 40. (B) Western blot with anti-M_2R. Lane Descriptions: 1 – GF-HPLC purified $His6_CM_2R$; 2 – concentrated IMAC fractions containing $His6_CM_2R$. 10µL of sample was loaded per well.

The molecular weight of $His6_CM_2R$ on the Western blot is slightly higher than observed in silver stained SDS-PAGE gel of the IMAC fractions (Figure 27) but this is likely due to the effect of running a sample with high protein and imidazole concentrations. The concentrated IMAC sample containing $His6_CM_2R$ was subject to Superdex-75 gel filtration (GF-HPLC) but did not elute as a single peak and eluted late in the GF-HPLC (Figure 29, indicated by a box). An estimated molecular weight of 2kDa was calculated for this protein peak, based on elution time of the peak and flow rate of the column. This does not correspond at all to the 50 – 60kDa protein observed in SDS-PAGE (Figure 28), suggesting the receptor is interacting with the GF-HPLC resin and being eluted later than expected.

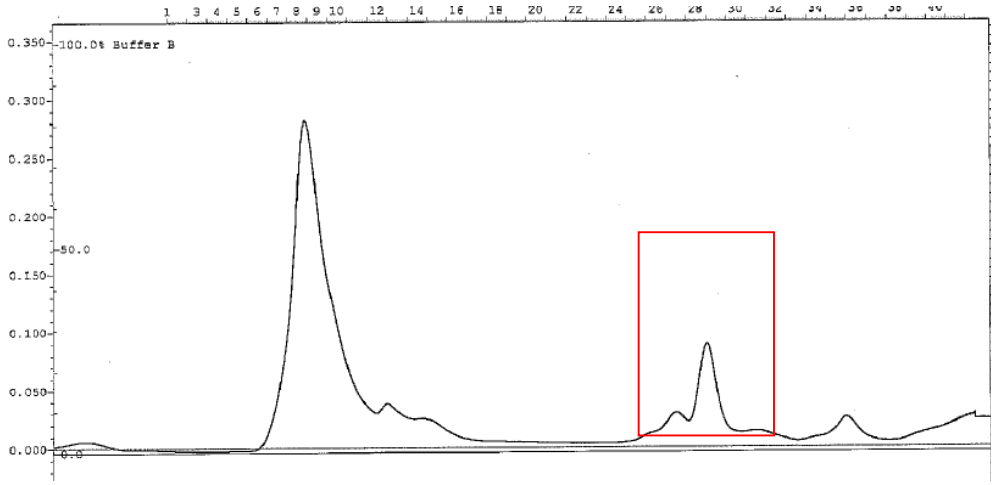

Figure 29. Absorbance profile for pooled $His6_CM_2R$ IMAC fractions. The protein sample was run on a 1 x 30cm Superdex-75 column using buffer containing 20mM DDM (see methods) and a flow rate of 0.2mL/min. 500µL fractions were collected. The red boxed area indicates fractions containing the $His6_cM_2R$.

In a separate purification however, elution of the $His6_CM_2R$ (along with contaminating proteins) began earlier (fraction 13), at time expected for a protein with an estimated molecular weight of ~30kDa (Figure 30, boxed).

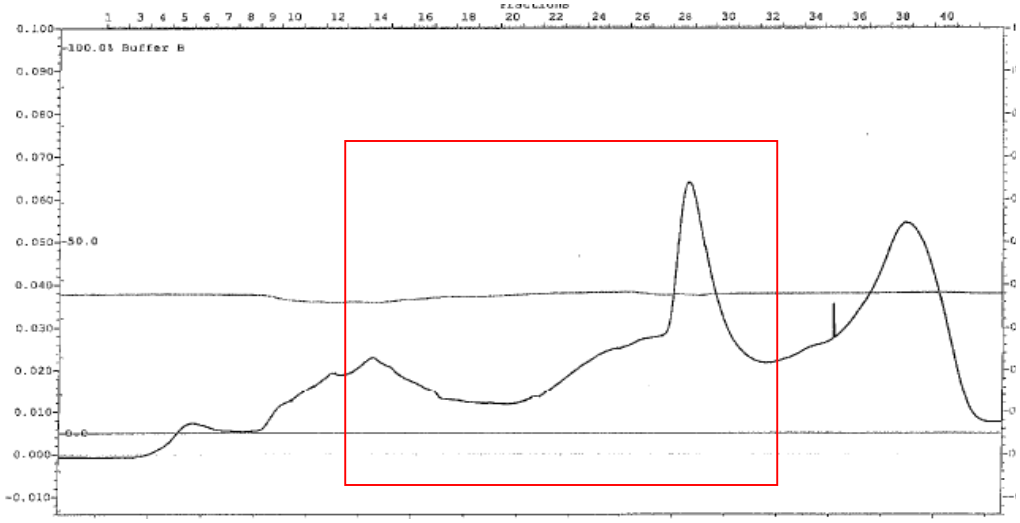

Figure 30. GF-HPLC absorbance profile for pooled $His6_CM_2R$ IMAC fractions. The protein sample was run on a 1 x 30cm Superdex-75 column using buffer containing 20mM DDM (see methods) and a flow rate of 0.2mL/min. 500µL fractions were collected. The red boxed area indicates fractions containing the $His6_cM_2R$.

The variability in the GF-HPLC absorbance profiles suggests the presence of a non-homogeneous population of glycosylated and non-glycosylated receptor. Glycosylated proteins may interact with the gel filtration resin causing a later than theoretically

calculated elution time. This corresponds with the results presented in Figures 25 and 26. However, as mentioned in section 3.4.9, technical problems related to running samples with high detergent concentration may also have caused variability in the GF-HPLC absorbance profiles. Furthermore, the $His6_CM_2R$ preparation eluted from the IMAC column was rather inhomogenous and the level of purity varied slightly between preparations, these factors may also affect the GF-HPLC profiles.

Silver stained SDS-PAGE (Figure 28, lane 6) confirmed the presence of a protein of between 50 and 60kDa as well as the presence of contaminating proteins as observed on the GF-HPLC absorbance profile (Figure 29). Fractions from this peak were pooled (total volume 1.5mL), concentrated and analysed by anti-M_2R Western blot (Figure 28B, lane 1). A single band was observed at ~60kDa at a slightly lower molecular weight than that observed in the concentrated $His6_CM_2R$ IMAC sample (Figure 28B, lane 2). This may be due to receptor degradation occurring between the IMAC and GF-HPLC steps but more likely, is due to the high imidazole and glycerol concentrations in the concentrated IMAC sample effecting sample running in the SDS-PAGE.

Whilst preliminary work with the $His6_CM_2R$ was carried out early in this study, large scale purifications were performed towards the end of the study, after work on the histamine receptor was completed. For this reason time limitations did not allow for further work with this receptor but the results presented here would go some way to developing a standardised purification protocol for the receptor.

3.5. Conclusions

The $His6_CM_2R$ and $His10_CH_1R$ were shown to functionally interact with purified G-protein subunits. Interestingly, $His10_CH_1R$ interacted with $G\alpha_{i1,}$ a member of the adenylyl cyclase inhibiting Gα family. Such an interaction has not been previously reported. The $His10_CH_1R$ was purified to near homogeneity using 7M urea treatment, nOG solubilisation, IMAC and GF-HPLC. 1mg of purified histamine receptor was obtained from 5L of insect cell culture with <5% of this receptor determined to be functional as defined by [^{3}H]-pyrilamine binding (in the presence of excess triprolidine). A preliminary solubilisation and purification protocol utilising DDM solubilisation, IMAC and GF-HPLC was developed for the $His6_CM_2R$ with receptor presence and purity determined by SDS-PAGE and Western blot with receptor specific antibodies.

4. *In meso* and two-dimensional crystallisation trials with the $His10_CH_1$ histamine receptor

4.1. Acknowledgements

Dr Connie Darmanin taught me everything in this chapter – *in meso* crystallisation, identifying and collecting crystals, using the X-ray generator at CSIRO, using the Australian synchrotron and using the electron microscope. Without her time and effort this chapter would not exist. Connie also helped with technical aspects of the *in meso* crystallisation such as preparing the plates and adapting them for automated imaging.

Dr Charlotte Conn helped to develop the methods for *in meso* crystallisation and gave technical advice about the surfactants and their cubic phase structures

Ms Lynne Waddington gave excellent technical assistance with use of the electron microscope and interpretation of initial EM images.

Dr Priya Bhakat demonstrated the EM image scanner and provided help with electron microscopy.

Dr Janet Newman helped with automation of crystal screening, provided all of the precipitant screens used in this study and was always helpful with technical advice. Janet and Dr Tom Peat gave helpful general discussions about crystallisation and kept me company on the weekends.

Glen from the CSIRO workshop helped with all of the hardware and "home-made" equipment used in this study, including preparation of the crystallisation plates.

Dr Victor Streltsov gave advice on X-ray and electron diffraction data analysis.

Dr Jose Varghese helped with the analysis of the electron and X-ray diffraction data.

4.2. Introduction

Crystallisation of membrane proteins is the next challenge of protein crystallography. Human seven transmembrane receptors are a highly desired and challenging target for atomic resolution structure determination. Until recently (2007) bovine rhodopsin was the only mammalian 7TMR for which the structure had been determined (Palczewski, et al., 2000). In 2007 the two reports were published on β_2 adrenergic receptor crystallisation and subsequent structure determination (Cherezov, et al., 2007; Rasmussen, et al., 2007). Protein crystallisation can take place in either two (ordered monolayer) or three dimensions. Two-dimensional (2D) crystallisation is performed either in suspension or by arraying of the protein, or a host lipid bilayer, onto a surface. Three-dimensional (3D) crystallisation can be achieved by either vapour diffusion (using either detergent solubilised or lipid reconstituted protein) or *in meso* methods.

In this study a C terminal 10x Histidine tagged Histamine H_1 receptor ($His10_CH_1R$) was used in suspension 2D crystallisation trials and *in meso* (3D) trials. 2D crystallisation was performed in suspension by reconstitution of the receptor into a lipid mixture followed by addition of a salt. 3D crystallisation of the receptor was trialed *in meso* using either monoolein or phytantriol in combination with a variety of commercially available precipitants.

4.3. Methods

4.3.1. Reagents

Unless otherwise stated in the text, all reagents were of analytical grade and were purchased from Sigma Aldrich. All buffers were prepared in milliQ treated water (mQH_2O)

4.3.2. GF-HPLC purification of $His6_NG\alpha_{i1}$

$His6_NG\alpha_{i1}$ was expressed and semi-purified as described in chapter 3. For crystallisation the G-protein was further purified using Superdex-75 HPLC and Gα gel filtration buffer (20mM Bis-Tris propane, 150mM NaCl, 5mM β-mercaptoethanol, 10μM guanosine diphosphate (GDP), pH 7.6).

4.3.3. Synthesis of surfactants

Phytantriol was synthesised by Dr Sharon Sagnella (CSIRO, Clayton). The viscous surfactant was stored at room temperature in a sealed glass vial. Monoolein was purchased from Sigma Aldrich. Cubic phase formation of both phytantriol and monoolein was characterised using small angle x-ray scattering (SAXS) by Dr Charlotte Conn (CSIRO, Clayton).

4.3.4. Development of custom made crystallisation viewing plates for *in meso* crystallography

Plates for the *in meso* crystallization set-up were prepared using a method based on that described by (Chelikani, et al., 2006). 1mm thick silicon rubber was cleaned thoroughly with household detergent, sonicated and cut to fit a typical glass microscope slide. Holes of 5mm diameter were punched into the silicon as a 3x3 grid that was a sufficient size to be covered by a single glass coverslip. The number of wells was optimised later in the study to 10 wells per plate (see section 4.4.1). The Silicon was pressed firmly onto the microscope slide. Following addition of protein, surfactant and precipitant, a glass coverslip was used to seal the wells. To increase the throughput, 96 well crystallisation plates were generously provided by Dr Connie Darmanin (CSIRO, Parkville). The plate was sealed using transparent packing tape (Scotch 3M). This decreased plate preparation time and brought the potential of automated crystal screening.

4.3.5. Preparation of H_1R/Surfactant for *in meso* Crystallisation

Protein/Surfactant Ratios

H_1R was prepared at 5mg/mL in 20mM Bis-Tris Propane pH 7.6, 150mM NaCl, 5mM β-mercaptoethanol and 20μM triprolidine. Protein was combined with surfactant at a ratio that would provide sufficient water content for cubosome formation of the given surfactant (examples are given in Table 1).

Table 1. Composition of H_1R/surfactant used for crystallization trials. S = surfactant, P = protein.

Surfactant	Ratio (S:P, w/v)	μL H_1R (5mg/mL)	mg Surfactant
Monoolein	60:40	9.8	14.7
Phytantriol	80:20	11.2	45

These ratios were determined using the reported phase diagrams for monoolein (Figure 1A; (Qiu and Caffrey, 2000)) and phytantriol (Figure 1B; (Barakaus and Landh, 2003)).

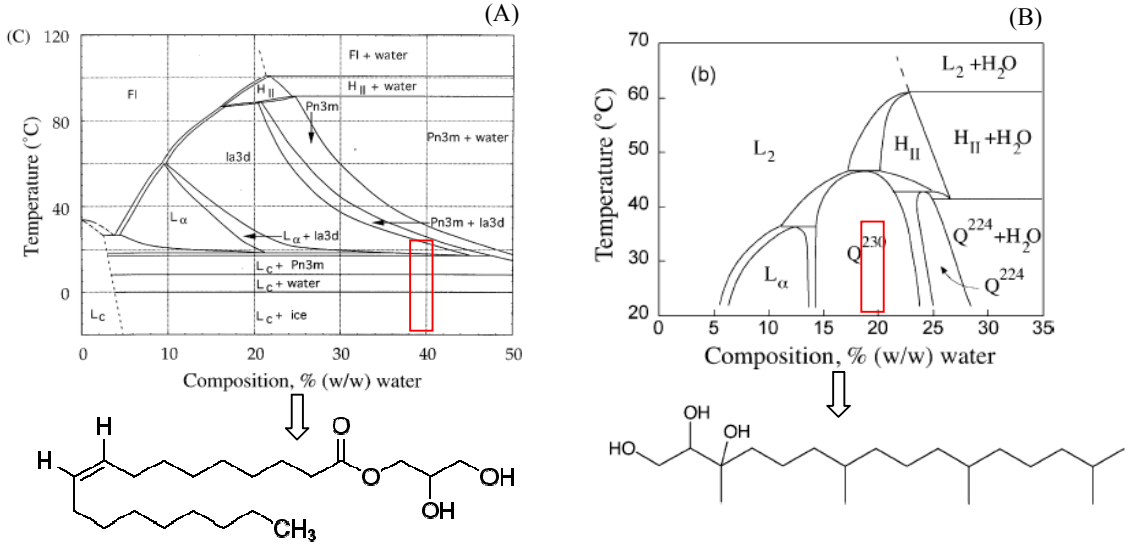

Figure 1. Phase diagrams and structures for surfactants used in this study. (A) Monoolein from (Qiu and Caffrey, 2000). (B) Phytantriol from (Barakaus and Landh, 2003). Structures are as follows: Pn3m – L_2 – reversed micellular; L_α – lamellar, Q^{230}/Ia3d and Q^{224} – (cubic) crystallographic space groups, H_{II} – hexagonal.

In this study the Pn3m or Ia3d cubic structures were preferred for protein crystallisation. At this stage of the study, the choice of cubic structure used was somewhat arbitrary since the exact dimensions of the cubic phases and the way in which the proteins resided in them were not known. The concentration of the protein used in the crystallisation trials may also require modification to aid the packing of the receptor within the cubic phase. Experiments

to determine these properties are currently under investigation by Dr Charlotte Conn (CSIRO, Clayton). At 20 to 25^{o}C and 40% w/w water, monoolein is at the border of the Ia3d/Pn3m cubic phases (Figure 1A, boxed). However when 20^{o}C is approached from typical room temperature (i.e. when setting up a crystallisation plate at ~25^{o}C and then placing the plate in a 20^{o}C incubator, as was done in this study) it is more likely that monoolein resides in a Pn3m structure as cubic structures tend to form at the temperatures shown in the heating direction but don't return to "cooler" structures when the temperature is decreased. (personal communication; Dr Charlotte Conn CSIRO, Clayton). For phytantriol the Ia3d structure (Q^{230}) is formed at 20% w/w water composition and between 20^{o}C and 30^{o}C (Figure 1B, boxed). Thus Ia3d would be the predominant cubic structure in these crystallisation experiments.

Preparation of protein containing cubic phase

Surfactant (+/- cholesterol, see the proceeding section) was measured into a 250μL Hamilton syringe and the protein suspension was pipetted into a second syringe (Figure 2A). The syringes were joined using a purpose-built stainless-steel coupler (Figure 2A, circled). The Hamilton syringe set up was based on the work of (Maruko, et al., 2005). The void volume of the coupled syringe system was approximately 15μL. Protein and surfactant were passed through the coupler 100 times until the suspension became viscous and transparent which indicated the formation of the mesophase. The suspension was allowed to equilibrate for 30 minutes to ensure homogeneity, before being passed through the coupler again 20 times. The syringe containing the protein/surfactant was removed from the coupler and connected to a Hamilton nano-dispenser (Figure 2B, coupling end circled). The protein/surfactant was injected into the 10μL syringe of the dispenser.

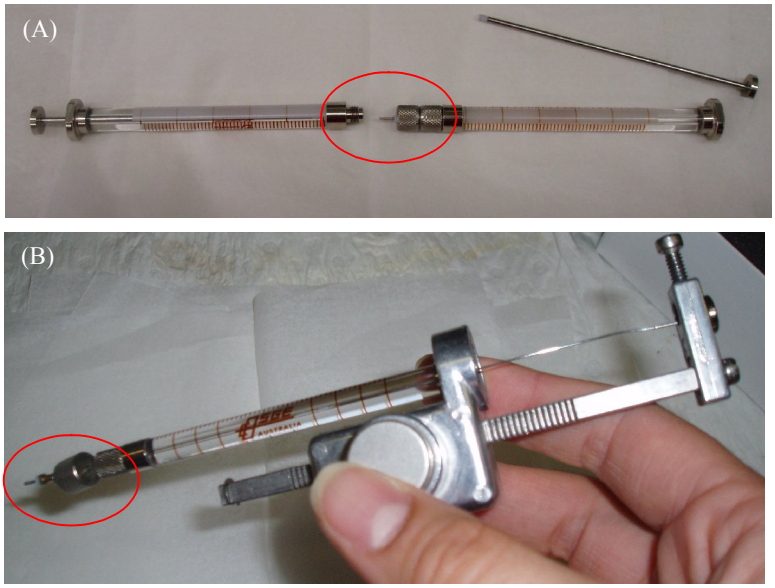

Figure 2. Apparatus for protein/*meso*-phase surfactant preparation. (A) Coupled Hamilton syringes, protein suspension is placed in one syringe and surfactant powder in the other, mixing of the two (through the coupler, circled) causes formation of the *meso* phase. (B) Hamilton nano-dispenser. Protein containing *meso* phase is transferred through a coupler at the dispensing end of the syringe (circled). 200nL drops can be dispensed.

The protein/surfactant mixture (0.2µL) was dispensed into each well. Precipitant (5µL) was immediately added and the well sealed as soon as all other wells in the 3x3 (or 1x5) grid were complete. For 96 well plates, the wells were sealed in sections of either one third or one half of the plate. Precipitant conditions were taken from the commercially available Crystal Screen^{TM}, Crystal Screen2^{TM} , PEG/Ion Screen, PEG/Ion 2 screen (Hampton Research) or PACT screen (Qiagen). All conditions were set up in duplicate. Plates were incubated at 20^{o}C.

Crystal wells were viewed with an Olympus SMZ12 stereomicroscope and were photographed using a Media cybernetics camera.

Modifications to the protein or surfactant

Modifications to either the His10$_C$H$_1$R suspension or the surfactant were carried out prior to preparation of the protein containing cubic phase.

For experiments containing cholesterol, 5% of the monoolein dry weight was replaced with cholesterol. The cholesterol was weighed into the same syringe as the monoolein. For

experiments containing $His6_N G\alpha_{i1}$ and $His10_C H_1 R$ the receptor (40µL, 5mg/mL) was mixed with the G-protein (10µL, 5mg/mL) and dialysed against 4 (50mL) changes of $H_1 R$ gel filtration buffer (20mM Bis Tris propane, 150mM NaCl, 30mM nOG, 10% (w/v) glycerol, pH7.4) containing Histamine (1mM) and GDP (10µM). The dialysis buffer was changed each hour for a total of 4 hours. Protein/surfactant cubic phase was then prepared at the ratio described in Table 1.

4.3.6. X-Ray diffraction analysis of crystals produced *in meso*

Crystals were removed and manipulated using tools from Hampton research. Where necessary these tools were used to remove all traces of surfactant from the crystal. Generally, cubic phase could be removed by transferring the crystal from the well to a fresh drop of the precipitant. The tools were then used to gently remove the attached cubic phase away from the crystals. For those crystals which had not grown in a condition containing a cryo-protectant (e.g. glycerol or PEG), the crystal was manipulated in a drop of the precipitant buffer with the addition of 20% (w/v) PEG. Crystals were mounted using CrystalCap Copper Magnetic™ based loops (Hampton Research) and placed into a stream of Nitrogen (≤100K, Figure 3A) directed onto the crystal stage/goniometer (Figure 3E) of the X-ray generator/detector. Crystals were analysed by X-ray either at CSIRO Molecular Health Technologies (CMHT), Parkville or at the Australian Synchrotron protein crystallography beamline.

X-ray diffraction at CSIRO MHT

For crystals screened by X-ray at CSIRO, a Rigaku RU-H2R generator and R-Axis IV detector were used (Figure 3). The Rigaku uses a rotating copper anode and a tungsten filament. The X-rays are focused using mirror optics to a 250 x 250µm beam. The X-ray generator was operated at 20mA and 40kV. At CSIRO Parkville the limit of diffraction is ~ 2.4 Å.

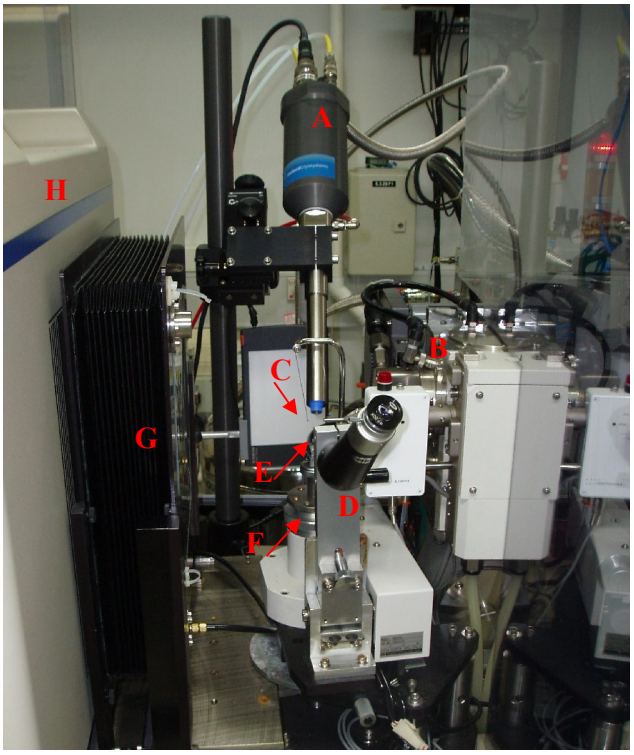

Figure 3. X-ray set up at CSIRO MHT Parkville. (A) "X-stream" Nitrogen stream (B) X-ray source (C) Backstop (D) Crystal viewing microscope (E) Magnetic crystal loop mount (F) Goniometer for aligning crystal in beam (G) Helium air scatter reducer (H) R-Axis imaging plates (detector).

Unless otherwise stated, the detector was set at 300mm from the crystal and oscillating crystal images (1^{o}) were collected over a period of 10 minutes.

X-ray diffraction at the Australian synchrotron

The Australian Synchrotron was officially opened in 2007 and is operated by the Australian Synchrotron Company (ASCo). The facility has the capacity for up to 30 beamlines, 4 of which are currently (December 2007) operating.

The 3BM1 protein crystallography beamline was used in this study. The Oxford Danfysik optics of the beamline are designed to produce a 250µm x 200µm monochromatic X-ray beam. The beam current was ~187mA. A Mar goniometer holds Hampton crystal cap magnetic loops and a Mar 165 charged coupled device (CCD) camera records diffracted X-rays. The user interface is provided by Blue-Ice software. The detector was placed 300mm

from the crystal and the crystal rotated 0.5^{o} over 10 seconds. The high beam intensity and rapid read-out from the CCD allowed for high-throughput screening of a large number of crystals (all salt or crystallised ligand) at the Australian synchrotron. At the Australian Synchrotron diffraction resolutions of ~0.9Å can be achieved.

4.3.7. His10$_C$H$_1$R lipid reconstitution and microdialysis for two-dimensional crystal trials.

The reported (and assumed) molecular weight for asolectin varies between ~740 to ~833gmol^{-1} (Fagan and Dewey, 1986; Niu, et al., 2002; Ratnala, et al., 2004). This variation is attributed to differences in fatty acid composition of the asolectin mixture. In this study the molecular weight of the lipid mixture was assumed to be 790gmol^{-1} (Niu, et al., 2002).

Purified His10$_C$H$_1$R (3.5mg/mL) in 'histamine gel filtration buffer' (described in chapter 3) was combined with asolectin (10mg/mL in histamine gel filtration buffer) to a final volume of 50µL. Several lipid:protein Molar ratios between 30:1 and 300:1 were trialed. The 50µL protein/lipid mixture was placed in a Slide-A-Lyzer mini-dialysis unit with a molecular weight cut-off of 10kDA (Pierce). Dialysis was performed against histamine gel filtration buffer which did not contain nOG, by one of two methods. Either the Slide-A-Lyzer was placed in a custom made dialysis plate and dialysed against histamine gel filtration buffer that did not contain nOG (1.5mL) and which was changed every 2 hours for a period of 10 hours followed by dialysis overnight. This process was repeated for a total of 2 overnight changes and a for a total of 3 days of dialysis. Following dialysis, the protein/lipid mixture was removed, placed in a 1.5mL tube (Eppindorf) and stored at room temperature until electron microscopy analysis. Alternatively, the Slide-A-Lyzer was placed in a beaker and dialysed overnight against 100mL of histamine gel filtration buffer. The following morning the buffer was changed every 3 hours for 9 hours. 98µL of protein/lipid mix was added to 2µL of the salt dodecyltrimethylammonium chloride (DTAC, 10mM stock, final concentration 200µM). The protein/lipid/DTAC mixture was left at room temperature until analysis by electron microscopy.

4.3.8. Sample preparation for electron microscopy and electron diffraction

Preparation of Carbon thin film

All mica and grid manipulations were carried out using tweezers and with gloved hands.

Mica (ProSciTech) was cleaved using adhesive tape to produce a clean, flat top layer. The mica was marked on one side with a permanent marker to designate the side which would not be coated with Carbon. Marked mica was placed on a glass microscope slide within a filter paper lined petri-dish which also contained a white tile, half of which was coated with vacuum sealing grease and a folded wedge of paper (Figure 4A). The tile and folded paper provide a visual measure of the thickness of the Carbon coating; the stronger the contrast between the grey Carbon layer and the white tile/paper the thicker the Carbon coating. The Petri-dish was placed into a Carbon coating chamber (Auto 306, Boc Edwards). Carbon coating was carried out under a 10^{-6} Torr vacuum with the current in the system being increased until Carbon evaporation became visible (dependent on carbon rods). The current was removed when the desired thickness of Carbon was obtained. Correct carbon thickness was determined by the comparing the darkness of the carbon coated area of the tile with previously prepared thin film carbon. For electron microscopy the sample thickness, which includes the grid thickness, should not be more than ~100nm.

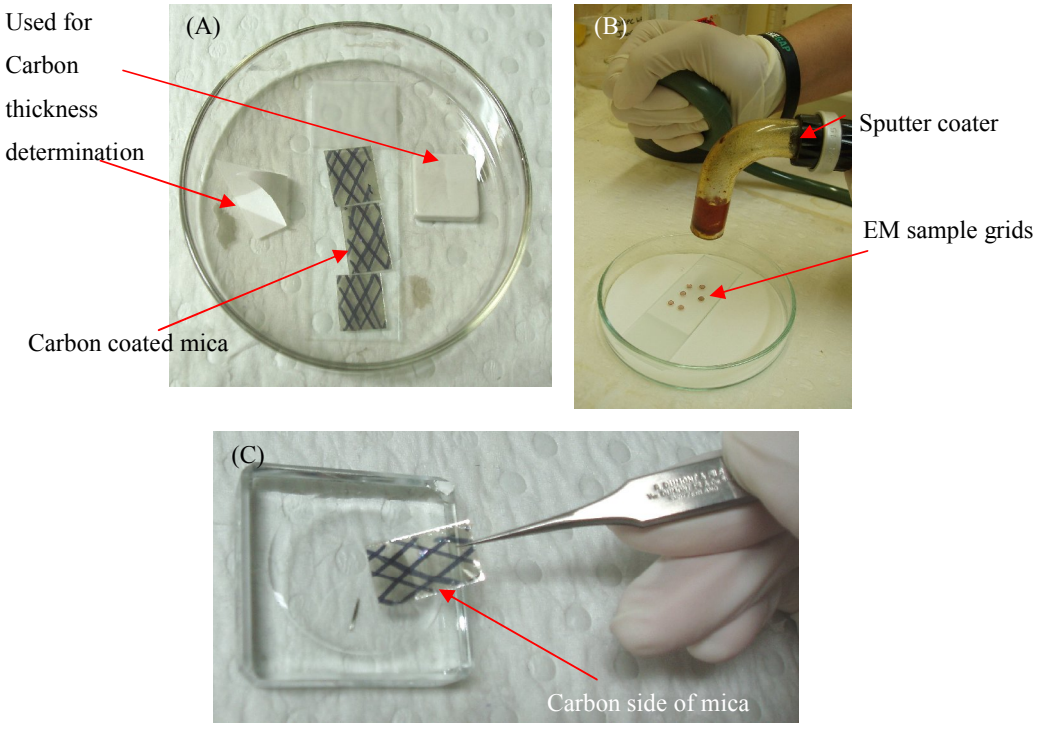

Figure 4. Images of apparatus used for preparation of carbon thin film coated electron microscopy (EM) grids. (A) set up for preparation of thin film carbon on mica. (B) coating of EM grids with neopropene. (C) preparation of floating thin film carbon on water reverse meniscus.

Preparation of carbon coated grids

400 mesh hexagonal carbon grids (ProSciTech), were placed in a single layer, with the shiney side down (this allows easier determination of which is the carbon face of the grid after carbon coating) onto a glass microscope slide. A hand pumped sputter coater was used to apply a thin layer of neopropene (5% v/v in toluene) to the grids (Figure 4B). The neopropene provides an adhesive for attachment of thin film carbon to the grid. 0.5mL of neopropene/toluene was sufficient to coat 15 to 20 grids. Freshly prepared mQH_2O was used to create a reverse meniscus in a small glass dish. Carbon coated mica was cut to a size approximately 15x that of a grid. With the carbon side up (facing away from the water), the mica was angled to the water such that when slowly placed through the meniscus the carbon layer detached from the mica and floated on the water surface (Figure 4C). A grid was griped with tweezers (shiny side away from the water), gently pressed into the floating carbon film, submerged and then rotated in the water such that the carbon face of the grid was now facing up. The carbon coated grid was placed carbon side up onto filter paper, covered with an up-turned Petri dish and allowed to dry before use. Dried carbon coated grids were stored in a grid box until use.

Preparation of uranyl acetate (negative) stained samples.

A carbon coated grid was held carbon face up using clamped tweezers. Protein sample (4µL) was pipetted onto the grid and adsorbed for 30 seconds, after which time filter paper was used to gently draw off the excess volume of sample by capillary action. $sMQH_2O$ (5µL) was pipetted onto the grid and drawn off after 20 seconds. This was followed by 5µL of uranyl acetate (2% w/v, centrifuged to produce a transparent supernatent) which was drawn off after 30 seconds. Grids (held in tweezers) were covered with an up-turned Petri dish and dried for at least 20 minutes before imaging.

Preparation of samples for cryo-electron microscopy

50µL drops of trehalose (1.5% w/v) were placed onto a strip of parafilm. A carbon coated grid was placed, carbon-side down into 3 sequential drops of the sugar. 2.5µL of the protein/lipid sample was pipetted onto the grid and adsorbed for 30 seconds before removal of excess sample by blotting with the edge of a filter paper. The grid was submerged into liquid Nitrogen within the cryo-stage (Gaton) and then, whilst remaining submerged in the liquid Nitrogen, was placed into the grid-holder of the cryo-stage. Care

was taken both when preparing samples for cryo-EM and when transferring sample grids to the EM. Once frozen at -173^{o}C, the temperature of the sample was not increased above -173^{o}C since even slight heating of the sample will lead to frosting which will decrease the quality of imaging.

4.3.9. Electron Microscopy and Electron Diffraction

Samples were imaged on a Technai 12 electron microscope (EM) equipped with a tungsten filament, a single tilt cryo-transfer system and a Megaview III soft imaging system (camera). The microscope was operated at 120kV. All samples were imaged using low dose mode.

Low dose image settings

In low dose mode, the grid is searched at low magnification and low beam intensity. On location of an area of interest the 'focus' option is selected allowing the beam to be focused (at high magnification) on an area of the grid which is away from the area of interest. Finally 'exposure' is selected and the original area is located and imaged at high magnification. The use of low dose limits damage to the crystal of interest by the electron beam. For this study the low dose settings were (generally) as follows: Search – 4,400x magnification, spot size 4 (spot size is a measure of beam intensity, the smaller the spot size the more intense the beam); Focus – sample was moved by 2µm and focused at magnification of 67,000x and a spot size of 4; Exposure – sample was returned to the area found in search mode and imaged at a magnification of 67,000x and a spot size of 4. Images of crystals and electron diffraction patterns were collected on electron image film (Estar thick base, Kodak) to enable future processing of the crystals. For recording crystal images on film, the exposure time was one second and for recording electron diffraction patterns on film the exposure time was 10 seconds. An image of the 2D crystal was recorded on film prior to observation of electron diffraction since it is the EM images that are used for phase determination (i.e. future analysis) and the intensity of the beam used for electron diffraction rapidly damages the crystal. For reporting purposes some crystals images were recorded using the MegaviewIII camera of the EM.

Development and scanning of EM film

Films were placed in developer (D19 developer, Kodak) for 12 minutes, washed in reverse osmosis (RO) water for 1.5 minutes and then placed in fixer (Photo-Flo 200 solution,

Kodak) for 2.5 minutes. Films were washed in running RO water for 20 minutes and then dried at room temperature overnight. Digital images of the films were prepared by scanning using either a Nikon Super Coolscan 8000 ED (for some crystal images, scans are suitable for further processing) or a Hewlett Packard Scanjet 5370C scanner (for diffraction images and/or reporting purposes only).

4.4. Results

4.4.1. Home-made crystallization plates for *in meso* crystallisation

Custom made crystallisation plates (Figure 5A, B and D) were a requirement for visualisation of the *in meso* crystallisation trials since the lipidic/protein drop (and the crystal formation within it) can not be easily visualised using traditional plastic crystallisation plates (Figure 5C). The glass plates were routinely used for both precipitant screening and crystal growth.

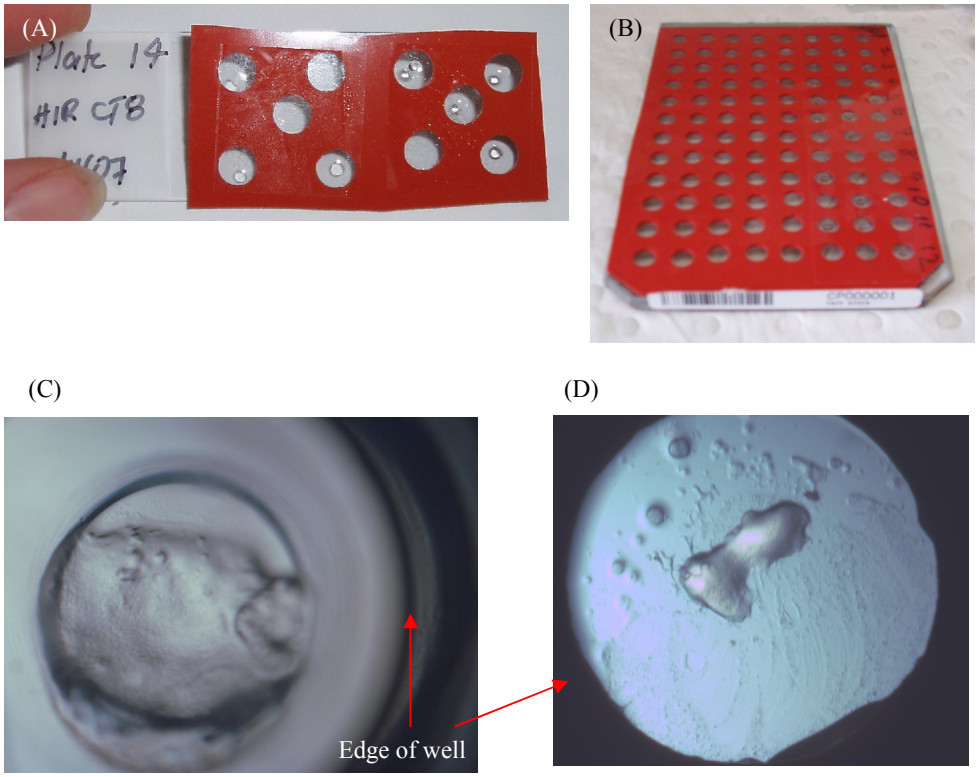

Figure 5. Images of custom made crystallisation plates and comparison to commercially available plastic plates. (A) 10 well glass plate for small scale *in meso* crystallisation trials. (B) 96 well plate for high-throughput crystallisation trials. Plates can be barcoded and used in automated crystal screening (CrystalTrak). (C) *In meso* crystallisation condition in a plastic plate. (D) *In meso* crystallisation condition in custom made glass plates.

Initially glass microscope slide crystallisation plates (e.g. Figure 5A) were prepared with two 3x3 grids of wells (i.e. 18 wells, not shown) and were sealed with glass coverslips. These plates suffered from movement of the rubber and subsequent mixing of precipitant conditions. For this reason the number of wells was optimised from 18 wells to 10 (5mm) wells per plate, five under each glass coverslip (Figure 5A). This substantially reduced movement of the rubber, buffer interaction between the wells and decreased drying out of the plates. When removing crystals for X-ray analysis, attempts to cut the glass coverslip around the well of interest (and so not disturb other wells) were generally unsuccessful and resulted in opening of other wells and contamination with glass fragments. Thus routinely the entire glass coverslip was removed, which of course meant that the other five wells under the coverslip were compromised. To increase the speed at which crystallisation trials could be performed (and for future work), 96 well plates were produced by Dr Connie Darmanin (CSIRO Parkville, Figure 5B). When sealed with either transparent packing tape or a plastic plate seal, the wells in the 96-well plate remained hydrated for weeks. Wells could be opened easily by simple cutting of the tape and so these plates offered a further advantage over the smaller plates in that individual wells could be opened to remove crystals. In addition, these plates could be bar-coded and used with the automated imaging system CrystalTrak (Rigaku).

4.4.2. Visualising Crystals

Traditional vapour diffusion crystallisation generally produces clearly distinguishable crystals (Figure 6A). *In meso* crystallisation conditions require a more thorough examination when looking for crystals. It is expected that protein crystals would be present in or around the cubic phase. When viewing *in meso* crystallisation conditions in the first few days after set up, generally, the surfactant/protein mixture is clearly visible (Figure 6B). With time, the morphology of the mixture may change and in some cases it appears that the cubic phase is diffusing into the precipitant (Figure 6C). This may represent a change of phase of the surfactant from the cubic or mesophase to the lamellar phase as the wells lose moisture (particularly for the smaller crystallisation plates which did not seal very well).

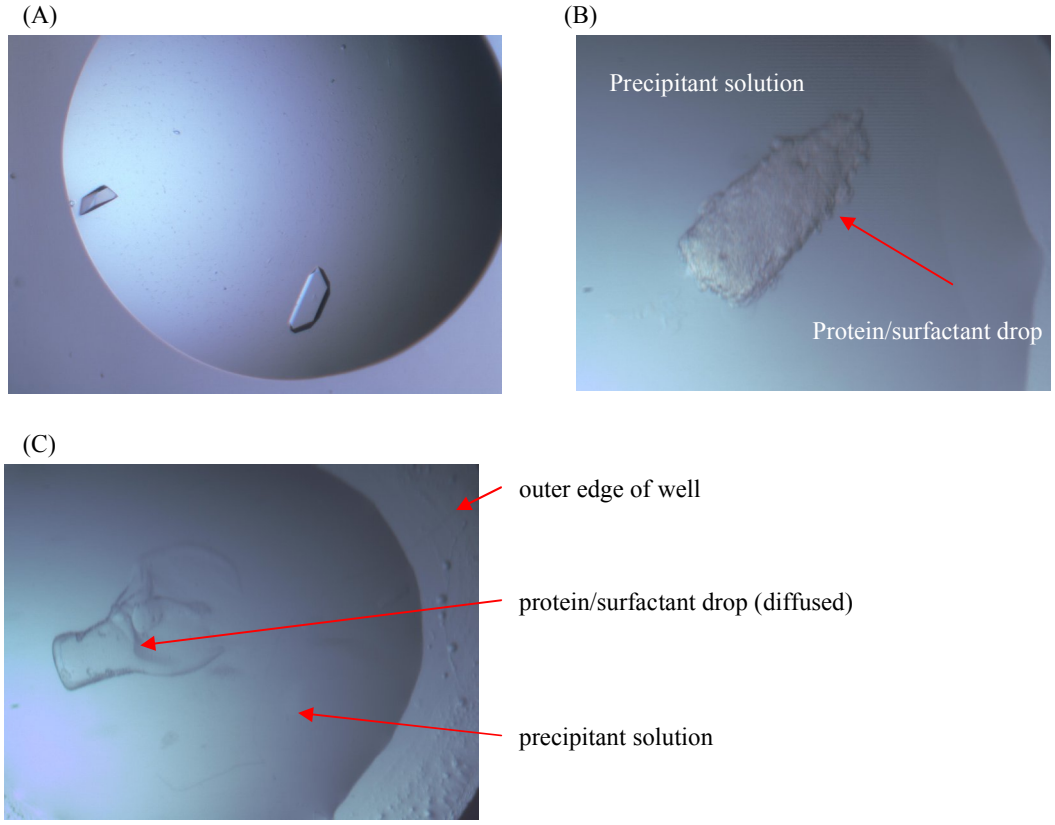

Figure 6. Digital camera images of *in meso* crystallisation trials. (A) antibody/antigen complex crystal produced under vapor diffusion conditions. Image was provided by Dr Janet Newman (CSIRO). (B) Condensed monoolein/His10$_C$H$_1$R drop, 30x magnification. (C) Diffused monoolein/His10$_C$H$_1$R drop, 30x magnification.

In the absence of an ultra violet microscope and with ready access to an X-ray generator, X-ray analysis was used to determine the identity of crystals produced in this study. Salt crystals produce easily recognisable diffraction patterns which are characterised by diffraction spots at high resolution and reflections which appeared smeared in the diffraction pattern (Figure 7).

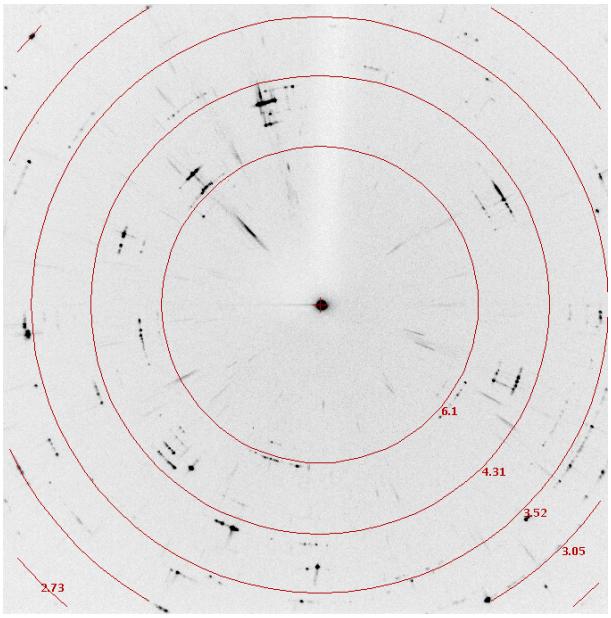

Figure 7. Image of X-ray diffraction from a salt crystal. The red rings denote the resolution in Å.

4.4.3. Conditions that produced interesting three-dimensional crystals

In the absence of an X-ray diffraction pattern 'interesting' crystals are just that – interesting; they might be protein, they might not. The crystals discussed in this section are those which still have a question mark associated with them. This may be due to either limited time meaning crystal conditions were not repeated/optimised, an inability to replicate conditions which initially produced crystals, or an inability to successfully transfer crystals to the X-ray stage (for particularly fragile/environment sensitive crystals). A total of 13 small scale (generally ≤ 48 conditions, in duplicate) $His10_CH_1R$ crystallisation trials were set up during this study. From a total of 3 cubic phases, 3 additives and 288 crystallisation buffers, approximately 784 conditions were trialled. Two cubic phase surfactants are discussed in this chapter – monoolein and phytantriol. A 3rd surfactant synthesised at CSIRO was also used but will not be discussed here due both to confidentiality issues and its failure to produce protein crystals which diffracted X-rays. Cholesterol, $His6_NG\alpha_{i1}$ and a monoclonal anti-H_1R antibody were used as additives in crystallisation trials. Crystallisation with the antibody will not be discussed here as it did not result in protein crystals. X-ray analysis demonstrated that greater than 90% of the crystals that formed from under the conditions tested in this study were salt. The crystals discussed in this section represent those that could not be definitively classified as salt crystals.

A combination of H_1R and the surfactant monoolein (MO) with 0.2M magnesium chloride, 0.1M HEPES (sodium salt) pH7.5 and 30% (w/v) PEG400 (Hampton Crystal Screen 1, condition 23) resulted in the growth of a crystal at between 25 and 37 days after set up (Figure 8, A1). The 180 x 216µm crystal was not visible at 40 days after set up and so was not analysed by X-ray. A repeat of this condition produced crystals of different morphology (Figure 8, A2 and A3) at between 15 and 20 days after set up. These crystals showed the diffraction pattern of a small molecule (salt, results not shown).

A precipitant condition of 0.1M HEPES pH7.5 and 20% (w/v) PEG 10K (Hampton Crystal Screen 2, condition 38) with the H_1R/MO cubic phase produced long thin crystals within 7 days of set up (Figure 8, B1 and B2). Unfortunately the crystals were particularly fragile and rapidly disintegrated when the well was unsealed and so were not analysed by X-rays. The HEPES/PEG condition was of particular interest since the precipitation buffer did not contain salt. Furthermore a similar precipitant buffer produced crystals (Figure 8C) of slightly different morphology but with the same instability. A combination of H_1R/MO, HEPES pH7.5, 10% (w/v) PEG8K and 8% (w/v) ethylene glycol (Hampton Crystal Screen 2, condition 37) resulted in the crystals presented in Figure 8C. The crystals had formed on the edge of what appeared to be diffused cubic phase surfactant. These crystals were also unstable and were not analysed by X-ray. The instability of crystals grown in the HEPES/PEG conditions to the atmospheric environment is interesting since generally such instability would be associated with inclusion of a volatile substance in the crystallisation condition. In future work these HEPES conditions should be optimised. Additives such as a sugar (e.g. trehalose) or a low concentration of salt may aid in the stability of the crystals. Alternatively the temperature of the crystallisation could be modified to bring about different cubic phase structures which may better fit/arrange the receptor. In addition to increasing the stability of the crystals, the precipitant needs to be optimised to promote larger crystals. The crystals presented in Figure 8B and 8C are particularly thin (<10µm) and would be difficult to manipulate. Furthermore, the ratio of X-ray beam size to crystal size would generate a low signal-to-noise ratio and may prevent observation of the X-ray diffraction from the crystal when the thin edge of the crystal is perpendicular to the X-ray beam.

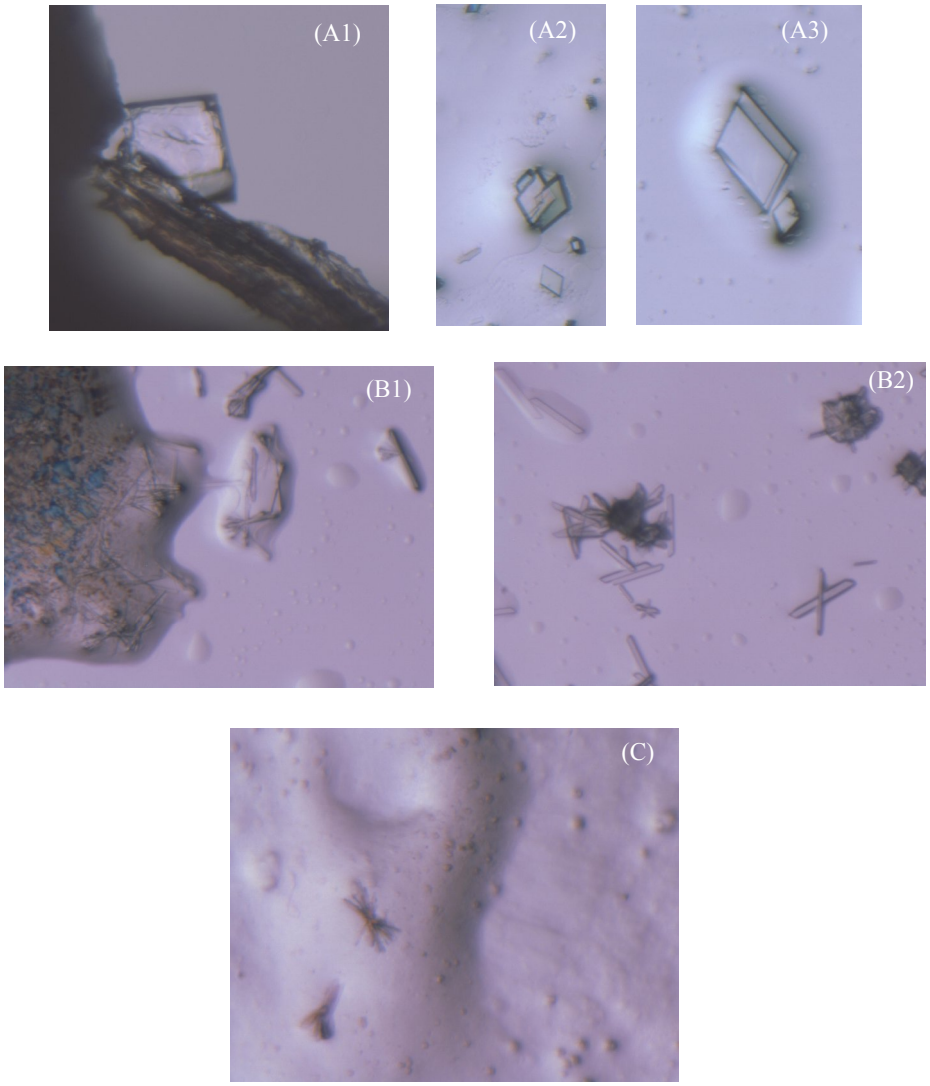

Figure 8. Images of 'interesting' crystals produced in this study. Unless otherwise stated, all images were taken at magnification of 144x
(A) Crystals formed in the presence of H_1R/MO, Mg, HEPES and PEG; (1) The crystal appeared between 25 and 37 days post set up and disappeared at day 40. (2) and (3) a repeat of the condition used to produce (1), crystals appeared between 15 and 20 days post set up.
(B) Crystals formed in the presence of H_1R/MO, HEPES and PEG; (1) and (2) The crystals appeared between 1 and 7 days of set up but were unstable when removed from the cubic phase.
(C) Crystals formed in the presence of HEPES, PEG and ethylene glycol. Crystals were formed within 7 days of set up.

Following the publication of the β_2-adrenergic receptor structure, the addition of cholesterol to the crystallisation conditions was trialled (Cherezov, et al., 2007). A mixture of His10$_C$H$_1$R/MO cubic phase, cholesterol and a screen using Qiagen PACT precipitants resulted in formation of crystals in the presence of 0.2M sodium malonate, 0.1M Bis Tris propane pH8.5, 20% (w/v) PEG3350 (PACT, condition 84, Figure 9, A1 and A2). The cubic crystals of ~30x30µm formed on and around the protein containing cubic phase,

making them of interest. Using the X-ray generator at CSIRO MHT, no X-ray diffraction pattern was observed for these crystals. It may be that these crystals are formed by disordered packing of the receptor. Given the large flexible regions of the receptor, such as the third intracellular loop, there is the likelihood for disordered crystalline packing; (this is discussed further at the end of this section). Alternatively, the crystals in Figure 9A are salt crystals. Given the highly defined structure of the crystals (near perfect cubes) salt crystals are probably more likely.

In addition to monolein, the surfactant phytantriol was also used in (separate) crystallisation trials with the His10$_C$H$_1$R in combination with the Hampton PEG/Ion screens. A combination of His10$_C$H$_1$R, phytantriol, 8% (w/v) tacsimate and 20% (w/v) PEG3350 (Hampton PEG/Ion 2 screen, condition 16) produced small cubic crystals. These crystals were less than 9x9 μm in dimension and were present on and within the cubic phase (Figure 9, B1 and B2).

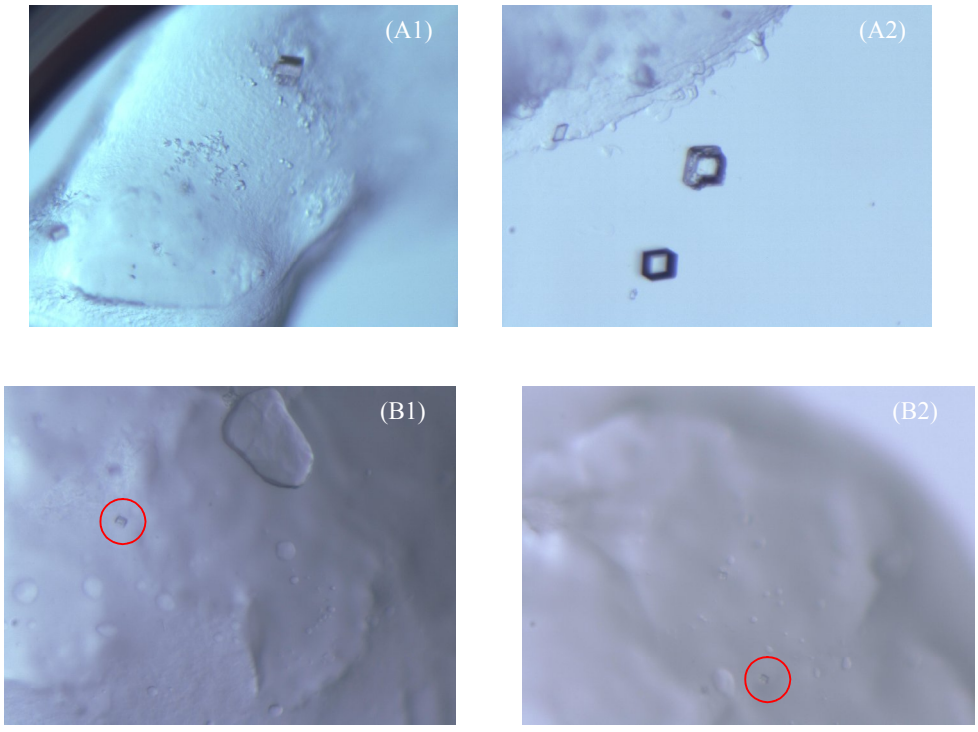

Figure 9. Images of 'interesting' crystals produced in this study. Unless otherwise stated, all images were taken at magnification of 144x.
(A1 and A2) Crystals formed in the presence sodium malonate, bis-tris propane and PEG. The cubic crystals were formed within 4 days of set up.
(B1 and B2) Crystals formed in the presence of tacsimate and PEG. The crystals were cubic and <9μm^2 in dimensions, here they are circled. The crystals could not be separated from the cubic phase.

The crystals shown in Figure 9B, formed between 1 and 10 days after crystallisation set up but an attempt to remove them from the cubic phase at 14 days was not successful. The crystals were not stable in the precipitant solution alone (i.e. in the absence of cubic phase), and due to their small size, were difficult remove from the cubic phase using tools alone. Stability of these crystals may be increased by modification of the precipitant conditions (for example by changing the pH). However, even if the crystals had been successfully removed it is unlikely that diffraction would have been observed since the size of the beam (250 x 250 μm) is significantly larger than the crystal and so the signal-to-noise ratio would be low. Crystals of this size require an X-ray beam that is focused to orders of magnitudes less than 10μm (for example the European Synchrotron Radiation Facility has an X-ray beam that can be focused to ~ 1x1 μm).

Encouragingly, all of the crystals shown in Figures 8 and 9 formed under conditions which are favourable for retention of protein functionality i.e. at pH 7.5 – 8.5 and in the presence of the precipitant PEG. However, whilst the crystals just discussed were not assigned as salt crystals, they are not definitely protein crystals either. Accordingly, in future experiments it may be more beneficial to determine if the crystal contains protein through methods other than X-ray diffraction, such as through use of ultra violet microscope, assessing the birefringence of the crystal or through protein staining. The first essential requirement for three-dimensional crystallisation of a protein is a high-quality preparation of the protein. The protein must be at least 90% pure and, regardless of other minor contaminants, the protein itself should be homogeneous i.e. without glycosylation, aggregation or existence of a mixed monomer/dimer population. Glycosylation was not apparent during purification of the $His10_CH_1R$ (although the occasional presence of a band at a slightly higher molecular weight than the $His10_CH_1R$ may still be of interest in that regard), nor was it reported by Ratnala, et al., (2004). It is possible that the receptor is present as dimers or other higher order aggregates in the detergent suspension. This is particularly the case since a definitive value for the % of functional protein in the final purified sample was not determined and non-functional protein may aggregate. Dynamic light scattering experiments may have proved useful in this regard, but were not completed during this study. In addition to purity and functionality of the protein, the structure of the protein itself plays an important factor in its ability to be crystallised. The H_1 histamine receptor, like many class A 7TMRs, has an extensive third intracellular loop which spans amino acids 211 to 418 of the 487 amino acid protein. The flexibility in the third

intracellular loop of the protein would be a hindrance to the ordered packing of the protein into a crystalline form and could be an explanation as to why some crystals produced in this study did not diffract. One recently published structure of the β_2 adrenergic receptor (β_2AR) replaced the third intracellular loop of the receptor with the lysozyme sequence (Cherezov, et al., 2007). Rasmussen, et al., (2007) removed 48 residues of the β_2AR C terminus to decrease flexibility associated with this region and stabilised other parts of the receptor using antibody fragments. Whilst structures lacking particular regions remain relevant and are most certainly a major achievement, the third intracellular loop of the receptor (for example) is known to be involved in Gα coupling and may have as yet undiscovered roles in receptor/G-protein interaction (Gether, 2000). Although regions of the receptor can be removed, the ideal (though ambitious) goal would be to have the complete receptor structure. If the complete receptor is to be crystallised, co-crystallisation with a receptor stabilising agent/protein is a likely requisite. The cubic phase is particularly amenable to co-crystallisation since the lipid surrounded aqueous channels in the cubic phase would provide the perfect environment for the intracellular, membrane associated G-proteins. In fact, activation of transducin by rhodopsin in the cubic phase has been demonstrated (Navarro, et al., 2002).

4.4.4. Powder diffraction of micro-crystals

In an attempt to stabilize the flexible intracellular loops of the $His10_CH_1R$, crystallisation was trialed in the presence of $His6_NG\alpha_{i1}$ a known interaction partner of the receptor (chapter 3, section 3.4.3). The protein mixture was combined with the H_1R agonist histamine and the $G\alpha_{i1}$ binding partner GDP. It was hypothesized that inclusion of the agonist (at mM amounts, in an attempt to out compete triprolidine) may prompt interaction of the receptor with the G-protein whilst the presence of GDP would retain the Gα in an inactive state and thus prevent its dissociation from the receptor. However, this dynamic interaction was only hypothetical and in future studies it would be necessary to determine if the 7TMR/Gα form a stable complex under these conditions. This could be achieved by gel filtration of the mixture – a stable complex should elute from the column as a single peak. $His10_CH_1R$ was used in a Molar excess (4:1) to $His6_NG\alpha_{i1}$ to try and reduce the possibility of the G-protein crystallising alone. Prior to inclusion in the crystallisation trial, $G\alpha_{i1}$ required additional purification (see chapter 3, Figure 1). $G\alpha_{i1}$ was purified to homogeneity, as determined by silver stained SDS-PAGE, using GF-HPLC (Figure 10).

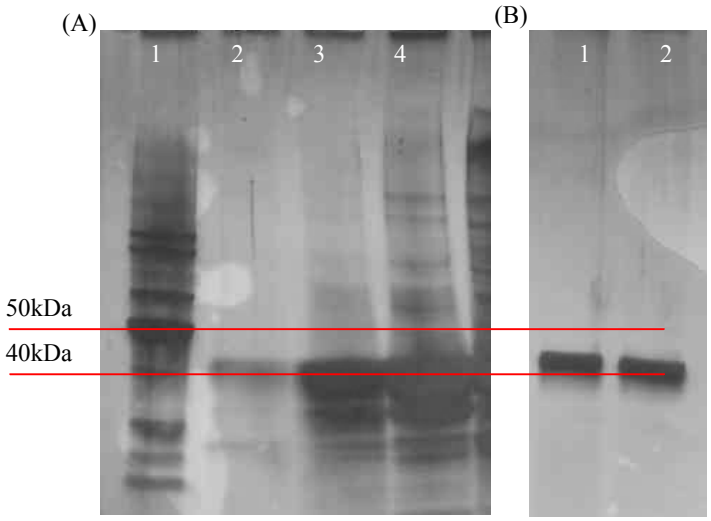

Figure 10. Silver stained SDS-PAGE gels of $His6_NG\alpha_{i1}$. (A) Lane Descriptions: 1 – BenchMark Marker (2µL, Invitrogen); 2-4 – IMAC purified $His6_NG\alpha_{i1}$ fractions. (B) Lane Descriptions: 1-2 – GF-HPLC purified $His6_NG\alpha_{i1}$ from IMAC fractions of the protein.

The protein/monoolein mixture was combined with precipitants from the Qiagen PACT screen. Sharp, thin bunches of crystals were formed within 3 days (Figure 11A) of crystallisation set up and grew for up to 3 weeks (Figure 11B). The crystals formed in the presence of 0.2M sodium sulphate, 0.1M Bis Tris propane pH7.5 and 20% (w/v) PEG3350 (Qiagen PACT, condition 80).

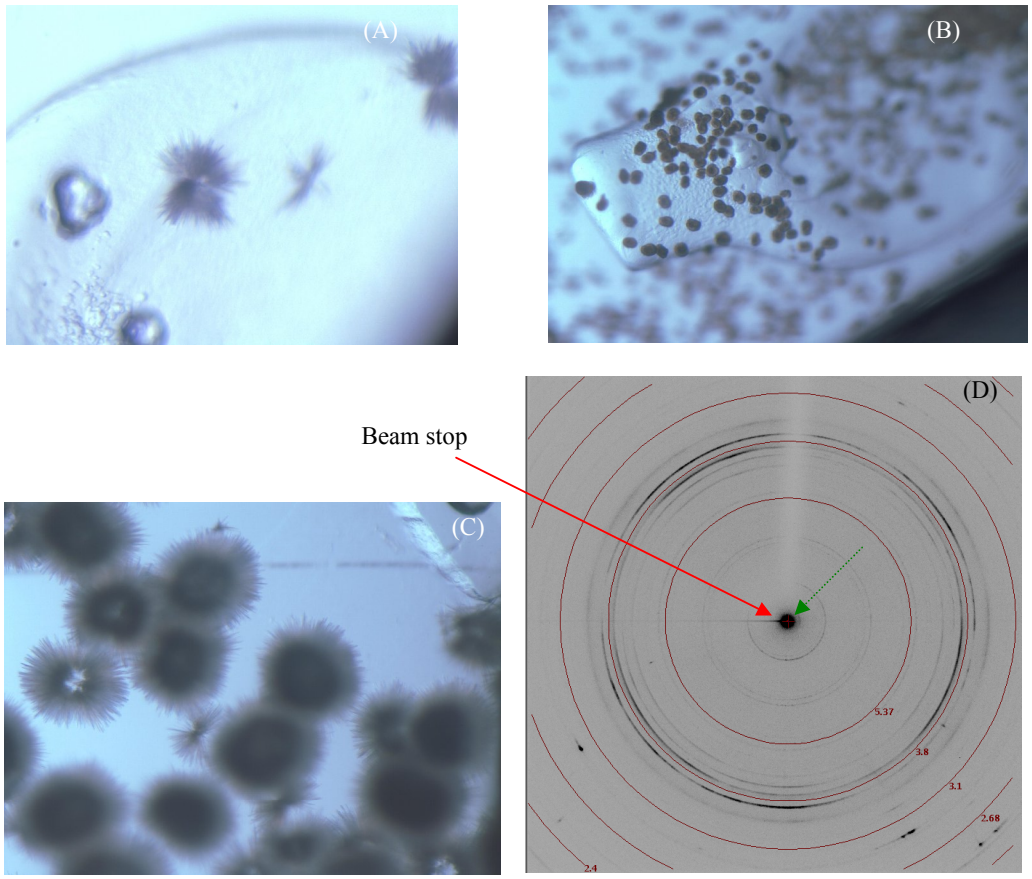

Figure 11. X-ray diffracting crystals formed in the presence of sodium sulphate, bis tris propane and PEG. (A) Beginning of crystal growth occurred within 3 days of set up. The image was taken at a magnification of 144x (B) Mature crystals at 3 weeks after set up. The image was taken at a magnification of 64x. (C) Mature crystals at 3 weeks after set up. The image was taken at a magnification of 144x. (D) X-ray diffraction of a bunch of the micro-crystals, the detector distance was 250mm and the crystals were rotated 1^{o} in the X-ray beam, over a period of 10 minutes

A bunch of these crystals was collected in a 75µm loop and analysed by X-ray (Figure 11D). Several rings, at high (< 5Å) and low resolutions (>17Å) were visible in the X-ray diffraction image. Rings are observed, as opposed to diffraction spots, since there is more than one crystal in the X-ray beam and so a powder diffraction pattern is produced. Rings appearing near the beam stop (Figure 11D green-dashed arrow) appear at a resolution of ~50Å. An attempt to index the data using powder diffraction software failed due to an inability to resolve the low resolution diffraction. Since the 50Å data was not included in the indexing the unit cell size could not be accurately calculated. Powder diffraction analysis would require oscillation of the crystal during the diffraction experiment and a large distance between the crystal and the detector to enable collection of the low angle

diffraction data. Ideally a synchrotron powder diffraction beamline would be used. These experiments are currently being investigated.

It was quite possible that the Gα protein would crystallise independently of the receptor but interestingly, when the same crystallisation conditions were repeated in the absence of receptor, no crystals formed. It is encouraging that these crystals formed under similar conditions to β_2AR – which were grown from a monoolein cubic phase (containing cholesterol) in the presence of 0.1M Bis-Tris propane pH6.5-7.5, 0.1-0.2M sodium sulphate, 30-35% (w/v) PEG400 and 5-7% (v/v) 1,4-butanediol. The next step would be to try and optimise the crystallisation/precipitant conditions such that single crystals are formed. Unfortunately this crystallisation trial used the last stock of receptor produced in this study and so the condition could not be repeated within the required time frame of this study. Following submission of this thesis, optimisation of the crystallisation condition may be attempted. However, whilst the results presented in Figure 11 are encouraging they are, once again, preliminary.

Concurrently with three dimensional *in meso* crystallisation trials, two-dimensional crystal trials were also being conducted with the $His10_CH_1R$.

4.4.5. Reconstitution of $His10_CH_1R$ into asolectin and formation of two dimensional crystals

Asolectin is a commercially available lipid mixture consisting of saturated fatty acids (24%), mono-unsaturated fatty acids (14%) and poly-unsaturated fatty acids (62%). Reconstitution of the $His10_CH_1R$ into asolectin for use in functional and nuclear magnetic resonance studies has been previously reported (Ratnala, et al., 2004) and for this reason it was selected for preliminary two-dimensional crystal trials. Electron diffracting crystals were formed under two conditions; either at a lipid:protein molar ratio of between 40:1 and 60:1 (0.65 and 0.8 ratio, w/w) prepared using dialysis method 1, in the absence of DTAC (Figure 12A). Or at a lipid:protein molar ratio of 180:1 when detergent removal was rapid and DTAC was added following membrane reconstitution of the protein (Figure 12B). The salt DTAC is a precipitant and has been used in two dimensional crystallisation of bacteriorhodopsin (Michel, et al., 1980).

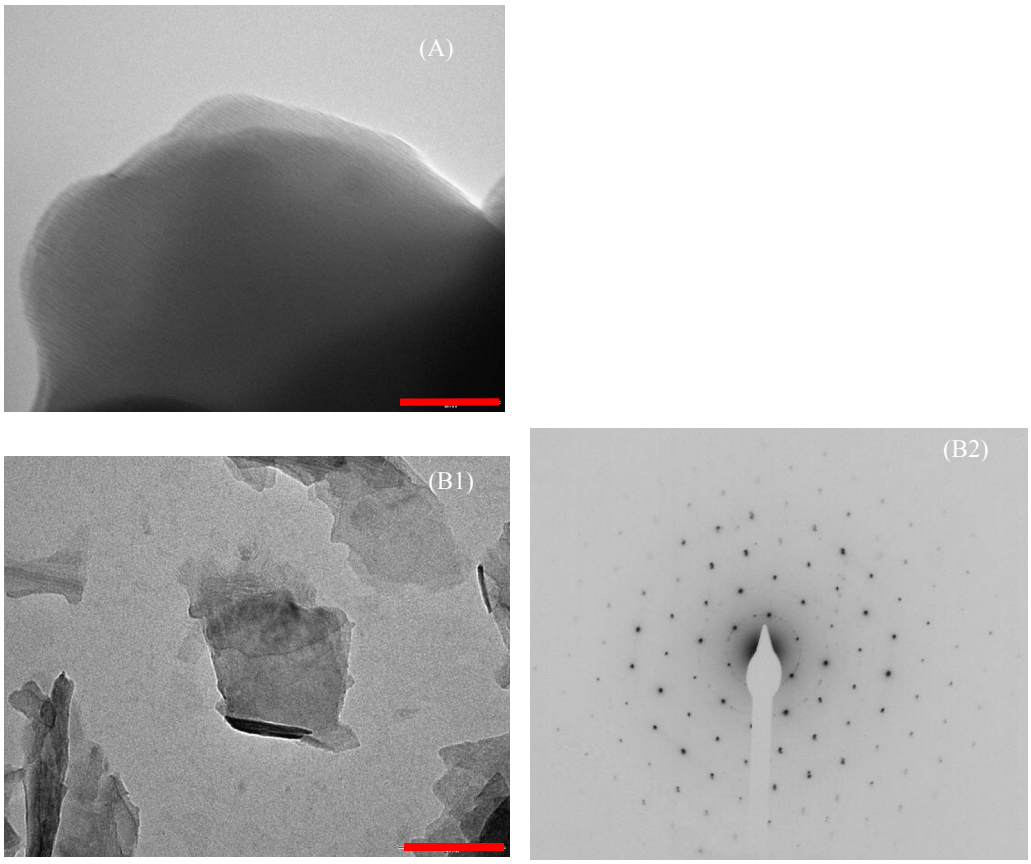

Figure 12. Electron microscopy images of two-dimensional crystals formed in the presence of $His10_CH_1R$/asolectin and, unless otherwise stated, DTAC.
(A) cryo-EM image of crystal prepared by dialysis in the absence of DTAC, scale bar = 5nm.
(B) Image of electron diffracting crystal; (1) Negatively stained two dimensional crystal, 97,000x magnification, scale bar (red) =200nm; (2) Electron diffraction of (B), 720mm camera distance, 10 second exposure time, scale bar = $6nm^{-1}$. The approximate distance from the centre of the beam to the outer diffraction spots is 0.15nm, or 1.5Å.

All subsequent crystals presented here were formed using DTAC addition to asolectin reconstituted $His10_CH_1R$. In separate work by another member of the laboratory (Dr Priya Bhakat, CSIRO), crystals were formed using lipid reconstitution only, without the presence of DTAC.

The two-dimensional crystals were observed between 4 and 14 days post set-up (Figure 13, A and B). $His10_CH_1R$/asolectin/DTAC samples collected and observed more than 14 days after crystallisation set up showed an overall decrease in the number of crystals which exhibited strong electron diffraction (Figure 14, A1 and A2). This suggests that the crystals were not stable for extended periods of time.

The predominant diffraction pattern observed reflected a hexagonal lattice for the crystals (Figures 12 and 13). However other diffraction patterns were also observed as shown in Figure 14 B2. In addition to the observation of different diffraction patterns, some areas which were clearly lipidic did not diffract (Figure 14C). On some crystals the hexagonal diffraction spots were visible to 4.5Å (Figure 12 B2) suggesting a highly ordered array within the crystal. At high magnifications (> 110,000x) some crystals had visible periodicity (lines in the image), which may represent the crystal lattice (Figure 13, B1). However greater than 90% of diffracting crystals were multilayered and did not give a defined diffraction pattern (Figure 12 and 13). Phase determination from 2D crystals requires excellent image collection – this means images of single layer crystals at a magnification of 60-70,000x. The formation of single layer crystals in suspension may be difficult due to the tendency for lipids to aggregate in solution. An alternative is to conduct 2D crystallisation on a surface (by lipid bilayer immobilisation), but this requires precise spacing of the tethered bilayer from the surface and may limit the conformations available to the protein thus hindering crystallisation further. Single layer crystals may be favoured by variation in the protein:lipid ratio, the type of lipid used, or alternatively, by changing the sample preparation method. Treatment of the EM grid surface using glow discharge prior to adsorbtion of the sample may aid in the preparation of single crystals. Whilst four good 2D crystal images are enough to determine a phase projection map for the protein, thousands of images may be screened before images of sufficient quality are discovered. In this regard it is useful, if not essential, to have access to an optical diffractometer which is used to direct a laser beam through the film image of the 2D crystal in order to determine its quality, (i.e. a well ordered, well imaged crystal recorded will be useful for phase determination if the film image of it diffracts the laser beam). Such a diffractometer was not available during this study.

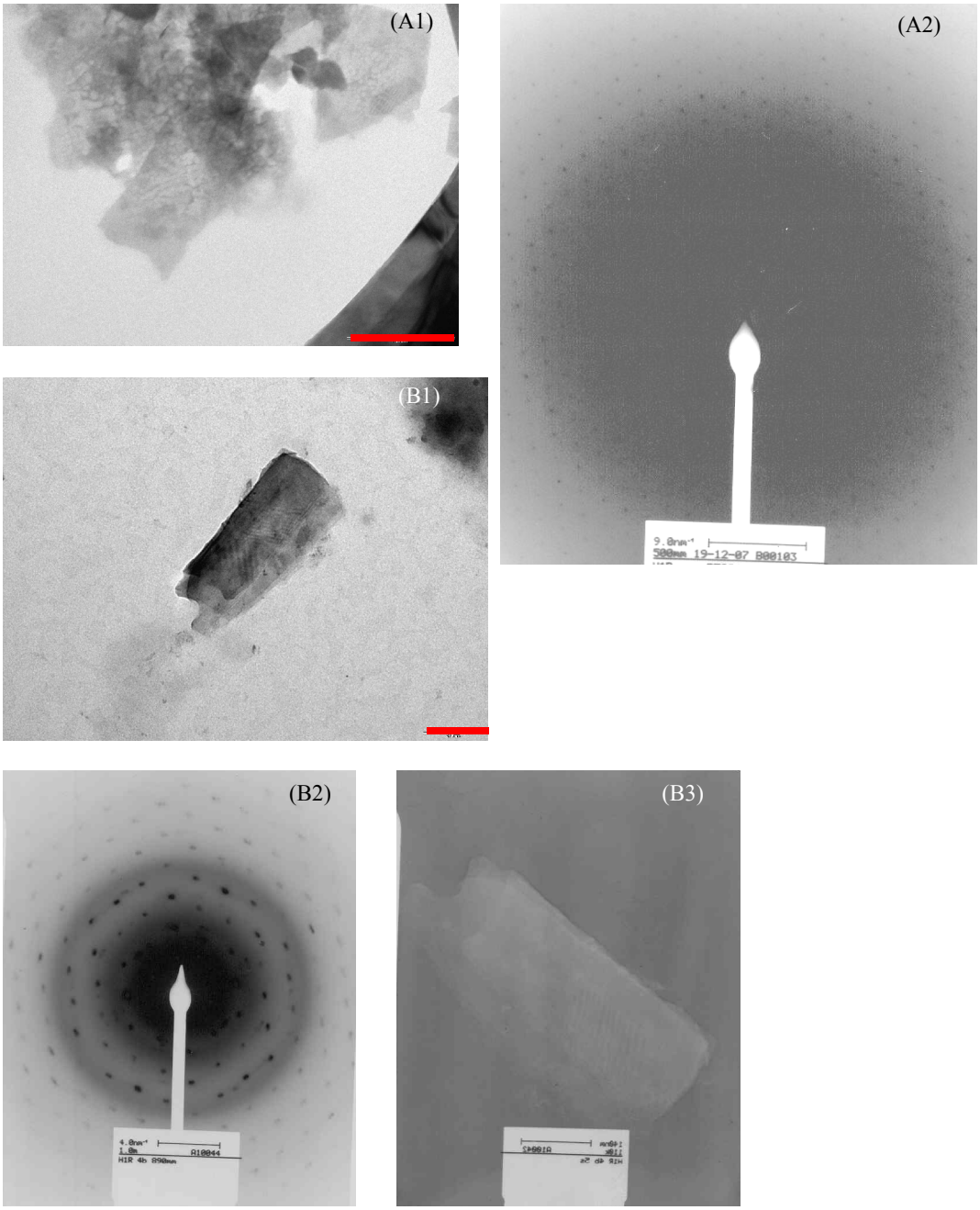

Figure 13. Electron microscopy and electron diffraction images for two-dimensional crystals formed in the presence of $His10_CH_1R$/asolectin and DTAC.
(A) cryo-EM prepared sample imaged 5 days after crystallisation set up; (1) two-dimensional crystal, 52,000x magnification, scale bar = 500nm; (2) electron diffraction of (1) d = 500mm, scale bar = $9nm^{-1}$.
(B) Negatively stained sample imaged 4 days after crystallisation set up: (1) 59,000x magnification, scale bar = 200nm; (2) electron diffraction of (1), d = 1000mm, scale bar = $4nm^{-1}$; (3) the same two-dimensional crystal recorded as an image on film, 110,000x magnification.

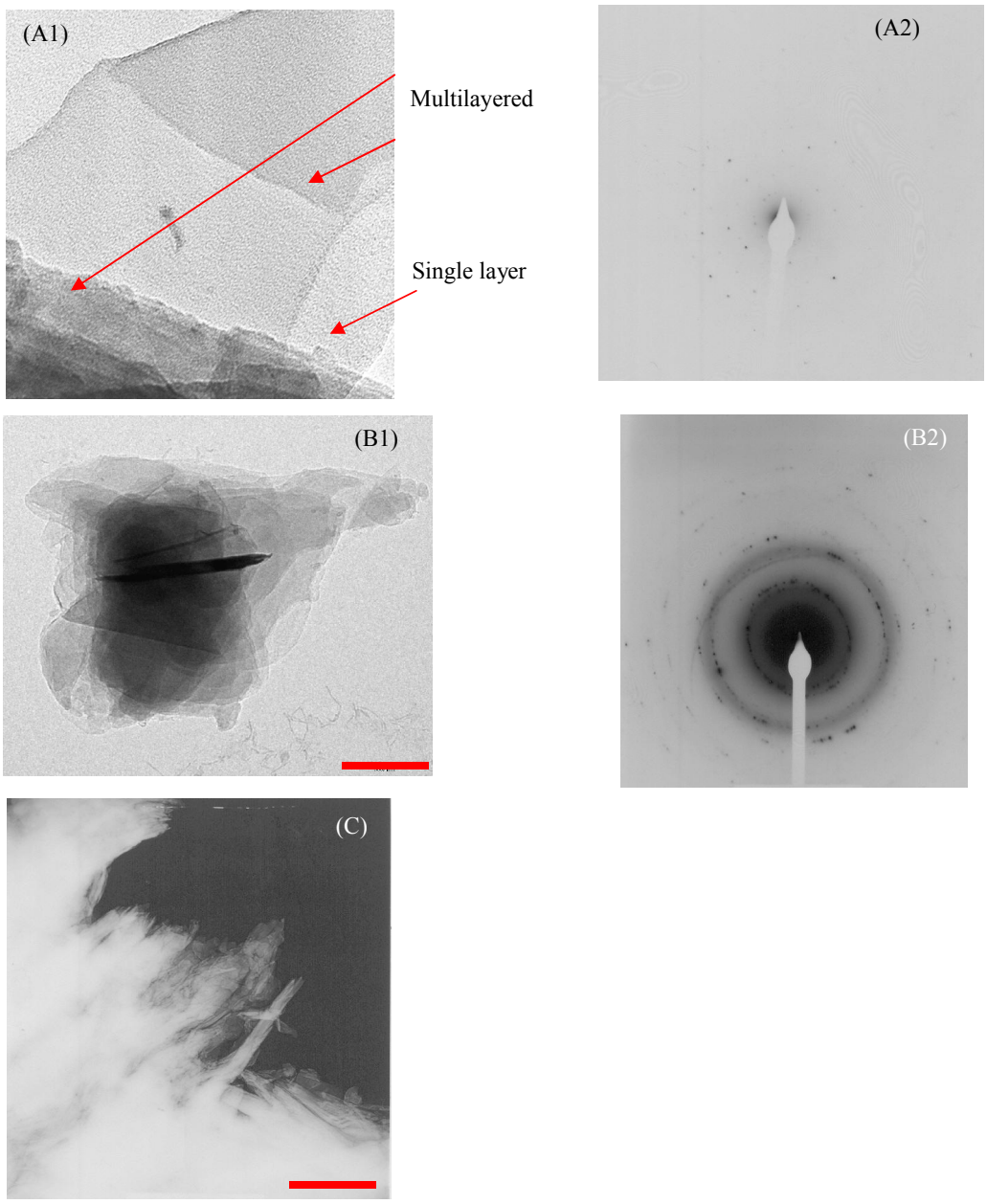

Figure 14. Electron microscopy and electron diffraction images of two-dimensional crystals formed in the presence of $His10_CH_1R$/asolectin and DTAC.
(A) negatively stained sample imaged 3 weeks after crystallisation set up; (1) two-dimensional crystals, 97,000x magnification; (2) electron diffraction of (1), d =750mm, scale bar = $6nm^{-1}$.
(B) negatively stained sample imaged 5 days after crystallisation set up: (1) two-dimensional crystals, 59,000x magnification, scale bar = 200nm; (2) electron diffraction of (1), d = 750mm, scale bar = $6nm^{-1}$.
(C) negatively stained sample imaged 5 days after crystallisation set up, 59,000x magnification, scale bar = 200nm

The electron diffraction pattern of 2D crystals formed from the $His10_CH_1R$/asolectin/DTAC mixture was interesting and appeared promising but, like the 'interesting' *in meso* crystals, in the absence of a structure from the diffraction, there is no

certainty as to what is causing the electron diffraction. Several controls were performed in an attempt to confirm that diffraction was from a protein crystal. The diffraction was not an artifact of negative staining or hexagonal ice since the same diffraction was observed using either cryo-EM conditions (i.e. in the absence of uranyl acetate, Figure 13A) or negative stained sample imaging (in the absence of ice). Nor was it a result of crystallisation of the DTAC since crystals formed in the absence of the salt also diffracted (Figure 12A and work of Dr Priya Bhakat, CSIRO). Whilst the carbon in the grids will diffract the electron beam, this is clearly distinguishable from the diffraction pattern presented here (results not shown). One strong concern was that the lipids themselves were forming ordered 2D arrays, perhaps in combination with the salt (150mM NaCl) and ligand (20μM triprolidine) in the histamine gel filtration buffer. Thus crystallisation experiments with the asolectin and histamine gel filtration buffer were performed under identical conditions as those described, but in the absence of $His10_CH_1R$. As anticipated, diffraction was observed (Figure 15). Ironically crystals formed in the absence of protein tended to be single. The observed diffraction pattern for protein-free crystals did not appear similar to that observed in the presence of the protein (compare Figure 15 A2/B2 to Figure 12/13 B).

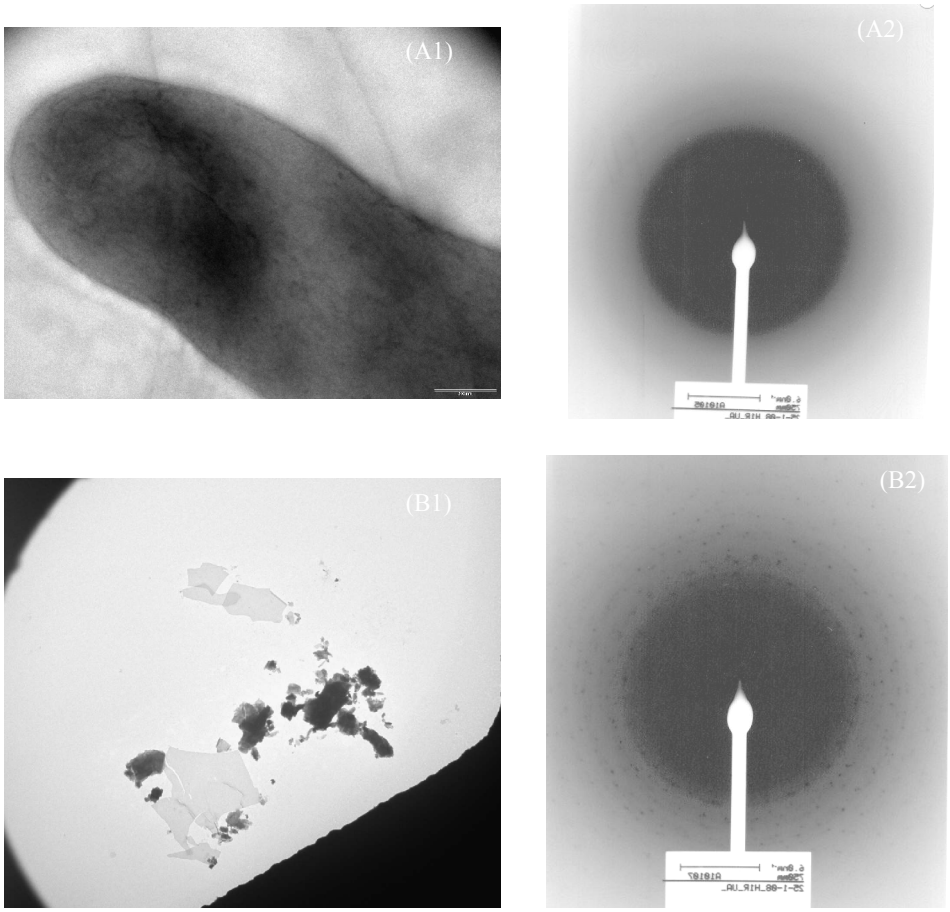

Figure 15. Electron microscopy and electron diffraction images of two-dimensional crystals formed in the absence of $His10_CH_1R$ and presence of asolectin and DTAC. All samples were prepared using negative staining.
(A): (1) two-dimensional crystal imaged at 5 days after crystallisation set up, 59,000x magnification, scale bar = 200nm; (2) electron diffraction of (1), d= 750mm, scale bar = $6nm^{-1}$.
(B): (1) two-dimensional crystal imaged at 5 days after crystallisation set up, scale bar = 5µm, (2) electron diffraction pattern of (1), d = 750mm, scale bar = $6nm^{-1}$.

At this stage, analysis of the electron diffraction patterns and electron microscopic images was proving difficult due to problems with the software and the shortage of single crystal images. Ideally the EM images are used to extract information about the crystal – which was where analysis effort was initially focused. Given the results from the control crystallisation experiments, the crystals formed in the presence of $His10_CH_1R$ looked indeed to contain the receptor. However, using the collected electron diffraction patterns, Bragg's law and basic geometric equations an approximate value for the d-spacing of the crystal was calculated.

4.4.6. Calculation of the d-spacing for 2D crystals formed in the presence of His10$_C$H$_1$R and asolectin.

For first order diffraction (i.e. n = 1), Bragg's law becomes $\lambda = 2d * \sin\theta$, since $\theta << 1$ this can be approximated to $d = \lambda/2\theta$ (equation 1). Basic geometry defines that $\tan(2\theta) = X/D$ (defined in Figure 16), since $\theta << 1$ this can be approximated to $\theta = X/2D$ (equation 2). X is measured directly from the electron diffraction pattern (Figure 16B) and is equal to 41mm/6 (average of the distance between 6 diffraction spots). D is a parameter of the experiment and in this case is 1000m. Using equation 2 and the λ of the electron beam, θ is determined as ~3.4×10^{-3}. This value is then used in equation 1 with the wavelength of the electron beam, which in this experiment was ~ 0.03349Å, giving a d spacing of ~5.0Å for the two dimensional crystal.

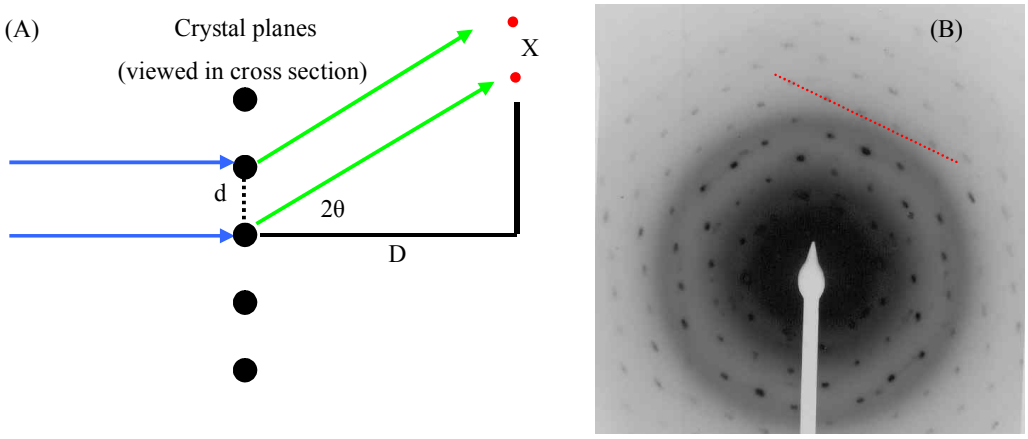

Figure 16. Calculation of the d-spacing for 2D crystals formed in the presence of His10$_C$H$_1$R and asolectin. (A) Schematic interpretation of Bragg's law and geometric considerations for calculation of d-spacing. Blue arrows represent the incident electron beam, green arrows the diffracted electron beam. Large black circles represent the crystal planes, small red circles represent the observed electron diffraction spots. Black lines represent the geometric considerations required for the calculation. D is the distance between sample (2D crystal) and detector, d is the spacing between the planes of the crystal, x is the distance between the diffraction spots and θ is the angle between the incident electron beam and the scattering planes of the crystal. (B) Example electron diffraction pattern, as described in Figure 13 of this chapter. Camera distance, (D), is 1000mm. The red line represents a distance of 41mm as measured directly from the film of the diffraction image.

5Å is far too small to be the d-spacing for a His10$_C$H$_1$R, which has a molecular weight of ~56kDa, containing crystal. For a protein of this size the d-spacing should be ~50Å. Thus it could be that the diffraction observed is in fact from ordering of the lipid, perhaps in conjunction with salts or the triprolidine in the crystallisation buffer. It is interesting that this diffraction was not observed in crystals formed in the absence of protein but this may simply be a reflection of the number of measurements taken, which was biased towards

crystallisation set up in the presence of receptor. Further work is required to determine what it is that is causing the observed diffraction pattern and if it is masking the diffraction of potential 2D protein crystals.

4.5. Conclusions

The $His10_CH_1R$ construct was used in *in meso* (3D) and 2D crystallisation trials. Preliminary results identified the combination of HEPES pH7.5, PEG and possibly a sodium salt as a useful starting point for crystallisation of the $His10_CH_1R$. Inclusion of $His6_N G\alpha_{i1}$ in *in meso* crystallisation trials with $His10_CH_1R$ and monolein, produced aggregated microcrystals which diffracted X-rays in the manner of a powder. The diffraction was not caused by salt or surfactant. These crystals did not form in the absence of $His10_CH_1R$ and so may represent 3D crystals of the receptor.

Reconstitution of $His10_CH_1R$ into asolectin produced multilayered 2D crystals. Electron diffraction demonstrated a hexagonal lattice for these crystals. However, an approximate calculation of the d-spacing demonstrated that this diffraction was not from a unit cell that was of sufficient size to incorporate the $His10_CH_1R$.

5. General discussions, future directions and conclusions of this study.

Purification of mammalian seven-transmembrane receptors in itself is a difficult task, while attempts to crystallise such purified proteins adds an extra level of difficulty. In this regard this was an ambitious PhD project which had a high-risk of failure. Despite the challenge and the inherent time limitations, some progress was made towards crystallisation of a 7TMR. Yet there remains areas in the pathway from expression to crystallisation which could be further optimised and other areas which were not completely addressed in this study. In this chapter a general discussion of the results of this study will be combined with directions which, in hindsight, may have been useful for this project or may be useful for future work with the project. Like the chapters in this thesis, the process from DNA to protein structure can be divided into three areas – expression of the protein, purification of the protein and crystallisation of the protein (followed by a fourth challenge of protein crystallography, or solving the structure of the protein). It is under these headings that this chapter will be discussed.

5.1.1. Protein Expression

The expression of three receptors; the M_2 muscarinic, H_1 histamine and $5HT_{2A}$ serotonin receptor was attempted in this study. If it is available (i.e. if the final aim is crystallisation of any 7TMR), the ability to select from a variety of receptors is particularly useful since expression levels of the receptors will vary substantially even in the same expression system. This was indeed observed in this study, with the $5HT_{2A}R$ not expressing at all (or at levels too low for definitive detection) and the H_1R expressing at an approximately 5x higher level than the M_2R. The choice of expression system is important but in reality it is the next two stages i.e. purification and crystallisation which will determine if the 7TMR will crystalise. The two essential requirements when choosing an expression system is that the receptor is produced in a functional form and the cell culture can be easily up-scaled. The second requirement reduces the dependence on high expression of the receptor, which is an inherent limitation of integral membrane proteins regardless of the choice of expression system. With modifications to the receptor, such as the work which has been reported for the neurotensin-1 receptor (NTR1), it may be possible to express the receptor of interest (in functional form) in *E. coli* (Grisshammer, et al., 1993; Hanninen, et al., 1994). This is an ideal situation since bacterial cultures are easily adapted to large scale culture and have a rapid growth rate enabling large quantities of protein can be produced. However without modification to the receptor, prokaryote expression will generally

produce non-functional/aggregated protein. In terms of 7TMRs, yeast is a somewhat neglected expression system but has been used successfully with a number of the receptors and may present a useful alternative to the baculovirus/insect cell expression system. Andre, et al., (2006) report expression levels of 39.1pmol/mg for both the D_2 dopamine and $5HT_{5A}$ serotonin receptors in the yeast system. Work in this study, and numerous others, suggests the baculovirus/insect cell expression system is particularly useful for 7TMR expression. The baculovirus/insect cell system produces functional 7TMRs in good yields (pmol/mg), is adaptable to large scale culture, and the cells themselves are relatively easy to maintain. The most time consuming part of baculovirus/insect cell expression is construction of the recombinant baculovirus. In an ideal situation the baculovirus can be constructed within 2 – 3 weeks as was the case for the $His6_CM_2R$ baculovirus but not for the $His12_CM_2R$ or $His6_NM_2R$ which took twice that time. However difficulties with cloning and in particular, recombination of the donor plasmid with the bacmid DNA within DH10Bac *E. coli* (a process over which one has little control) can extend this time substantially. Furthermore, if non-recombinant bacmid is isolated in-conjunction with recombinant bacmid (this can occur if the colour reaction demonstrating DH10Bac containing non-recombinant bacmid is not complete when colonies are selected), protein expression will gradually decrease as the virus is amplified and non-recombinant bacmid becomes favoured in the viral population. In this regard, amplification of the virus at a low MOI (such as 0.1, which was used in this study) can reduce the ability of any non-recombinant baculoviruses to dominate. A possible disadvantage of the baculovirus/insect cell system, is the lytic nature of the virus. This limits the ability to perform further investigation of the receptor expression such as assessing the trafficking of the receptor to the membrane; it is highly likely that incompletely processed receptor is aggregated within the insect cell. If the receptors are being produced for cell based functional studies, as well as for purification, the vector pIZ/V5 (Insect Select, Invitrogen) allows both transient and stable expression in insect cells. It does however use a different promoter (OpIE2, as compared to polyhedrin for the baculovirus) for expression of the gene and subsequently expression levels of the receptor may vary between the two systems.

If one does wish to try a variety of cell types for expression, the Gateway® cloning system (Invitrogen) may be worth investigation. In this system the gene is cloned into an entry vector which subsequently can be recombined with a variety of destination vectors, via attenuation sites on each vector and the enzyme 'Gateway® LR Clonase™. Hence the

cloning procedure is only performed once. Destination and expression vectors are available for mammalian, *E. coli* and baculovirus expression systems. This technology may prove useful for future work with the $5HT_{2A}R$ which was purchased in the Gateway™ destination vector pDEST8 (Invitrogen).

5.1.2. Protein Purification

In comparison to intracellular or peripheral membrane proteins, 7TMRs are incredibly difficult to purify. Every step of the 7TMR purification protocol as well as every associated procedure required (such as the binding assay and the Western blot) seemed to involve difficulties which could only be attributed to the proteins under investigation, since the protocols and procedures for the G-proteins could be performed with relative ease. The challenge begins at solubilisation of the membrane protein. Loss of functional protein is predominantly due to removal of the receptor from the membrane (i.e. solubilisation) in combination with the time required for purification – loss of solubilised functional protein is time (and temperature) dependent. Thus there are at least two areas in which functional protein yields may be increased. With the exception of the initial purification trials, which required some optimisation of parameters, in this study the purification was carried out in the shortest time frame possible which from cell lysis to purified protein was minimised at 3 days. Although extensions to this time occasionally came from slow-running columns etc. Whilst it was not always available in this study, ideally all steps including chromatography should be performed at 4^oC. Initial IMAC experiments in this study were performed at 4^oC but later were performed at room temperature due to the availability of a HPLC chromatography workstation. It may also be useful to try additives other than receptor ligand at the solubilisation step, for example decaethylene glycol monododecyl ether ($C_{12}E_{10}$), cholesterol or a cholesterol derivative such as cholesteryl hemisuccinate. The primary purpose of the solubilisation step is essentially to allow purification of the receptor, since using current techniques the receptor cannot be separated from other integral membrane proteins whilst still in the cell membrane. In this respect it is possible that *in vitro* receptor expression may be of benefit by negating the solubilisation step. If receptors can be expressed independently of the expression of other proteins and directed to a simple artificial lipid bilayer (which is deemed compatible with crystallisation) or into surfactants (which can then be prepared as meso-phase structures) the requirement for detergent solubilisation would be negated.

Without doubt the limitation of this study was an inability to report conclusive values for radioligand binding to the receptor following its solubilisation. In the initial phases of this work, when the purification procedures were being optimised and initial results demonstrated that the radioligand binding assay for soluble/ligand bound receptor would be difficult, the focus became producing purified receptor and detecting it by Western blot using antibodies to both the poly-Histidine tag and the receptor itself. Once these methods were established, and in fact after crystallisation trials had begun, the strategy then was to refocus on the binding assay. Since the binding assay had not been properly established, a high-affinity ligand was incorporated throughout the purification protocol (for both the muscarinic and histamine receptors) to stabilise the receptor following its removal from the cell membrane. The ideal situation, as mentioned in chapter 3, would be the use of two distinct receptor binding sites i.e. both orthosteric and allosteric sites, one for stabilisation during purification and the other for detection of functional protein.

Rather than trialling a variety of purification procedures in this study, emphasis was placed instead on the IMAC method. This method was successful in that it lead to partial purification of the receptor, but other methods may have favoured for the retention of protein functionality and/or selected for functional protein. For example, the use of a ligand-affinity column would select for receptors which had retained functionality during solubilisation. Ideally a ligand affinity column would be used as the final chromatography step. A ligand-affinity column is not a simple task for either the muscarinic or the histamine receptor since there are no commercially available ligand resins. However, pyrilamine derivatives have been synthesised and attached to resin for purification of the H_1 histamine receptor and ABT has been coupled to resin for purification of the M_2 muscarinic receptor (Haga and Haga, 1983; Ruat, et al., 1992). This chromatographic method would however suffer the same difficulty of purifying ligand bound receptor, in that the receptor must be dissociated from the ligand. This is generally achieved by modification of the buffer compositions (such as an increase in ionic strength or change in pH), but one would need to select carefully to ensure receptor functionality is not lost during the elution process. In addition to their potential use in stabilisation of the receptor, allosteric modulators and Gα based peptides (see CADEN biosciences; http://www.cadenbiosciences.com/index.php?id=2) would provide useful tools for receptor purification. In particular, such peptides may be useful for purification since they are amenable to attachement to a solid support, either through thiol-maleimide or ester

linkage of the amino acids to resin. Alternatively a biotinylation sequence could be added to the peptide and then biotin used to couple the peptides to (commercially available) streptavidin resin.

5.1.3. Protein Crystallisation

Once the 7TMR has passed through the rigors of purification, the next challenge becomes that of crystallisation. Although in this study the percentage of functional receptor in the final purified $His10_CH_1R$ sample was not conclusively demonstrated, it was decided to attempt crystallisation. The decision to attempt crystallisation of the $His10_CH_1R$ was based on a number of factors – 1) it had not been demonstrated that all receptor was non-functional and even the presence of a small amount of functional receptor allows the potential for crystallisation of functional receptor; 2) even if non-functional receptor was crystallised it may still provide useful structural information; 3) regardless of the protein, methods for *in meso* crystallisation required development and it seemed logical to at least try the $His10_CH_1R$ and 4) of course there were time limitations for this study and preliminary crystallisation experiments provided a good point for completion of the work. Substantial additional work will be required to define the properties of the crystals observed in this study. The co-crystallisation experiments with $His6_N G\alpha_{i1}$ should be further investigated by attempting to collect and analyse further powder diffraction data and by attempting to grow single crystals. While some of the crystallisation results are particularly encouraging, without the final confirmation which would come from structure determination, it is difficult to draw conclusions about the formation of $His10_CH_1R$ crystals. Furthermore, a significant back-catalogue of work preceded crystallistion of the β_2 adrenergic receptor and it would be particularly fortunate to achieve the same result with substantially less work.

Generally, crystallisation of 7TMRs is another challenging step towards structure determination at the atomic level. Many 7TMRs contain long flexible regions, for example the third intracellular loop of the M_2 and H_1 receptors. If the aim is crystallisation, it may be desirable to remove these regions of the receptor at the cloning stage. Investigations with the M_2R have suggested that amino acids 233 – 380 (in the third intracellular loop) can be removed without effecting receptor interaction with G-proteins (Sarramegna, et al., 2003). This is similar for other type A 7TMRs, however removing parts of the receptor would not provide a holistic overview of the receptor function. An alternative to removal

of regions of the protein is stabilisation using a secondary protein such as antibody fragments, which have been successfully used for crystallisation of the β_2AR (Rasmussen, et al., 2007). A more appealing alternative is to co-crystalise with the natural receptor binding partners to the G-proteins, in particular the Gα subunit. As well as stabilising regions of the receptor, co-crystallisation of the receptor with G-proteins would provide a unique insight into the interaction between the two proteins and may allow for the molecular replacement method to be used to solve the phase problem when determining structure. It may also be beneficial/necessary to modify the G-protein to provide a more stable interaction between G-protein and receptor. Once again, high affinity Gα based peptides may have a role in this regard.

Whilst modifications can be made to the receptor or to the methods used for crystallisation, the ideal situation is not to change the proteins themselves but to change the methods by which they are studied. This will become increasing possible as the dialogue between biologists and physicists increases. One upcoming and promising field is single molecule diffraction (Hajdu, 2000). The development of X-ray free-electron lasers (FELs) will enable the production of a 100 femto-second duration beam with a brilliance 10 to 11 orders of magnitude higher than that which can be produced by current synchrotrons. The femto second beam time and high energies allow each molecule to be shot once, with radiation damage subsequently destroying the molecule. Thus a spray/vapour of the molecules is directed into the beam, each molecule is shot once, and then averaging is used to construct the structure of the molecule. Two such lasers are being built, one at Stanford (http://www-ssrl.slac.stanford.edu/lcls/) and the other in Germany (http://tesla-new.desy.de/). This technology would be ideal for membrane proteins as it would avoid the current requirement for crystallisation and, potentially, the requirement for purification.

Whilst FELs are still in development, microfocus X-ray beams are already available for use at the European Synchrotron Radiation Facility (France), Swiss Light Source (Switzerland), Advanced Photon Source (U.S.A) and the Photon Factory (Japan). These beams use advanced X-ray optics to focus the X-ray beam to dimensions down to less than 1μm whilst retaining high flux. Thus microfocus beamlines allow for the diffraction of very small crystals – which are commonly produced when membrane proteins are crystallised. Both structures of the β_2AR were calculated from protein crystal diffraction of microfocus beamlines.

Whilst electron crystallographic technologies have not significantly advanced in the past decade (particularly in comparison to X-ray crystallography), the formation of two-dimensional crystals remains appealing. By definition, two-dimensional crystals should be simpler to form since order is only required in two dimensions and the receptor is being reconstituted into a 'natural like' environment of the artificial bilayer. It is also interesting to note that β_2AR crystals formed using the bicelle method were reported to be stacks of two-dimensional crystals (Rasmussen, et al., 2007). Thus the formation of two-dimensional crystals may be an initial step toward three-dimensional crystallisation and crystallography.

5.1.4. Final conclusions of this study

Expression of poly-Histidine tagged M_2 muscarinic receptor and H_1 histamine receptor was demonstrated using the baculovirus/insect cell system. Expression of the $5HT_{2A}$ serotonin receptor in the baculovirus/insect cell system could not be conclusively demonstrated. Addition of receptor specific ligands to baculovirus infected insect cell cultures of the muscarinic and histamine receptor modulated the density of receptors in the cell membranes. Purification of the $His6_CM_2R$ and $His10_CH_1R$ was achieved using IMAC and gel-filtration with receptor presence being confirmed by Western blot. *In meso* (three-dimensional) and two-dimensional crystallisation trials were conducted using purified $His10_CH_1R$. Preliminary results suggest the presence three-dimensional crystals which were formed in the presence of $His10_CH_1R$ and $His6_N G\alpha_{i1}$. Initial results suggested the formation of 2D $His10_CH_1R$ crystals. However, calculation of the d-spacing for the two-dimensional crystals determined the crystal unit cell size to be too small to contain the $His10_CH_1R$. Work on the three-dimensional crystals formed in the presence of $His10_CH_1R$ is ongoing.

6. References

Alberts B, Bray D, Lewis J, Raff M, Roberts K and Watson JD. (1994). *Molecular biology of the cell.* Garland Publishing,

Alper J. (2002). Breaching the membrane. *Science* 296: 838.

An JY, Yun HS, Lee YP, et al. (2002). The intracellular pathway of the acetylcholine-induced contraction in cat detrusor muscle cells. *British Journal of Pharmacology* 137: 1001-1010.

Andre N, Cherouati N, Prual C, et al. (2006). Enhancing functional production of G protein-coupled receptors in pichia pastoris to levels required for structural studies via a single expression screen. *Protein Science : A Publication of the Protein Society* 15: 1115-1126.

Arechaga I and Fotiadis D. (2007). Reconstitution of mitochondrial ATP synthase into lipid bilayers for structural analysis. *Journal of Structural Biology* 160: 287-294.

Arechaga I, Miroux B, Karrasch S, et al. (2000). Characterisation of new intracellular membranes in escherichia coli accompanying large scale over-production of the b subunit of F(1)F(o) ATP synthase. *FEBS Letters* 482: 215-219.

Babcock GJ, Mirzabekov T, Wojtowicz W, et al. (2001). Ligand binding characteristics of CXCR4 incorporated into paramagnetic proteoliposomes. *The Journal of Biological Chemistry* 276: 38433-38440.

Bakker RA, Timmerman H and Leurs R. (2002). Histamine receptors: Specific ligands, receptor biochemistry, and signal transduction. *Clinical Allergy and Immunology* 17: 27-64.

Barakaus J and Landh T. (2003). Phase behavior of the phytantriol/water system. *Langmuir* 19: 9562.

Barton CS, Glatz RV, Martin S, et al. (2007). Interaction of self-assembled monolayers incorporating NTA disulfide with multilength histidine-tagged ga_{i1} subunits . *Journal of Bionanoscience* 1: 22.

Bayburt TH and Sligar SG. (2003). Self-assembly of single integral membrane proteins into soluble nanoscale phospholipid bilayers. *Protein Science* 12: 2476-2481.

Bonner TI. (1992). Domains of muscarinic acetylcholine receptors that confer specificity of G protein coupling. *Trends in Pharmacological Science* 13:48-50.

Bradford MM. (1976). A rapid and sensitive method for the quantitation of microgram quantities of protein utilizing the principle of protein-dye binding. *Analytical Biochemistry* 72: 248-254.

Brady AE and Limbird LE. (2002). G protein-coupled receptor interacting proteins: Emerging roles in localization and signal transduction. *Cellular Signalling* 14: 297-309.

Brandt J, Andersen AS and Kristensen C. (2001). Dimeric fragment of the insulin receptor alpha-subunit binds insulin with full holoreceptor affinity. *The Journal of Biological Chemistry* 276: 12378-12384.

Caffrey M. (2003). Membrane protein crystallization. *Journal of Structural Biology* 142: 108.

Caron MG, Srinivasan Y, Pitha J, et al. (1979). Affinity chromatography of the beta-adrenergic receptor. *The Journal of Biological Chemistry* 254: 2923-2927.

Cerione RA, Strulovici B, Benovic JL, et al. (1983). Reconstitution of beta-adrenergic receptors in lipid vesicles: Affinity chromatography-purified receptors confer catecholamine responsiveness on a heterologous adenylate cyclase system. *Proceedings of the National Academy of Sciences of the United States of America* 80: 4899-4903.

Chalmers DT and Behan DP. (2002). The use of constitutively active GPCRs in drug discovery and functional genomics. *Nature Reviews.Drug Discovery* 1: 599-608.

Chasse SA and Dohlman HG. (2003). RGS proteins: G protein-coupled receptors meet their match. *Assay and Drug Development Technologies* 1: 357-364.

Chelikani P, Reeves PJ, Rajbhandary UL, et al. (2006). The synthesis and high-level expression of a beta2-adrenergic receptor gene in a tetracycline-inducible stable mammalian cell line. *Protein Science : A Publication of the Protein Society* 15: 1433-1440.

Cherezov V and Caffrey M. (2007). Membrane protein crystallization in lipidic mesophases. A mechanism study using X-ray microdiffraction. *Faraday Discussions* 136: 195-213-219.

Cherezov V, Rosenbaum DM, Hanson MA, et al. (2007). High-resolution crystal structure of an engineered human {beta}2-adrenergic G protein coupled receptor. *Science* 318: 1258-1265.

Ciccarone V, Polayes D and Luckow V (1997) Generation of recombinant baculovirus DNA in *E.coli* using a baculovirus shuttle vector, in (Anonymous) pp 213-235,

Civjan NR, Bayburt TH, Schuler MA, et al. (2003). Direct solubilization of heterologously expressed membrane proteins by incorporation into nanoscale lipid bilayers. *BioTechniques* 35: 556-60, 562-3.

Crespo P, Xu N, Simonds WF, et al. (1994). Ras-dependent activation of MAP kinase pathway mediated by G-protein beta gamma subunits. *Nature* 369: 418-420.

Cvejic S and Devi LA. (1997). Dimerization of the delta opioid receptor: Implication for a role in receptor internalisation. *The Journal of Biological Chemistry* 272: 26959-26964.

Daeffler L, Schmidlin F, Gies JP, et al. (1999). Inverse agonist activity of pirenzepine at M2 muscarinic acetylcholine receptors. *British Journal of Pharmacology* 126: 1246-1252.

Daniels MJ, Chrispeels MJ and Yeager M. (1999). Projection structure of a plant vacuole membrane aquaporin by electron cryo-crystallography. *Journal of Molecular Biology* 294: 1337-1349.

Day PW, Rasmussen SG, Parnot C, et al. (2007). A monoclonal antibody for G protein-coupled receptor crystallography. *Nature Methods* 4: 927-929.

Day PW, Wedegaertner PB and Benovic JL. (2004). Analysis of G-protein-coupled receptor kinase RGS homology domains. *Methods in Enzymology* 390: 295-310.

De Lean A, Stadel JM and Lefkowitz RJ. (1980). A ternary complex model explains the agonist-specific binding properties of the adenylate cyclase-coupled beta-adrenergic receptor. *The Journal of Biological Chemistry* 255: 7108-7117.

Degrip WJ, Vanoostrum J and Bovee-Geurts PH. (1998). Selective detergent-extraction from mixed detergent/lipid/protein micelles, using cyclodextrin inclusion compounds: A novel generic approach for the preparation of proteoliposomes. *The Biochemical Journal* 330 (Pt 2): 667-674.

Deisenhofer J, Epp K, Huber R, et al. (1985). Structure of the protein subunits in the photosynthetic reaction centre of *rhodopseudomonas viridis* at 3A resolution. *Nature* 318: 618.

DeLapp NW. (2004). The antibody-capture [(35)S]GTPgammaS scintillation proximity assay: A powerful emerging technique for analysis of GPCR pharmacology. *Trends in Pharmacological Sciences* 25: 400-401.

Denisov IG, Grinkova YV, Lazarides AA, et al. (2004). Directed self-assembly of monodisperse phospholipid bilayer nanodiscs with controlled size. *Journal of the American Chemical Society* 126: 3477-3487.

Endo Y and Sawasaki T. (2004). High-throughput, genome-scale protein production method based on the wheat germ cell-free expression system. *Journal of Structural and Functional Genomics* 5: 45-57.

Fagan MH and Dewey TG. (1986). Resonance energy transfer study of membrane-bound aggregates of the sarcoplasmic reticulum calcium ATPase. *The Journal of Biological Chemistry* 261: 3654-3660.

Fitzsimons CP, Monczor F, Fernandez N, et al. (2004). Mepyramine, a histamine H1 receptor inverse agonist, binds preferentially to a G protein-coupled form of the receptor and sequesters G protein. *The Journal of Biological Chemistry* 279: 34431-34439.

Florio VA and Sternweis PC. (1985). Reconstitution of resolved muscarinic cholinergic receptors with purified GTP-binding proteins. *The Journal of Biological Chemistry* 260: 3477-3483.

Furukawa H and Haga T. (2000). Expression of functional M2 muscarinic acetylcholine receptor in escherichia coli. *Journal of Biochemistry* 127: 151-161.

Garnovskaya M, Nebigil C, Arthur J, et al. (1995). 5-Hydroxytryptamine$_{2A}$ receptors expressed in rat renal mesangial cells inhibit cyclic AMP accumulation. *Molecular Pharmacology* 230: 230.

Gether U. (2000). Uncovering molecular mechanisms involved in activation of G protein-coupled receptors. *Endocrine Reviews* 21: 90.

Gether U, Lin S, Ghanouni P, et al. (1997). Agonists induce conformational changes in transmembrane domains III and VI of the beta2 adrenoceptor. *The EMBO Journal* 16: 6737-6747.

Goodwin JA, Hulme EC, Langmead CJ, et al. (2007). Roof and floor of the muscarinic binding pocket: variations in the binding modes of orthosteric ligands. *Molecular Pharmacology* 72(6): 1484-1486.

Gordeliy VI, Labahn J, Moukhametzianov R, et al. (2002). Molecular basis of transmembrane signalling by sensory rhodopsin II-transducer complex. *Nature* 419: 484-487.

Graber SG, Figler RA and Garrison JC. (1994). Expression and purification of G-protein alpha subunits using baculovirus expression system. *Methods in Enzymology* 237: 212-226.

Granier S, Kim S, Shafer AM, et al. (2007). Structure and conformational changes in the C-terminal domain of the beta2-adrenoceptor: Insights from fluorescence resonance energy transfer studies. *The Journal of Biological Chemistry* 282: 13895-13905.

Grisshammer R, Averbeck P and Sohal AK. (1999). Improved purification of a rat neurotensin receptor expressed in escherichia coli. *Biochemical Society Transactions* 27: 899-903.

Grisshammer R, Duckworth R and Henderson R. (1993). Expression of a rat neurotensin receptor in escherichia coli. *The Biochemical Journal* 295 (Pt 2): 571-576.

Grunewald S, Haase W, Molsberger E, et al. (2004). Production of the human D2S receptor in the methylotrophic yeast P. pastoris. *Receptors & Channels* 10: 37-50.

Gutowski S, Smrcka A, Nowak L, et al. (1991). Antibodies to the alpha q subfamily of guanine nucleotide-binding regulatory protein alpha subunits attenuate activation of phosphatidylinositol 4,5-bisphosphate hydrolysis by hormones. *The Journal of Biological Chemistry* 266: 20519-20524.

Haga K and Haga T. (1983). Affinity chromatography of the muscarinic acetylcholine receptor. *The Journal of Biological Chemistry* 258: 13575-13579.

Hajdu J. (2000). Single-molecule x-ray diffraction. *Current Opinion in Structural Biology* 10: 569.

Hanninen AL, Bamford DH and Grisshammer R. (1994). Expression in escherichia coli of rat neurotensin receptor fused to membrane proteins from the membrane-containing bacteriophage PRD1. *Biological Chemistry Hoppe-Seyler* 375: 833-836.

Harding PJ, Attrill H, Ross S, et al. (2007). Neurotensin receptor type 1: Escherichia coli expression, purification, characterization and biophysical study. *Biochemical Society Transactions* 35: 760-763.

Harrison C and Traynor JR. (2003). The [35S]GTPgammaS binding assay: Approaches and applications in pharmacology. *Life Sciences* 74: 489-508.

Harvey L, Reid RE, Ma C, et al. (2003). Human genetic variations in the 5HT2A receptor: A single nucleotide polymorphism identified with altered response to clozapine. *Pharmacogenetics* 13: 107-118.

Hasler L, Heymann JB, Engel A, et al. (1998). 2D crystallization of membrane proteins: Rationales and examples. *Journal of Structural Biology* 121: 162-171.

Hassaine G, Wagner R, Kempf J, et al. (2006). Semliki Forest virus vectors for overexpression of 101 G protein-coupled receptors in mammalian host cells. *Protein Expression and Purification* 45: 343-351.

Hayashi MK and Haga T. (1997). Palmitoylation of muscarinic acetylcholine receptor m2 subtypes: Reduction in their ability to activate G proteins by mutation of a putative palmitoylation site, cysteine 457, in the carboxyl-terminal tail. *Archives of Biochemistry and Biophysics* 340: 376-382.

Hayashi MK and Haga T. (1996). Purification and functional reconstitution with GTP-binding regulatory proteins of hexahistidine-tagged muscarinic acetylcholine receptors (m2 subtype). *Journal of Biochemistry* 120: 1232-1238.

Hepler JR and Gilman AG. (1992). G proteins. *Trends in Biochemical Sciences* 17: 383.

Hepler JR, Kozasa T, Smrcka AV, et al. (1993). Purification from Sf9 cells and characterization of recombinant gq alpha and G11 alpha. activation of purified phospholipase C isozymes by G alpha subunits. *The Journal of Biological Chemistry* 268: 14367-14375.

Hermans E. (2003). Biochemical and pharmacological control of the multiplicity of coupling at G-protein-coupled receptors. *Pharmacology & Therapeutics* 99: 25-44.

Houston C, Wenzel-Seifert K, Burckstummer T, et al. (2002). The human histamine H2-receptor couples more efficiently to Sf9 insect cell gs-proteins than to insect cell gq-proteins: Limitations of Sf9 cells for the analysis of receptor/Gq-protein coupling. *Journal of Neurochemistry* 80: 678-696.

Huang XP, Nagy PI, Williams FE, et al. (1999). Roles of threonine 192 and asparagine 382 in agonist and antagonist interactions with M1 muscarinic receptors. *British Journal of Pharmacology* 126: 735-745.

Hulme EC, Birdsall NJ and Buckley NJ. (1990). Muscarinic receptor subtypes. *Annual Review of Pharmacology and Toxicology* 30: 633-673.

Hulme EC, Saldanha JW, Bee MS. (2003). Structure and activation of muscarinic acetylcholine receptors. *Biochemical Society Transactions* 31(1): 29-34.

Jackson AM, Boutell J, Cooley N, et al. (2004). Cell-free protein synthesis for proteomics. *Briefings in Functional Genomics & Proteomics* 2: 308-319.

Jahn T, Dietrich J, Andersen B, et al. (2001). Large scale expression, purification and 2D crystallization of recombinant plant plasma membrane H+-ATPase. *Journal of Molecular Biology* 309: 465-476.

Jakubik J, Bacakova L, el-Fakahany EE, et al. (1995). Constitutive activity of the M1-M4 subtypes of muscarinic receptors in transfected CHO cells and of muscarinic receptors in the heart cells revealed by negative antagonists. *FEBS Letters* 377: 275-279.

Janssen JJ, Bovee-Geurts PH, Merkx M, et al. (1995). Histidine tagging both allows convenient single-step purification of bovine rhodopsin and exerts ionic strength-dependent effects on its photochemistry. *The Journal of Biological Chemistry* 270: 11222-11229.

Jarvis DL and Finn EE. (1995). Biochemical analysis of the N-glycosylation pathway in baculovirus-infected lepidopteran insect cells. *Virology* 212: 500-511.

Jasper JR, Lesnick JD, Chang LK, et al. (1998). Ligand efficacy and potency at recombinant alpha2 adrenergic receptors: Agonist-mediated [^{35}S]GTPgammaS binding. *Biochemical Pharmacology* 55: 1035-1043.

Jongejan A, Leurs R. (2005). Delineation of receptor-ligand interactions at the human H_1 receptor by a combined approach of site-directed mutagenesis and computational techniques – or – how to bind the H_1 receptor. *Archiv der Pharmazie* 338: 248-259.

Key TA, Vines CM, Wagener BM, et al. (2005). Inhibition of chemoattractant N-formyl peptide receptor trafficking by active arrestins. *Traffic* 6: 87-99.

Kitanaka J, Kitanaka N, Tatsuta T, et al. (2007). Blockade of brain histamine metabolism alters methamphetamine-induced expression pattern of stereotypy in mice via histamine H1 receptors. *Neuroscience* 147: 765-777.

Klabunde T and Hessler G. (2002). Drug design strategies for targeting G protein-coupled receptors. *Chembiochem : A European Journal of Chemical Biology* 3: 928-944.

Klammt C, Schwarz D, Eifler N, et al. (2007). Cell-free production of G protein-coupled receptors for functional and structural studies. *Journal of Structural Biology* 158: 482-493.

Knight AR, Misra A, Quirk K, et al. (2004). Pharmacological characterisation of the agonist radioligand binding site of 5-HT_{2A}, 5-HT_{2B} and 5-HT_{2C} receptors. *Naunyn Schmiedebergs Arch.Pharmacol.* 370: 114.

Kobilka BK. (1995). Amino and carboxyl terminal modifications to facilitate the production and purification of a G protein-coupled receptor. *Analytical Biochemistry* 231: 269-271.

Kobilka BK. (1990). The role of cytosolic and membrane factors in processing of the human beta-2 adrenergic receptor following translocation and glycosylation in a cell-free system. *The Journal of Biological Chemistry* 265: 7610-7618.

Kobilka BK and Deupi X. (2007). Conformational complexity of G-protein-coupled receptors. *Trends in Pharmacological Sciences*. 28(8): 397 - 406.

Koning RI, Keegstra W, Oostergetel GT, et al. (1999). The 5 A projection structure of the transmembrane domain of the mannitol transporter enzyme II. *Journal of Molecular Biology* 287: 845-851.

Kozasa T. (2004). Purification of G protein subunits from Sf9 insect cells using hexahistidine-tagged alpha and beta gamma subunits. *Methods in Molecular Biology* 237: 21-38.

Krebs A, Villa C, Edwards PC, et al. (1998). Characterisation of an improved two-dimensional p22121 crystal from bovine rhodopsin. *Journal of Molecular Biology* 282: 991-1003.

Kuno T, Kubo N and Tanaka C. (1985). Molecular size of histamine H-1 receptor determined by target size analysis. *Biochemical and Biophysical Research Communications* 129: 639-644.

Labrecque J, Fargin A, Bouvier M, et al. (1995). Serotonergic antagonists differentially inhibit spontaneous activity and decrease ligand binding capacity of the rat 5-hydroxytryptamine type 2C receptor in Sf9 cells. *Molecular Pharmacology* 48: 150-159.

Lagerström MC and Schiöth HB. (2008). Structural diversity of G protein-coupled receptors and significance for drug discovery. *NatureReviews Drug Discovery* 7(4): 339 – 357.

Laible PD, Scott HN, Henry L, et al. (2004). Towards higher-throughput membrane protein production for structural genomics initiatives. *Journal of Structural and Functional Genomics* 5: 167-172.

Landau EM, Rummel G, Cowan-jacob S, et al. (1997). Crystallization of a polar protein and small molecules from the aqueous compartment of lipidic cubic phases. *The Journal of Physical Chemistry B* 101: 1935.

Latif R, Graves P and Davies TF. (2001). Oligomerization of the human thyrotropin receptor: Fluorescent protein-tagged hTSHR reveals post-translational complexes. *The Journal of Biological Chemistry* 276: 45217-45224.

Lee KB, Ptasienski JA, Bunemann M, et al. (2000). Acidic amino acids flanking phosphorylation sites in the M2 muscarinic receptor regulate receptor phosphorylation, internalisation, and interaction with arrestins. *The Journal of Biological Chemistry* 275: 35767-35777.

Lefkowitz RJ. (2004). Historical review: A brief history and personal retrospective of seven-transmembrane receptors. *Trends in Pharmacological Sciences* 25: 413-422.

Leifert WR, Aloia AL, Bucco O, et al. (2005a). G-protein-coupled receptors in drug discovery: Nanosizing using cell-free technologies and molecular biology approaches. *Journal of Biomolecular Screening : The Official Journal of the Society for Biomolecular Screening* 10: 765-779.

Leifert WR, Aloia AL, Bucco O, et al. (2005b). GPCR-induced dissociation of G-protein subunits in early stage signal transduction. *Molecular Membrane Biology* 22: 507-517.

Leopoldt D, Harteneck C and Nurnberg B. (1997). G proteins endogenously expressed in sf 9 cells: Interactions with mammalian histamine receptors. *Naunyn-Schmiedeberg's Archives of Pharmacology* 356: 216-224.

Leurs R, Smit MJ, Meeder R, et al. (1995). Lysine200 located in the fifth transmembrane domain of the histamine H1 receptor interacts with histamine but not with all H1 agonists. *Biochemical and Biophysical Research Communications* 214: 110-117.

Leurs R, Smit MJ, Tensen CP, et al. (1994a). Site-directed mutagenesis of the histamine H1-receptor reveals a selective interaction of asparagine207 with subclasses of H1-receptor agonists. *Biochemical and Biophysical Research Communications* 201: 295-301.

Leurs R, Traiffort E, Arrang JM, et al. (1994b). Guinea pig histamine H1 receptor. II. stable expression in chinese hamster ovary cells reveals the interaction with three major signal transduction pathways. *Journal of Neurochemistry* 62: 519-527.

Levy D, Chami M and Rigaud JL. (2001). Two-dimensional crystallization of membrane proteins: The lipid layer strategy. *FEBS Letters* 504: 187-193.

Levy D, Mosser G, Lambert O, et al. (1999). Two-dimensional crystallization on lipid layer: A successful approach for membrane proteins. *Journal of Structural Biology* 127: 44-52.

Liitti S, Matikainen MT, Scheinin M, et al. (2001). Immunoaffinity purification and reconstitution of human alpha(2)-adrenergic receptor subtype C2 into phospholipid vesicles. *Protein Expression and Purification* 22: 1-10.

Lim WK and Neubig RR. (2001). Selective inactivation of guanine-nucleotide-binding regulatory protein (G-protein) alpha and betagamma subunits by urea. *The Biochemical Journal* 354: 337-344.

Luecke H, Richter HT and Lanyi JK. (1998). Proton transfer pathways in bacteriorhodopsin at 2.3 angstrom resolution. *Science (New York, N.Y.)* 280: 1934-1937.

Lundstrom K. (2005). Structural genomics of GPCRs. *Trends in Biotechnology* 23: 103-108.

Marinissen MJ and Gutkind JS. (2001). G-protein-coupled receptors and signaling networks: Emerging paradigms. *Trends in Pharmacological Sciences* 22: 368-376.

Maruko T, Nakahara T, Sakamoto K, et al. (2005). Involvement of the betagamma subunits of G proteins in the cAMP response induced by stimulation of the histamine H1 receptor. *Naunyn-Schmiedeberg's Archives of Pharmacology* 372: 153-159.

Massotte D. (2003). G protein-coupled receptor overexpression with the baculovirus-insect cell system: A tool for structural and functional studies. *Biochimica Et Biophysica Acta* 1610: 77-89.

Matsuyama K, Ichikawa T, Nitta Y, et al. (2006). Localized expression of histamine H1 receptors in syncytiotrophoblast cells of human placenta. *Journal of Pharmacological Sciences* 102: 331-337.

May LT, Lin Y, Sexton PM, et al. (2005). Regulation of M2 muscarinic acetylcholine receptor expression and signaling by prolonged exposure to allosteric modulators. *The Journal of Pharmacology and Experimental Therapeutics* 312: 382-390.

Michel H, Oesterhelt D and Henderson R. (1980). Orthorhombic two-dimensional crystal form of purple membrane. *Proceedings of the National Academy of Sciences of the United States of America* 77: 338.

Milligan G. (2003). Principles: Extending the utility of [35S]GTP gamma S binding assays. *Trends in Pharmacological Sciences* 24: 87-90.

Milligan G and Bond RA. (1997). Inverse agonism and the regulation of receptor number. *Trends in Pharmacological Sciences* 18: 468-474.

Milligan G, Ramsay D, Pascal G, et al. (2003). GPCR dimerisation. *Life Sciences* 74: 181-188.

Milligan G and White JH. (2001). Protein-protein interactions at G-protein-coupled receptors. *Trends in Pharmacological Sciences* 22: 513-518.

Mirshahi T, Jin T and Logothetis DE. (2003). G beta gamma and KACh: Old story, new insights. *Science's STKE : Signal Transduction Knowledge Environment* 2003: PE32.

Mitsuhashi M and Payan DG. (1989). Receptor glycosylation regulates the affinity of histamine H1 receptors during smooth muscle cell differentiation. *Molecular Pharmacology* 35: 311-318.

Miyoshi K, Das AK, Fujimoto K, et al. (2006). Recent advances in molecular pharmacology of the histamine systems: Regulation of histamine H1 receptor signaling by changing its expression level. *Journal of Pharmacological Sciences* 101: 3-6.

Miyoshi K, Kawakami N, Horio S, et al. (2004). Homologous and heterologous phosphorylations of human histamine H1 receptor in intact cells. *Journal of Pharmacological Sciences* 96: 474-482.

Moguilevsky N, Varsalona F, Noyer M, et al. (1994). Stable expression of human H1-histamine-receptor cDNA in chinese hamster ovary cells. pharmacological characterisation of the protein, tissue distribution of messenger RNA and chromosomal localisation of the gene. *European Journal of Biochemistry* 224: 489-495.

Morfis M, Christopoulos A and Sexton PM. (2003). RAMPs: 5 years on, where to now? *Trends in Pharmacological Sciences* 24: 596-601.

Mukerji G, Yiangou Y, Grogono J, et al. (2006). Localization of M2 and M3 muscarinic receptors in human bladder disorders and their clinical correlations. *The Journal of Urology* 176: 367-373.

Murata Y, Miyoshi A, Kitamura Y, et al. (2004). Up-regulation of histamine H(1) receptors in an allergic rat nasal mucosa model. *Inflammation Research* 53 Suppl 1: S11-2.

Navarro J, Landau EM and Fahmy K. (2002). Receptor-dependent G-protein activation in lipidic cubic phase. *Biopolymers* 67: 167-177.

Nelson CP, Nahorski SR and Challiss RA. (2006). Constitutive activity and inverse agonism at the M2 muscarinic acetylcholine receptor. *The Journal of Pharmacology and Experimental Therapeutics* 316: 279-288.

Neuwald AF. (2007). Galpha gbetagamma dissociation may be due to retraction of a buried lysine and disruption of an aromatic cluster by a GTP-sensing arg trp pair. *Protein Science : A Publication of the Protein Society* 16: 2570-2577.

Ng GY, Varghese G, Chung HT, et al. (1997). Resistance of the dopamine D2L receptor to desensitization accompanies the up-regulation of receptors on to the surface of Sf9 cells. *Endocrinology* 138: 4199-4206.

Niu L, Kim JM and Khorana HG. (2002). Structure and function in rhodopsin: Asymmetric reconstitution of rhodopsin in liposomes. *Proceedings of the National Academy of Sciences of the United States of America* 99: 13409-13412.

Ohta K, Hayashi H, Mizuguchi H, et al. (1994). Site-directed mutagenesis of the histamine H1 receptor: Roles of aspartic acid107, asparagine198 and threonine194. *Biochemical and Biophysical Research Communications* 203: 1096-1101.

Okada T, Le Trong I, Fox BA, et al. (2000). X-ray diffraction analysis of three-dimensional crystals of bovine rhodopsin obtained from mixed micelles. *Journal of Structural Biology* 130: 73-80.

Okada T, Sugihara M, Bondar AN, et al. (2004). The retinal conformation and its environment in rhodopsin in light of a new 2.2 A crystal structure. *Journal of Molecular Biology* 342: 571-583.

Okamura N, Yanai K, Higuchi M, et al. (2000). Functional neuroimaging of cognition impaired by a classical antihistamine, d-chlorpheniramine. *British Journal of Pharmacology* 129: 115-123.

Osband M and McCaffrey R. (1979). Solubilization, separation, and partial characterization of histamine H1 and H2 receptors from calf thymocyte membranes. *The Journal of Biological Chemistry* 254: 9970-9972.

Paas Y, Cartaud J, Recouvreur M, et al. (2003). Electron microscopic evidence for nucleation and growth of 3D acetylcholine receptor microcrystals in structured lipid-detergent matrices. *Proceedings of the National Academy of Sciences of the United States of America* 100: 11309-11314.

Palczewski K, Kumasaka T, Hori T, et al. (2000). Crystal structure of rhodopsin: A G protein-coupled receptor. *Science (New York, N.Y.)* 289: 739-745.

Pals-Rylaarsdam R and Hosey MM. (1997). Two homologous phosphorylation domains differentially contribute to desensitization and internalisation of the m2 muscarinic acetylcholine receptor. *The Journal of Biological Chemistry* 272: 14152-14158.

Park P, Sum CS, Hampson DR, et al. (2001). Nature of the oligomers formed by muscarinic m2 acetylcholine receptors in Sf9 cells. *European Journal of Pharmacology* 421: 11-22.

Park PS and Wells JW. (2003). Monomers and oligomers of the M2 muscarinic cholinergic receptor purified from Sf9 cells. *Biochemistry* 42: 12960-12971.

Parker EM, Kameyama K, Higashijima T, et al. (1991). Reconstitutively active G protein-coupled receptors purified from baculovirus-infected insect cells. *The Journal of Biological Chemistry* 266: 519-527.

Peralta EG, Ashkenazi A, Winslow JW, et al. (1988). Differential regulation of PI hydrolysis and adenylyl cyclase by muscarinic receptor subtypes. *Nature* 334: 434-437.

Peroutka SJ and Snyder SH. (1981). 3H]mianserin: Differential labeling of serotonin and histamine receptors in rat brain. *The Journal of Pharmacology and Experimental Therapeutics* 216: 142-148.

Peterson GL, Toumadje A, Johnson WC,Jr, et al. (1995). Purification of recombinant porcine m2 muscarinic acetylcholine receptor from chinese hamster ovary cells. circular dichroism spectra and ligand binding properties. *The Journal of Biological Chemistry* 270: 17808-17814.

Pfeiffer M, Koch T, Schroder H, et al. (2001). Homo- and heterodimerization of somatostatin receptor subtypes. inactivation of sst(3) receptor function by heterodimerization with sst(2A). *The Journal of Biological Chemistry* 276: 14027-14036.

Pfleger KD, Dalrymple MB, Dromey JR, et al (2007). Monitoring interactions between G-protein-coupled receptors and beta-arrestins. *Biochemical Society Transactions* 35(4): 764-767.

Pierce KL, Premont RT and Lefkowitz RJ. (2002). Seven-transmembrane receptors. *Nature Reviews.Molecular Cell Biology* 3: 639-650.

Ponimaskin EG, Schmidt MF, Heine M, et al. (2001). 5-hydroxytryptamine 4(a) receptor expressed in Sf9 cells is palmitoylated in an agonist-dependent manner. *The Biochemical Journal* 353: 627-634.

Popot JL and Engelman DM. (1990). Membrane protein folding and oligomerization: The two-stage model. *Biochemistry* 29: 4031-4037.

Qiu H and Caffrey M. (2000). The phase diagram of the monoolein/water system: Metastability and equilibrium aspects. *Biomaterials* 21: 223-234.

Qutub Y, Reviakine I, Maxwell C, et al. (2004). Crystallization of transmembrane proteins in cubo: Mechanisms of crystal growth and defect formation. *Journal of Molecular Biology* 343: 1243-1254.

Ramsay D, Kellett E, McVey M, et al. (2002). Homo- and hetero-oligomeric interactions between G-protein-coupled receptors in living cells monitored by two variants of bioluminescence resonance energy transfer (BRET): Hetero-oligomers between receptor subtypes form more efficiently than between less closely related sequences. *The Biochemical Journal* 365: 429-440.

Rasmussen SG, Choi HJ, Rosenbaum DM, et al. (2007). Crystal structure of the human beta2 adrenergic G-protein-coupled receptor. *Nature* 450: 383-387.

Ratnala VR, Swarts HG, VanOostrum J, et al. (2004). Large-scale overproduction, functional purification and ligand affinities of the his-tagged human histamine H1 receptor. *European Journal of Biochemistry* 271: 2636-2646.

Ratnala VR, Kiihne SR, Buda F, et al. (2007). Solid-state NMR evidence for a protonation switch in the binding pocket of the H1 receptor upon binding of the agonist histamine. *Journal of the American Chemical Society* 129: 867-872.

Reeves PJ, Callewaert N, Contreras R, et al. (2002). Structure and function in rhodopsin: high-level expression of rhodopsin with restricted and homogenous N-glycosylation by a tetracycline-inducible N-acetylglucosaminyltransferase 1-negative HEK293S stable mammalian cell line. *Proceedings of the National Academy of Science* 99(21): 13419-13424.

Reilander H and Weiss HM. (1998). Production of G-protein-coupled receptors in yeast. *Current Opinion in Biotechnology* 9: 510-517.

Reiter E and Lefkowitz RJ (2006). GRKs and beta-arrestins: roles in receptor silencing, trafficking and signalling. *Trends in Endocrinology and Metabolism* 17(4): 159-165.

Rhodes G. (2000). *Crystallography made crystal clear.* Elsevier Academic Press,

Rigaud J, Chami M, Lambert O, et al. (2000). Use of detergents in two-dimensional crystallization of membrane proteins. *Biochimica Et Biophysica Acta* 1508: 112-128.

Rigaud JL, Mosser G, Lacapere JJ, et al. (1997). Bio-beads: An efficient strategy for two-dimensional crystallization of membrane proteins. *Journal of Structural Biology* 118: 226-235.

Rigaud JL, Pitard B and Levy D. (1995). Reconstitution of membrane proteins into liposomes: Application to energy-transducing membrane proteins. *Biochimica Et Biophysica Acta* 1231: 223-246.

Rinken A. (1996). Formation of the functional complexes of m2 muscarinic acetylcholine receptors with GTP-binding regulatory proteins in solution. *Journal of Biochemistry* 120: 193-200.

Rinken A and Haga T. (1993). Solubilization and characterization of atrial muscarinic acetylcholine receptors in sucrose monolaurate. *Archives of Biochemistry and Biophysics* 301: 158-164.

Rinken A, Kameyama K, Haga T, et al. (1994). Solubilization of muscarinic receptor subtypes from baculovirus infected Sf9 insect cells. *Biochemical Pharmacology* 48: 1245-1251.

Ruat M, Traiffort E, Garbarg M, et al. (1992). Design of an affinity matrix for purification of the histamine H1 receptor from guinea pig cerebellum. *Journal of Neurochemistry* 58: 350-356.

Salim K, Fenton T, Bacha J, et al. (2002). Oligomerization of G-protein-coupled receptors shown by selective co-immunoprecipitation. *The Journal of Biological Chemistry* 277: 15482-15485.

Sander LE, Lorentz A, Sellge G, et al. (2006). Selective expression of histamine receptors H1R, H2R, and H4R, but not H3R, in the human intestinal tract. *Gut* 55: 498-504.

Sansuk K, Balog C, van der Does A, et al. (2008). GPCR proteomics: mass spectrometric and functional analysis of histamine H1 receptor after baculovirus-driven and in vitro cell free expression. *Journal of Proteome Research*. 7: 621-629.

Sarramegna V, Talmont F, Demange P, et al. (2003). Heterologous expression of G-protein-coupled receptors: Comparison of expression systems fron the standpoint of large-scale production and purification. *Cellular and Molecular Life Sciences : CMLS* 60: 1529-1546.

Schonwetter BS, Luedtke RR, Kung MP, et al. (1989). Characterization of membrane-bound and soluble D2 receptors in canine caudate using [125I]IBZM. *The Journal of Pharmacology and Experimental Therapeutics* 250: 110-116.

Seeman P, Corbett R and Van Tol HH. (1997). Atypical neuroleptics have low affinity for dopamine D_2 receptors and are selective for D_4 receptors. *Neuropsychopharmacology* 16: 93.

Seifert R, Grunbaum L and Schultz G. (1994). Histamine H1-receptors in HL-60 monocytes are coupled to gi-proteins and pertussis toxin-insensitive G-proteins and mediate activation of Ca2+ influx without concomitant Ca2+ mobilization from intracellular stores. *Naunyn-Schmiedeberg's Archives of Pharmacology* 349: 355-361.

Sen S, Jaakola VP, Heimo H, et al. (2002). Development of a scintiplate assay for recombinant human alpha(2B)-adrenergic receptor. *Analytical Biochemistry* 307: 280-286.

Service RF. (2004). Materials research society meeting. sushi-like discs give inside view of elusive membrane proteins. *Science (New York, N.Y.)* 304: 674.

Shorr RG, Strohsacker MW, Lavin TN, et al. (1982). The beta 1-adrenergic receptor of the turkey erythrocyte. molecular heterogeneity revealed by purification and photoaffinity labeling. *The Journal of Biological Chemistry* 257: 12341-12350.

Shupak A and Gordon CR. (2006). Motion sickness: Advances in pathogenesis, prediction, prevention, and treatment. *Aviation, Space, and Environmental Medicine* 77: 1213-1223.

Sigel E, Stephenson FA, Mamalaki C, et al. (1983). A gamma-aminobutyric acid/benzodiazepine receptor complex of bovine cerebral cortex. *The Journal of Biological Chemistry* 258: 6965-6971.

Simons FE. (2004). Advances in H1-antihistamines. *The New England Journal of Medicine* 351: 2203-2217.

Smit MJ, Bloemers SM, Leurs R, et al. (1992). Short-term desensitization of the histamine H1 receptor in human HeLa cells: Involvement of protein kinase C dependent and independent pathways. *British Journal of Pharmacology* 107: 448-455.

Smit MJ, Leurs R, Alewijnse AE, et al. (1996). Inverse agonism of histamine H2 antagonist accounts for upregulation of spontaneously active histamine H2 receptors.

Proceedings of the National Academy of Sciences of the United States of America 93: 6802-6807.

Spirin AS. (2004). High-throughput cell-free systems for synthesis of functionally active proteins. *Trends in Biotechnology* 22: 538-545.

Spirin AS, Baranov VI, Ryabova LA, et al. (1988). A continuous cell-free translation system capable of producing polypeptides in high yield. *Science (New York, N.Y.)* 242: 1162-1164.

Stanasila L, Pattus F and Massotte D. (1998). Heterologous expression of G-protein-coupled receptors: Human opioid receptors under scrutiny. *Biochimie* 80: 563-571.

Starr S, Kozell LB and Neve KA. (1995). Drug-induced up-regulation of dopamine D2 receptors on cultured cells. *Journal of Neurochemistry* 65: 569-577.

Tashiro M and Yanai K. (2007). Molecular imaging of histamine receptors in the human brain. *Brain and Nerve = Shinkei Kenkyu no Shinpo* 59: 221-231.

Tate CG and Grisshammer R. (1996). Heterologous expression of G-protein-coupled receptors. *Trends in Biotechnology* 14: 426-430.

Tetlow LC and Woolley DE. (2005). Demonstration of histamine H1 and H2 receptors in chondrocytes of human osteoarthritic cartilage. *Inflammation Research* 54 Suppl 1: S74-5.

Toll L and Snyder SH. (1982). Solubilization and characterization of histamine H1 receptors in brain. *The Journal of Biological Chemistry* 257: 13593-13601.

Treherne JM and Young JM. (1988). Digitonin-solubilised histamine H1-receptors bind to polyethylenimine-treated glass-fibre filters. *The Journal of Pharmacy and Pharmacology* 40: 730-733.

Tsai CJ, Ejsing CS, Shevchenko A, et al. (2007). The role of lipids and salts in two-dimensional crystallization of the glycine-betaine transporter BetP from corynebacterium glutamicum. *Journal of Structural Biology* 160: 275-286.

Unger VM, Hargrave PA, Baldwin JM, et al. (1997). Arrangement of rhodopsin transmembrane alpha-helices. *Nature* 389: 203-206.

Unger VM, Kumar NM, Gilula NB, et al. (1999). Expression, two-dimensional crystallization, and electron cryo-crystallography of recombinant gap junction membrane channels. *Journal of Structural Biology* 128: 98-105.

Uustare A, Nasman J, Akerman KE, et al. (2004). Characterization of M2 muscarinic receptor activation of different G protein subtypes. *Neurochemistry International* 44: 119-124.

Valenzuela D, Han X, Mende U, et al. (1997). G alpha(o) is necessary for muscarinic regulation of Ca2+ channels in mouse heart. *Proceedings of the National Academy of Sciences of the United States of America* 94: 1727-1732.

van Koppen CJ and Nathanson NM. (1990). Site-directed mutagenesis of the m2 muscarinic acetylcholine receptor. analysis of the role of N-glycosylation in receptor expression and function. *The Journal of Biological Chemistry* 265: 20887-20892.

van Rhee M and Jacobson K. (1996). Molecular architecture of G protein-coupled receptors. *Drug Development Research* 37: 1.

Vaughn JL, Goodwin RH, Tompkins GJ, et al. (1977). The establishment of two cell lines from the insect spodoptera frugiperda (lepidoptera; noctuidae). *In Vitro* 13: 213-217.

Vorobiov D, Bera AK, Keren-Raifman T, et al. (2000). Coupling of the muscarinic m2 receptor to G protein-activated K(+) channels via galpha(z) and a receptor-galpha(z) fusion protein. fusion between the receptor and galpha(z) eliminates catalytic (collision) coupling. *The Journal of Biological Chemistry* 275: 4166-4170.

Wang YX and Kotlikoff MI. (2000). Signalling pathway for histamine activation of non-selective cation channels in equine tracheal myocytes. *The Journal of Physiology* 523 Pt 1: 131-138.

Warne T, Chirnside J and Schertler GF. (2003). Expression and purification of truncated, non-glycosylated turkey beta-adrenergic receptors for crystallization. *Biochimica Et Biophysica Acta* 1610: 133-140.

Weill C, Autelitano F, Guenet C, et al. (1997). Pharmacological and structural integrity of muscarinic M2 acetylcholine receptors produced in Sf9 insect cells. *European Journal of Pharmacology* 333: 269-278.

Wess J. (1997). G-protein-coupled receptors: Molecular mechanisms involved in receptor activation and selectivity of G-protein recognition. *The FASEB Journal : Official Publication of the Federation of American Societies for Experimental Biology* 11: 346-354.

Whorton MR, Bokoch MP, Rasmussen SG, et al. (2007). A monomeric G protein-coupled receptor isolated in a high-density lipoprotein particle efficiently activates its G protein. *Proceedings of the National Academy of Sciences of the United States of America* 104: 7682-7687.

Wikipedia (2007). William lawrence bragg.
http://en.wikipedia.org/wiki/William_Lawrence_Bragg

Windh RT and Manning DR. (2002). Analysis of G protein activation in Sf9 and mammalian cells by agonist-promoted [35S]GTP gamma S binding. *Methods in Enzymology* 344: 3-14.

Xu J, He J, Castleberry AM, et al. (2003). Heterodimerization of alpha 2A- and beta 1-adrenergic receptors. *The Journal of Biological Chemistry* 278: 10770-10777.

Xu ZQ, Zhang X and Scott L. (2007). Regulation of G protein-coupled receptor trafficking. *Acta Physiologica (Oxford, England)* 190: 39-45.

Yao X, Parnot C, Deupi X, et al. (2006). Coupling ligand structure to specific conformational switches in the beta2-adrenoceptor. *Nature Chemical Biology* 2: 417-422.

Yao Z and Kobilka B. (2005). Using synthetic lipids to stabilize purified beta2 adrenoceptor in detergent micelles. *Analytical Biochemistry* 343: 344-346.

Yoshino T, Takahashi M, Takeyama H, et al. (2004). Assembly of G protein-coupled receptors onto nanosized bacterial magnetic particles using Mms16 as an anchor molecule. *Applied and Environmental Microbiology* 70: 2880-2885.

Zhu Y, Michalovich D, Wu H, et al. (2001). Cloning, expression, and pharmacological characterization of a novel human histamine receptor. *Molecular Pharmacology* 59: 434-441.

Zhuang J, Prive GG, Werner GE, et al. (1999). Two-dimensional crystallization of escherichia coli lactose permease. *Journal of Structural Biology* 125: 63-75.

7. Appendix for Chapter 2

7.1. Production of Baculoviruses

Figure 3. [^{3}H]-scopolamine binding to *Sf*9 infected with His6$_C$M$_2$R recombinant baculovirus.

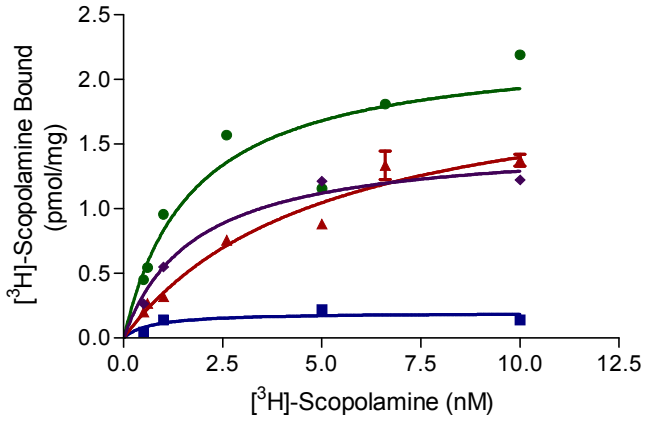

Figure 3. [^{3}H]-Scopolamine binding to cells infected with His(6_c)M$_2$ recombinant baculovirus. Cells were collected at 24 hour intervals post baculovirus addition and assayed for specific [^{3}H]-Scopolamine binding. Non-specific binding was determined in the presence of 10µM atropine. Data points are as follows: blue squares 24hpi; red triangles 48hpi; green circles 72hpi; purple diamonds 96hpi. Data points represent the mean ± S.E.M, n = 3.

Figure 4. [^{3}H]-pyrilamine binding to cells infected with His10$_C$H$_1$ recombinant baculovirus.

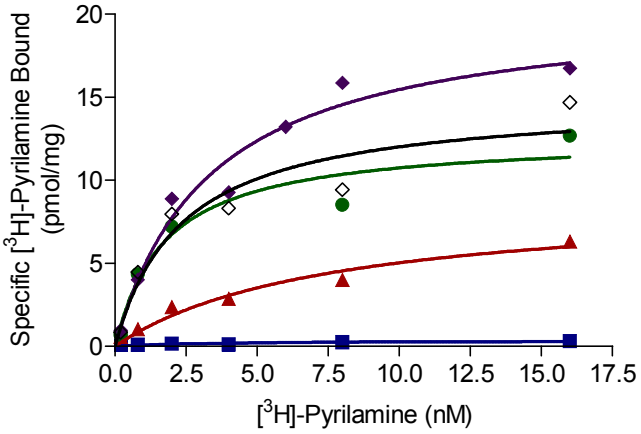

Figure 4. [^{3}H]-pyrilamine binding to *Sf*9 cells infected with recombinant His(10_C)H$_1$ baculovirus. Cells were collected at 24 (blue squares), 48 (red triangles), 72 (green circles), 96 (purple diamonds) and 120 (black diamonds) hours post baculovirus addition and assayed for specific [^{3}H]-pyrilamine binding. Non-specific binding was determined in the presence of 10µM triprolidine. Each point is representative of a single experiment..

7.2. Expression of the M_2 muscarinic receptors

Figure 7. [^{3}H]-scopolamine binding to Histidine tagged M_2 muscarinic receptors.

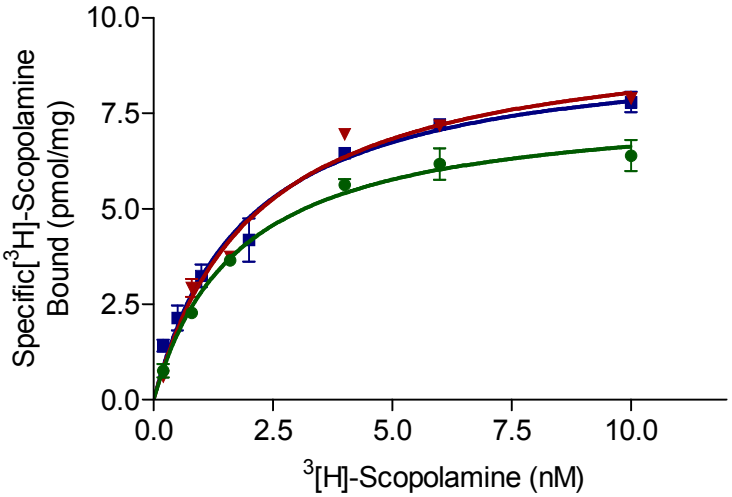

Figure 7. [^{3}H]-Scopolamine binding to Histidine tagged M_2 Muscarinic receptors in membranes prepared from *Sf*9 cells infected with recombinant baculovirus. N terminal hexa-Histidine tagged M_2R (blue squares), C terminal hexa-Histidine tagged M_2R (red triangles) and C terminal dodeca-Histidine tagged M_2R (green circles). K_d values were calculated using single site non-linear regression and were 1.9, 2.2 and 1.8 nM respectively. B_{max} values were calculated as 9.3pmol/mg, 9.7pmol/mg and 7.8pmol/mg for the $His6_NM_2R$, $His6_CM_2R$ and the $His12_CM_2R$ respectively. Non-specific binding was determined in the presence of 10μM atropine and was less than 10%. Data points represent the mean ± S.E.M, n=3.

7.3. Ligand Culture

Figure 14. [^{3}H]-scopolamine binding to $His6_CM_2R$ membranes prepared from ligand treated *Sf*9 cells.

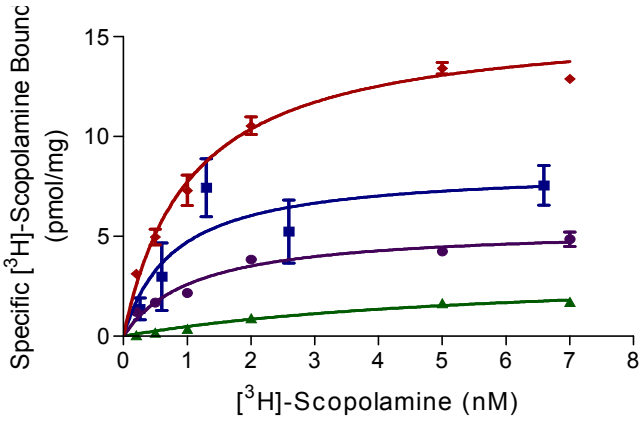

Figure 14. [^{3}H]-scopolamine binding in membranes prepared from ligand treated, $His(6_C)M_2R$ baculovirus infected *Sf*9 cells. Blue squares no ligand treatment, red triangles treatment with atropine, purple circles treatment with pirenzepine, green triangles treatment with acetylcholine. B_{max} and K_d values were calculated from one site saturation binding analysis (n=3) and were as follows: control (8.4 pmol/mg, 0.7nM), atropine (15.8pmol/mg, 1.0nM), pirenzepine (5.5pmol/mg, 1.1nM) and acetylcholine (3.3pmol/mg, 5.8nM).

Figure 15. [^{3}H]-pyrilamine binding to His10$_C$H$_1$R membranes prepared from ligand treated *Sf*9 cells.

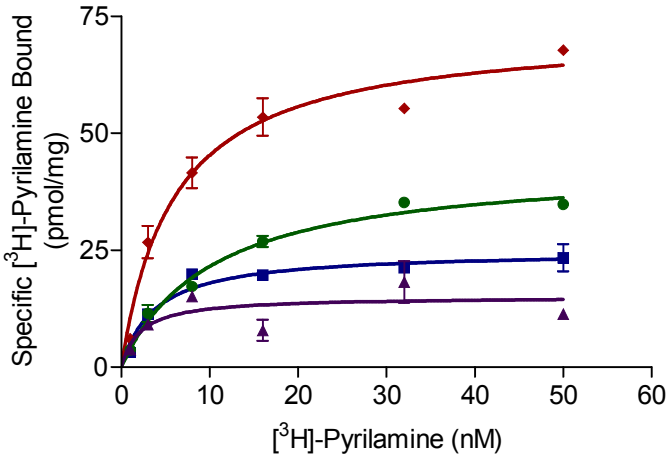

Figure 15. [^{3}H]-pyrilamine binding in membranes prepared from ligand treated, His(10_C)H$_1$R baculovirus infected *Sf*9 cells. Blue squares no ligand treatment, red diamonds treatment with triprolidine, green cricles treatment with pyrilamine, purple triangles treatment with histamine. B_{max} and K_d values were calculated from one site saturation binding analysis (n=3) and were as follows: control (25pmol/mg, 3.8nM), triprolidine (72pmol/mg, 5.9nM), pyrilamine (44pmol/mg, 10.2nM) and histamine (15pmol/mg, 2.1nM).

Figure 16. [^{3}H]-spiperone binding to His6$_C$D$_{2L}$R membranes prepared from ligand treated *Sf*9 cells.

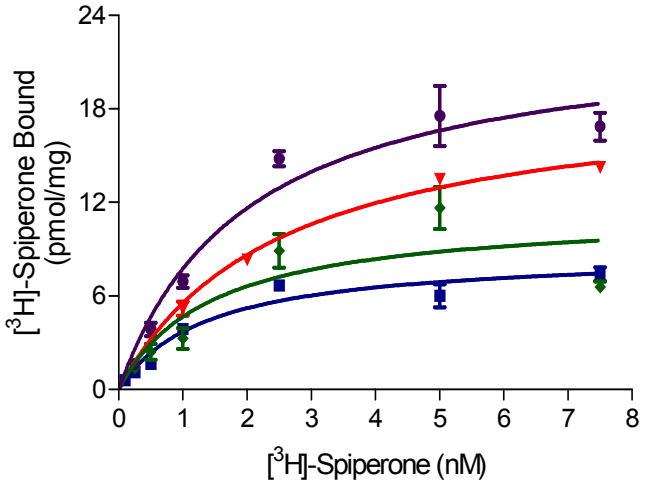

Figure 16. [^{3}H]-spiperone binding to His6$_C$D$_{2L}$R membranes prepared from ligand treated *Sf*9 cells. Blue squares no ligand treatment, red triangles treatment with bromocryptine, purple circles treatment with NPA, green diamonds treatment with haloperidol. B_{max} and K_d values were calculated from one site saturation binding analysis (n=3) and were as follows: control (8.7pmol/mg, 1.3nM), bromocryptine (19.4pmol/mg, 2.5nM), haloperidol (11.3pmol/mg, 1.4nM) and NPA (23.3pmol/mg, 2.0nM).